

**The Development of a Novel Technique for AFM Thermal
Analysis of Individual Phases in Polymer Mixtures after
Separation and Identification via LC-FTIR**

by

E. de Goede



Thesis presented in partial fulfilment of the requirements for the degree of

Master of Science (Polymer Science)

at the

University of Stellenbosch

Study Leader:
Prof. R.D. Sanderson

Stellenbosch
April 2004

Declaration

I, the undersigned, hereby declare that the work contained in this thesis is my own original work and that I have not previously in its entirety or in part, submitted it at any university for a degree.

Signature

Date

Abstract

In the ongoing search for better and faster ways to characterize complex polymer systems, it is often necessary to couple different analytical techniques in order to obtain information on more than one distributed property. In this study, the coupling of chromatography and spectroscopy to atomic force microscopy (AFM) was attempted for the first time, and thus the term “LC-FTIR-AFM” was coined. This new hyphenated technique combines the separation power of liquid chromatography (LC) and the ability of infrared spectroscopy (IR) to identify almost any organic compound, with the AFM’s ability to be used for thermal analysis of individual phases in polymer mixtures.

The first two steps of this new technique comprise (i) the separation of compounds in a mixture via gradient polymer elution chromatography (GPEC) and (ii) the identification of each compound by means of LC-FTIR analysis. In the final step, LC-FTIR analysis is coupled to AFM through the use of the LC-FTIR interface.

A number of polymer mixtures were analysed by means of the novel technique that was developed, in order to establish its validity and value as a characterization technique of the future. The influence of film thickness and molar mass on the thermal parameters of individual components in mixtures, measured by this technique, were also investigated. This technique adds a new dimension to conventional thermal analysis methods, since it allows the thermal transitions of individual polymer phases in multiphase polymers to be resolved directly after separation and identification.

Opsomming

In die voortdurende soektog na beter en vinniger maniere om komplekse polimeersisteme te karakteriseer, is dit soms nodig om verskillende analitiese tegnieke met mekaar te koppel ten einde inligting aangaande twee of meer verspreide eienskappe te bekom. Gedurende hierdie studie is daar gepoog om chromatografie en spektroskopie met atoominteraksie-mikroskopie (atomic force microscopy, AFM) te koppel. Gevolglik het die term “LC-FTIR-AFM” ontstaan. Hierdie nuwe koppelingstegniek kombineer die kragtige skeidingspotensiaal van vloeistofchromatografie en die vermoë van infrarooispektroskopie om byna enige organiese verbinding positief te identifiseer, met die atoominteraksie-mikroskoop se potensiaal om as ‘n termiese analise metode vir individuele fases in polimeermengsels te dien.

Die eerste twee stappe van die tegniek behels (i) die skeiding van verbindings in ‘n mengsel deur middel van gradient-hoë-druk-vloeistofchromatografie en (ii) die identifisering van afsonderlike verbindings deur vloeistofchromatografie gekoppel aan infrarooispektroskopie. Gedurende die finale stap word vloeistofchromatografie en infrarooispektroskopie aan die atoominteraksie-mikroskoop gekoppel deur gebruik te maak van die LC-FTIR koppelingsapparaat.

‘n Aantal polimeermengsels is geanaliseer deur die nuwe tegniek hierbo beskryf, ten einde die geldigheid en waarde daarvan as ‘n analitiese metode vir die toekoms vas te stel. Die invloed van film diktes en molekulêre massa op die termiese oorgange van individuele komponente in mengsels, soos gemeet deur hierdie metode, is ook ondersoek. Hierdie tegniek voeg ‘n nuwe dimensie tot konvensionele termiese analise metodes deurdat dit die bepaling van termiese oorgange van individuele polimeerfases in multifase polimere, direk na afloop van skeiding en identifikasie moontlik maak.

Acknowledgements

First, I would like to thank my study leader, Prof. Ron Sanderson, for his interest in this project and for the opportunity to study at this world-class institution. The technical staff at Polymer Science, Aneli, Calvin, Erinda, Mr. Bonthuys and Margie, is sincerely thanked for their assistance. The students at Polymer Science, especially André and Martina are also thanked for their contribution to this project. I would also like to thank the National Research Foundation (NRF) and the Division of Polymer Science for financial support received during the time of this project.

On a more personal note I thank my parents and my brothers for providing me with all the opportunities necessary to achieve my goals and for encouraging me to further my studies in this field. Also to Kenneth and Celeste, thanks for your friendship and interest in my studies over the last year. Finally, I would like to thank Phillip for his friendship, patience and support. Thank you very much.

List of Contents

List of Figures	vi
------------------------	----

List of Tables and Schemes	ix
-----------------------------------	----

List of Symbols and Abbreviations	x
--	---

Chapter 1: General Introduction and Objectives

1.1	Introduction	1
1.2	Objectives	5
1.3	Layout of thesis	6
1.4	References	7

Chapter 2: Historical Overview

2.1	Developments in liquid chromatography	8
2.1.1	Introduction	8
2.1.2	Gradient elution chromatography	9
2.1.2.1	The gradient former	10
2.1.2.2	Analysis of oligomers by gradient elution	11
2.1.2.3	Normal-phase and reversed-phase gradient elution	12
2.1.2.4	Separation according to chemical composition and critical conditions	14

2.2	Hyphenation in liquid chromatography	15
2.2.1	The need for hyphenation in the characterisation of polymers	15
2.2.2	LC-FTIR analysis	17
2.2.3	Gradient elution chromatography coupled to FTIR detection	19
2.3	The development of scanning probe microscopy	19
2.3.1	From optical microscopy to scanning probe microscopy	19
2.3.2	The atomic force microscope	20
2.3.2.1	The origin of atomic force microscopy	20
2.3.2.2	Polymer thin film characteristics	22
2.3.2.3	The glass transition temperature	23
2.3.2.4	Thermal analysis by AFM	24
2.4	References	25

Chapter 3: Theoretical Background

3.1	Gradient polymer elution chromatography	30
3.1.1	The solvent gradient or program	31
3.1.1.1	The nature of solvents A and B	32
3.1.1.2	Gradient steepness	33
3.1.1.3	Gradient shape	34
3.1.2	The separation process	35
3.1.2.1	Effect of specific solvents A and B on separation	37
3.1.2.2	Effect of gradient steepness on separation	38
3.1.2.3	Effect of gradient shape on separation	38
3.1.3	Other factors affecting separation in gradient elution	40
3.1.3.1	Solvent degassing	40
3.1.3.2	Baseline stability	40
3.1.3.3	Column regeneration	41
3.1.3.4	Sampling effects	41

3.1.4	Normal-phase and reversed-phase separation in gradient elution	41
3.1.4.1	The precipitation-redissolution mechanism in reversed-phase separation	42
3.1.5	Normal-phase gradient elution	45
3.1.5.1	The adsorption mechanism	46
3.1.5.2	Effect of eluent strength	46
3.1.5.3	Effect of solubility	47
3.2	Liquid chromatography-Fourier transform infrared spectroscopy	48
3.2.1	Flow-cell LC-FTIR	49
3.2.2	Solvent-elimination LC-FTIR	49
3.3	Scanning probe microscopy	50
3.3.1	System operation and signal detection	51
3.3.2	Atomic force microscopy	53
3.3.2.1	Force-distance relationship	54
3.3.2.2	Contact mode AFM	56
3.3.2.3	Non-contact mode AFM	56
3.3.3	Micro-thermal analysis of polymers by SPM	56
3.3.3.1	Thermal analysis of polymers by AFM	57
3.3.3.2	The interaction mode	58
3.3.3.3	The melting point	60
3.3.3.4	The glass transition	61
3.4	References	63

Chapter 4: Experimental

4.1	Materials	66
4.1.1	Choice of materials	66
4.1.2	Sample preparation	67

4.2	HPLC analysis	68
4.2.1	HPLC equipment and experimental conditions	68
4.2.2	Solvents	69
4.2.3	Experimental setup for gradient analysis	69
4.2.4	The solvent gradient	71
4.3	LC-FTIR analysis	72
4.3.1	Sample preparation	72
4.3.2	The LC-FTIR interface	73
4.3.3	Experimental conditions	75
4.4	AFM analysis	76
4.4.1	AFM instrumentation	76
4.4.2	System operation for resonance frequency measurements	77
4.5	Proposed strategy for the development of the LC-FTIR-AFM technique	79
4.5.1	Route diagram of the work proposed	79
4.5.2	Strategy followed during LC-FTIR analysis	80
4.5.3	Development of the LC-FTIR-AFM technique	81
4.6	References	81

Chapter 5: Results and Discussion

5.1	Analysis of oligoethylenes	83
5.1.1	HPLC separation of an oligoethylene mixture	83
5.1.2	LC-FTIR analysis of an oligoethylene mixture	84
5.1.3	LC-AFM analysis of an oligoethylene mixture	86

5.2	Analysis of polystyrenes	87
5.2.1	HPLC separation of a polystyrene mixture	87
5.2.2	LC-FTIR analysis of a polystyrene mixture	89
5.2.3	LC-AFM analysis of a polystyrene mixture	91
5.2.3.1	Molar mass dependence of the T_g	93
5.2.3.2	Film thickness dependence of the T_g	95
5.3	Analysis of a mixture of oligoethylene and polystyrene	97
5.3.1	HPLC separation of a mixture of oligoethylene and polystyrene	98
5.3.2	LC-FTIR analysis of a mixture of oligoethylene and polystyrene	99
5.3.3	LC-AFM analysis of a mixture of oligoethylene and polystyrene	100
5.4	Analysis of a mixture of poly(ethyl methacrylate) and polystyrene	101
5.4.1	HPLC separation of a mixture of PEMA and PS	102
5.4.2	LC-FTIR analysis of a mixture of PEMA and PS	103
5.4.3	LC-AFM analysis of the mixture of PEMA and PS	104
5.5	Analysis of an unknown emulsion	105
5.5.1	HPLC analysis of an unknown emulsion	105
5.5.2	LC-FTIR analysis of an unknown emulsion	107
5.5.3	LC-AFM analysis of an unknown emulsion	110
5.6	References	113

Chapter 6: Summary and Conclusions

6.1	Summary	115
6.2	Conclusions	116

List of Figures

Chapter 3: Theoretical Background

- Figure 3.1: Illustration of a number of solvent gradients of various shapes.
- Figure 3.2: The fractional migration (r) of a band of compound X along the column as a function of time; and the band k' value as a function of time (instantaneous value k_t).
- Figure 3.3: The effect of gradient shape on the peak profile appearance of the chromatogram.
- Figure 3.4: Schematic representation of three different stages a, b, and c in the precipitation-redissolution mechanism of gradient elution.
- Figure 3.5: The relationship between $\log M$ and retention time (RT) for separation in gradient HPLC.
- Figure 3.6: Illustration of the general design principle of all SPMs.
- Figure 3.7: Representation of the forces present between the AFM tip and a sample surface when the tip is in close proximity of the sample.
- Figure 3.8: Diagram of a typical AFM force-vs-distance curve.
- Figure 3.9: The resonance frequency of the cantilever as a function of temperature.
- Figure 3.10: The melting point of octadecane as indicated by the kink at 31.7 °C in the resonance frequency plot.
- Figure 3.11: The glass transition of a random copolymer, as indicated by the plateau at about 21°C.

Chapter 4: Experimental

- Figure 4.1: Schematic representation of the gradient HPLC experimental setup used.
-

-
- Figure 4.2: The LC-Transform design concept, illustrating the two independent modules: (A) the sample collection module, and (B) the optics module.
- Figure 4.3: Schematic diagram of the nozzle depositing a solute track onto the germanium substrate.
- Figure 4.4: The position of the sample during AFM measurements.

Chapter 5: Results and Discussion

- Figure 5.1: GPEC chromatogram of a mixture of two oligoethylene standards.
- Figure 5.2: Gram-Schmidt chromatogram of a mixture of two oligoethylenes.
- Figure 5.3: IR spectrum of the C20 oligoethylene.
- Figure 5.4: IR spectrum of the C28 oligoethylene.
- Figure 5.5: R_f spectrum of the C20 oligoethylene.
- Figure 5.6: R_f spectrum of the C28 oligoethylene.
- Figure 5.7: GPEC chromatogram of a mixture of five PS standards.
- Figure 5.8: Gram-Schmidt representation of the mixture of five PS standards.
- Figure 5.9: IR spectrum of PS taken at 17.18 minutes.
- Figure 5.10: R_f plot of the highest molar mass region of the mixture of the five PS standards.
- Figure 5.11: T_g of the lowest MM region of the PS deposit.
- Figure 5.12: T_g of the mid-MM region of the PS deposit.
- Figure 5.13: The change in the T_g plateau width and onset as a function of film thickness for PS with a molar mass of $142\,500\text{ g}\cdot\text{mol}^{-1}$.
- Figure 5.14: Average T_g plateau width as a function of film thickness for PS with a molar mass of $142\,500\text{ g}\cdot\text{mol}^{-1}$.
- Figure 5.15: The onset of the T_g plateau as a function of film thickness.
- Figure 5.16: GPEC chromatogram of a mixture of oligoethylene and PS.
- Figure 5.17: Gram-Schmidt representation of the mixture of oligoethylene and PS.
- Figure 5.18: IR spectrum of the oligoethylene component of the mixture.
- Figure 5.19: IR spectrum of the PS component of the mixture.
- Figure 5.20: R_f plot of the oligoethylene component of the mixture.
- Figure 5.21: R_f plot of the PS component of the mixture.
-

- Figure 5.22: GPEC chromatogram of a mixture containing PEMA and PS.
- Figure 5.23: Gram-Schmidt representation of a mixture of PEMA and PS.
- Figure 5.24: IR spectrum of PEMA at 7.71 minutes.
- Figure 5.25: IR spectrum of PS at 15.24 minutes.
- Figure 5.26: The R_f plot of the PEMA in the mixture.
- Figure 5.27: The R_f plot of the PS in the mixture.
- Figure 5.28: GPEC chromatogram of a commercial paper coating emulsion system.
- Figure 5.29: Gram-Schmidt representation of the commercial paper coating emulsion.
- Figure 5.30: IR spectrum of the component at 14.12 minutes.
- Figure 5.31: IR spectrum of the component at 20.74 minutes.
- Figure 5.32: Comparison of the unknown second component of the paper coating emulsion with a reference spectrum in the IR library (closest match).
- Figure 5.33: Stack plot of the two major components in the paper coating emulsion system.
- Figure 5.34: R_f plot of the oligoethylene component of the unknown sample.
- Figure 5.35: R_f plot of the copolymer component of the unknown sample.
- Figure 5.36: Illustration of the technique used to recover deposits from the LC-FTIR collection disc.
-

List of Tables and Schemes

Chapter 3: Theoretical Background

Scheme 3.1: Different solvent systems in binary and ternary gradients.

Chapter 4: Experimental

Table 4.1: Specifications of the columns used for HPLC analysis.

Scheme 4.1: Representation of the gradient used during gradient analysis.

Table 4.2: Specifications of the silicon discs used for sample collection.

Scheme 4.2: Route diagram of the path followed during the development of the new LC-FTIR-AFM technique.

Chapter 5: Results and Discussion

Table 5.1: IR absorption data for oligoethylene.

Table 5.2: IR absorption data for PS.

Table 5.3: IR data of the functional groups of PEMA.

List of Symbols and Abbreviations

Abbreviations

ACN	acetonitrile
AFM	atomic force microscopy
ATR	attenuated total reflection
BLS	Brillouin light scattering
CCD	chemical composition distribution
CE	capillary electrophoresis
CE-MS	capillary electrophoresis coupled to mass spectrometry
CSC	critical solvent composition
DMA	dynamic mechanical analysis
DSC	differential scanning calorimetry
ELSD	evaporative light scattering detector
FFM	friction force microscopy
FTD	functionality-type distribution
FTIR	Fourier transform infrared spectroscopy
GC	gas chromatography
GC-FTIR	gas chromatography coupled to Fourier transform infrared spectroscopy
GC-MS	gas chromatography coupled to mass spectrometry
GPEC	gradient polymer elution chromatography
GS	Gram-Schmidt
HPLC	high-performance liquid chromatography
HPLC-MS	high-performance liquid chromatography coupled to mass spectrometry
IR	infrared spectroscopy

LAC	liquid absorption chromatography
LC	liquid chromatography
LCCC	liquid chromatography at critical conditions
LC-FTIR	liquid chromatography coupled to Fourier transform infrared spectroscopy
LC-FTIR-AFM	liquid chromatography coupled to Fourier transform infrared spectroscopy and atomic force microscopy
LC-MS	liquid chromatography coupled to mass spectrometry
LC-NMR	liquid chromatography coupled to nuclear magnetic resonance
LFM	lateral force microscopy
LSS	linear solvent strength
MAA	methacrylic acid
MAD	molecular architecture distribution
MALDI-MS	matrix-assisted laser desorption/ionization mass spectrometry
MDSC	modulated differential scanning calorimetry
MM	molar mass
MMD	molar mass distribution
MS	mass spectrometry
NMR	nuclear magnetic resonance
NP-GPEC	normal-phase gradient polymer elution chromatography
PEMA	poly(ethyl methacrylate)
PMMA	poly(methyl methacrylate)
PS	polystyrene
RFM	resonance frequency measurement
RP-GPEC	reversed-phase gradient polymer elution chromatography
RT	retention time
SEC	size exclusion chromatography
SEM	scanning electron microscopy
SFM	scanning force microscopy
SMFM	shear modulation force microscopy
SNOM	scanning near-field optical microscopy

SPM	scanning probe microscopy
STM	scanning tunneling microscopy
TA	thermal analysis
THF	tetrahydrofuran
TLC	thin layer chromatography
UV	ultraviolet

Symbols

a^*	absorption coefficient
C	empirical parameter
d	depth of the near-interface polymer layer
D	depth of the polymer surface layer
D	diameter of the cantilever
D	polydispersity
E	elastic modulus
F_{rate}	flow rate of the mobile phase eluent
G'	storage modulus
G''	loss modulus
G^*	shear modulus
ΔG_m	Gibbs free energy of mixing
ΔH	interaction enthalpy
ΔH_m	mixing enthalpy
k	capacity factor
k'	capacity factor
k_x	capacity factor for compound x
K	empirical constant
L	length of column
L	length of cantilever
M_n	number-average molar mass
M_w	weight-average molar mass

N	column plate number
N	average length of polymer chain in units of segments
r^*	reflection coefficient
R_s	resolution
RT	retention time
ΔS	conformational entropy
t	time
t_0	column dead time
t_d	gradient delay time
t_G	gradient time
t_H	gradient hold time
t_R	solute retention time
t_x	retention time of compound x
T	temperature
T_g	glass transition temperature
T_{g0}	glass transition temperature of the surface
T_g^∞	glass transition temperature at an infinitely large molar mass
T_m	melting temperature
$T\Delta S_m$	entropy of mixing
U_E	linear velocity of the eluent
U_p	linear velocity of a polymer molecule in the interstitial volume
V_0	column dead volume
V_I	interstitial volume
V_{mob}	volume accessible by the eluent
V_P	pore volume of the packing material
Z_a^*	imaginary acoustic impedance of air
Z_p^*	imaginary acoustic impedance of polymer
α	material constant
α_i	isocratic separation factor for two adjacent solute bands, equal to the ratio of their k-values

δ	strength of film-surface interaction
ρ	density
ϕ'	gradient steepness
ϕ''	gradient steepness equal to $\phi' t_0$
w	baseline bandwidth
ω_r	resonance frequency

Chapter 1

General Introduction and Objectives

1.1 Introduction

In an industrial world where technology advances rapidly and new complex polymers are synthesised daily, the demand for better and faster analytical methods by which to analyse them has created a challenging task for chemists in the field of polymer characterisation. Over the past few years there has been a significant increase in the quest to correlate the structure of synthetic polymers to their properties, in order to explain and manipulate the behaviour of polymer materials and to ensure more suitable products for specific applications.

Most synthetic polymers are highly complex multi-component materials, consisting of molecules of different chain lengths, chemical compositions, and molecular architectures. Such materials are heterogeneous in more than one distributed property, for example, linear copolymers that are distributed in both molar mass and chemical composition. Polymer analysis is therefore concerned with the following heterogeneities [1]: molar mass distribution (MMD), functionality-type distribution (FTD), chemical composition distribution (CCD), and molecular architecture distribution (MAD). These heterogeneities can also be superimposed on one another, making it a very difficult task to fully characterise complex polymer systems.

Until recently, the most popular techniques for polymer characterisation have been nuclear magnetic resonance spectroscopy (NMR), Fourier transform infrared spectroscopy (FTIR) and size exclusion chromatography (SEC). With the development of new complex polymer systems such as copolymers, blends, alloys, laminates and core-shell particles, these conventional techniques have become less popular and sometimes insufficient for adequate characterisation. NMR and FTIR are still valued for their ability to determine the type of monomer building blocks and functional groups present, but they cannot provide any information on the way in which monomer units are included in the chain structure. Functional end groups in long-chain molecules can also not be determined, since they are usually present in relatively low concentrations.

SEC provides information on the size of macromolecules, which can then be related to their molar mass via a calibration curve method, but once again some complications need to be kept in mind. SEC separates molecules according to their hydrodynamic volume, and since polymers in mixtures may have overlapping hydrodynamic volumes, it might be impossible to separate such macromolecules. The size distribution of polymers can unfortunately only be correlated with molar mass distribution within a single heterogeneity type. SEC also does not provide any information on the chemical composition of macromolecules, and should therefore always be coupled to a composition-sensitive detector for complete characterisation of any polymer system.

It is therefore obvious that meaningful characterisation of complex synthetic polymers often requires more than one analytical technique. The techniques combined for this purpose should each be selective towards a specific heterogeneity type. This can be accomplished either through two-dimensional chromatography [2,3] where different chromatographic modes are coupled, or via coupling of a chromatographic separation technique with a selective detector. In 1980 Hirshfeld proposed the term “hyphenation” to describe the close relationship or marriage between two separate devices or techniques via appropriate interfaces [4]. Another term used in this regard is “coupling” [5] of analytical techniques, but this was considered less appropriate, since it creates the idea of

two individual instruments simply being connected to each other via tubing, whereas adjustments to the experimental setup are always needed.

In the past, hyphenated techniques have mostly been applied for the analysis of low molar mass organic compounds found in very low concentrations within environmental and biological samples. Mass spectrometry (MS) was often used as the detector for components separated by capillary gas chromatography (GC), high performance liquid chromatography (HPLC) and capillary electrophoresis (CE). Hyphenated techniques such as GC-MS, HPLC-MS and CE-MS ensure fast and efficient separation as well as identification of compounds in one single run. As far as polymers are concerned, one needs to understand the influence of molecular parameters on polymer properties and performance. Information on molar mass distribution and chemical composition may be insufficient for establishing such structure-property relationships. It has become necessary to employ multidimensional approaches instead of conventional techniques that yield only average properties of the bulk sample.

One analytical technique capable of separating polymers according to chemical composition is gradient elution analysis, or gradient polymer elution chromatography (GPEC), invented by Tiselius and co-workers in 1952 [6]. The mobile phase consists of at least two solvents, the composition of which changes with time during the run, to create a so-called gradient or program. Gradient polymer elution can be coupled to other analytical techniques, depending on the information required. The most efficient way to obtain information on different distribution types is by combining different chromatographic techniques, each one selective towards a certain heterogeneity type, e.g. MMD, CCD, FTD, and MAD. This two-dimensional approach is called “orthogonal chromatography” [7]. Chromatographic separation has also been coupled to various spectroscopic detectors over the past few years, giving rise to the following most popular hyphenated techniques: LC-NMR [8], LC-MS [9] and LC-FTIR [10].

When coupling liquid chromatography to FTIR spectroscopy, the main problem is the strong absorption of IR radiation by the mobile phase solvents. This problem was solved

by Gagel and Biemann [11-13], when they invented a LC-FTIR interface that eliminated the LC mobile phase prior to FTIR analysis. LC-FTIR analysis yields a complete IR spectrum for each sample fraction, therefore individual polymer components separated by gradient analysis can be identified on the basis of their IR spectra, wherever reference spectra are available.

Polymer surfaces and thin polymer films are currently gaining importance due to their involvement in a wide variety of technological applications varying from improvements in lubrication and adhesion [14,15], to the development of water and oil repellence [16]. Such advances require new developments in analytical sciences, especially microscopy, for exploring the relation between the molecular structure and macroscopic properties. Apart from the information obtainable via imaging in scanning probe microscopy (SPM), certain chemical and physical properties of thin polymer films, including thermal transitions, can also be measured by means of appropriate SPM modes.

The thermal parameters of a polymer, such as the glass transition temperature (T_g) and melting point (T_m), can be determined by a number of analytical techniques. Two conventional methods of thermal analysis include differential scanning calorimetry (DSC) and dynamic mechanical analysis (DMA). The disadvantage of both these respective methods is that they can only provide an average result of the parameter measured, for the entire sample. Thermal transitions of individual phases in structured polymer systems cannot be measured locally on a molecular scale. A new analytical technique for the local measurement of thermal transitions of polymer blends or structured systems was recently developed by Meincken [17]. The T_g of both the core and shell of a core-shell polymer [18] could be measured by means of this technique. The atomic force microscope (AFM) is operated in a stationary non-contact mode in a way comparable to the functioning of the DMA. Molecules are excited mechanically in order to measure their response, but on a much smaller scale. Therefore, the term "nano-DMA" was proposed.

During this study, the coupling of liquid chromatography with atomic force microscopy was attempted for the first time. This will allow the determination of thermal properties of individual components in polymer mixtures or blends after separation and identification via gradient elution chromatography and LC-FTIR analysis, respectively. Such a technique should not only provide information on the chemical composition of analytes separated by chromatography, but also give the analyst insight into the thermal properties of individual components which might be useful for determining whether a certain polymer is suitable for a specific application.

1.2 Objectives

The main objective of this study was to develop a new analytical technique for the determination of thermal properties of individual polymer components in a mixture or blend directly after separation and identification by means of LC-FTIR analysis. Three well-established characterization methods were to be combined to create this technique: HPLC (more specifically, gradient elution chromatography), LC coupled to FTIR spectroscopy (LC-FTIR) and AFM.

During the first stage of the development process, gradient elution chromatography had to be coupled to FTIR spectroscopy to ensure continuous semi-on-line detection of the LC effluent. This facilitates the identification of individual components in a blend after separation by liquid chromatography.

The aim of the second stage of this study was to develop a novel hyphenated technique in which the AFM could be used as a “detector” for HPLC of macromolecules. For the purpose of coupling HPLC to AFM, the LC-FTIR interface was used. A certain modification had to be made however to allow continuous deposition of the LC-effluent onto a substrate suitable for thermal analysis by AFM. This novel technique LC-FTIR-AFM, allows the determination of thermal properties of individual components

in a polymer blend, whereas all other thermal analysis techniques yield only an average value of the thermal parameter measured.

1.3 Layout of thesis

The various chapters in this thesis will provide an understanding of the different analytical techniques used during this study, i.e., HPLC, LC-FTIR, and AFM. The thesis is divided into the following chapters:

Chapter 2: Historical overview

Key moments in the development of the three analytical techniques used during this study are discussed together with selected applications of each technique. Recognition is paid to those researchers responsible for the development of each technique.

Chapter 3: Theoretical background

The basic theoretical principles of each technique are discussed. These principles are used to explain the experimental results obtained from this study.

Chapter 4: Experimental

The experimental procedures followed during the analysis of various polymers and oligomers are provided, together with a route diagram indicating the path followed during the development of the novel technique.

Chapter 5: Results and discussion

All results obtained from this study are presented as HPLC chromatograms, Gram-Schmidt representations, IR spectra and resonance frequency plots. These results are explained and discussed by means of the theoretical principles provided in chapter 3.

Chapter 6: Summary and conclusions

A summary of the work performed during this study is provided and conclusions are formulated from the results presented in chapter 5.

1.4 References

- [1] H. Pasch, B. Trathnigg, HPLC of Polymers, Springer-Verlag, Heidelberg, Berlin, 1998.
 - [2] J. Adrian, E. Esser, G. Hellman, H. Pasch, Polym. J. **41** (2000) 2439.
 - [3] H. Pasch, K. Mequanint, J. Adrian, e-Polymers **005** (2002).
 - [4] T. Hirschfeld, Anal. Chem. **52** (1980) 279A.
 - [5] K. Grob, J. Chromatogr. **626** (1992) 25.
 - [6] R.S. Alm, R.J.P. Williams, A. Tiselius, Acta Chem. Scand. **6** (1952) 826.
 - [7] H. Pasch, Adv. Polym. Sci. **150** (2000) 1.
 - [8] K. Albert, J. Chromatogr. A **703** (1995) 123.
 - [9] W.M.A. Niessen, J. Chromatogr. A **856** (1999) 179.
 - [10] G.W. Somsen, C. Gooijer, U.A.T. Brinkman, J. Chromatogr. A **856** (1999) 213.
 - [11] J.J. Gagel, K. Biemann, Anal. Chem. **58** (1986) 2184.
 - [12] J.J. Gagel, K. Biemann, Anal. Chem. **59** (1987) 1266.
 - [13] J.J. Gagel, K. Biemann, Mikrochim. Acta **11** (1988) 185.
 - [14] D. Julthongpiput, H.-S. Ahn, A. Sidorenko, D.-I. Kim, V.V. Tsukruk, Tribol. Int. **35** (2002) 829.
 - [15] D. Hegemann, H. Brunner, C. Oehr, Nucl. Instrum. Methods Phys. Res., Sect. B **208** (2003) 281.
 - [16] K. Li, P. Wu, Z. Han, Polymer **43** (2002) 4079.
 - [17] M. Meincken, S. Graef, K. Mueller-Nedebock, R.D. Sanderson, Appl. Phys. A **74** (2002) 371.
 - [18] M. Meincken, PhD Dissertation: University of Stellenbosch; Stellenbosch, South Africa (2001).
-

Chapter 2

Historical Overview

2.1 Developments in liquid chromatography

2.1.1 Introduction

This chapter will provide an overview of the most important events in the development of liquid chromatography, and the coupling of this powerful technique to various detectors. The origin of a well-established hyphenated technique LC-FTIR is discussed, together with a number of applications. The historical overview is concluded with a brief discussion of the development of scanning probe microscopy and a few novel applications reported over the last few years.

During the first few decades after the discovery of chromatography, the three chromatographic techniques most often used were: thin layer chromatography (TLC), gas chromatography (GC) and size exclusion chromatography (SEC). Although they have been used extensively through the years, these techniques each have certain associated disadvantages. TLC was basically invented to replace paper chromatography, but its poor reproducibility has caused it to lose some of its popularity. Nowadays, it is mainly used as a test run to establish solvent systems for large-scale column chromatography or as a convenient assay tool for column eluents, using a variety of visualization techniques. GC is limited in terms of the volatility of samples. SEC, although an excellent technique for obtaining molar mass and molar mass distribution

information, cannot provide any information on the chemical composition of high molar mass molecules.

Over the past 30 years high performance liquid chromatography has become one of the most powerful analytical techniques in the chemical sciences. Even in its early stages it was evident that this technique would become one of great importance, since numerous chemical substances are either too polar or have too high a molar mass for volatilization in gas chromatography. Before 1941 gas chromatography was considered much more powerful than liquid chromatography due to its superior speed and resolution. Therefore, many small polar molecules were often derivatised for volatilization and analysis by gas chromatography. It was however subsequently realized that very polar, high molar mass molecules could not be separated and analysed in the gas phase. It all began in 1941 when Martin and Synge [1] predicted that efficient analysis of such molecules would require very small stationary phase particles and high pressure. Their prediction was later confirmed by Huber [2] in the late 1960s. In years to follow, various modes for separation in HPLC were reported, the three most important ones being the size exclusion mode (SEC), the liquid adsorption mode (LAC) and the critical mode (LC-CC). The principles of these three separation modes, as well as a detailed description of the instrumentation needed and examples of polymers typically separated by each mode, is provided by Pasch and Trathnigg in a book entitled "HPLC of polymers", published in 1998 [3]. A section on two-dimensional chromatography of complex polymer systems also forms part of this publication.

2.1.2 Gradient elution chromatography

Depending on the mobile phase composition, HPLC can be divided into isocratic and gradient elution. Polymers that are homogeneous in chemical nature and chain length, can be separated successfully by isocratic elution, where the mobile phase composition remains constant throughout the chromatographic run. It is however inadequate for the separation of complex mixtures of high molar mass polymers due to problems associated with their characteristic adsorption and solubility behaviour.

This gap in chromatography was filled by Tiselius' group in 1952, when they discovered gradient elution chromatography for the analysis of compound mixtures [4]. Whereas isocratic elution is carried out with a fixed mobile phase composition, this technique involves the continuous variation of the composition of the eluting medium during a chromatographic run, which gives rise to the so-called solvent gradient. The advantages of gradient elution chromatography are: (i) the reduction of excessive tailing which results from solute chemisorption and column overloading, (ii) increased sensitivity of strongly retained analytes, and (iii) the elimination of band-broadening associated with conventional elution chromatography.

During the 1960s, investigations by L.R. Snyder provided much of the theoretical basis upon which the theory of gradient elution relies today. He published a series of seven articles on the fundamentals of gradient elution between 1961 and 1964 [5-11], dealing with various theoretical principles such as the influence of the adsorbent and the solute structure on separation. A number of theoretical relationships for retention, bandwidth, and resolution were also investigated and formulated by him, which lead to his publication of the "linear solvent strength model" (LSS) in 1980 [12] and again in 1998 [13]. These two publications provide a detailed explanation of the theoretical principles of gradient elution, as well as some practical considerations for the optimisation of gradient systems. L.R. Snyder has therefore provided the basis for understanding gradient elution, and the theoretical principles formulated by him are used to explain the basics of gradient elution in this thesis.

2.1.2.1 The gradient former

Perhaps the most important part of the experimental gradient elution setup is the gradient former. The two basic requirements of the gradient former are: (i) to provide accurate proportioning of the gradient solvents at each point during the run, and (ii) to ensure proper solvent mixing prior to entering the column. During the early stages of gradient elution, inefficient gradient formers were often responsible for poor reproducibility and

inaccurate results. Another problem was the absence of a suitable detection method for substances that lack the presence of a chromophore. Only polymers containing UV-absorbing groups could be detected in column gradient separations. This problem was, however, solved in 1986 by Mourey [14], when he first introduced the use of evaporative light scattering detection (ELSD) for the analysis of poly(alkyl acrylate) and poly(alkyl methacrylate) homopolymers and copolymers eluted from silica with toluene-2-butanone solvent gradients. This allowed the detection of polymers that used to be difficult to detect by spectrophotometric methods, and also permitted the use of good solvents that are strongly UV absorbing. This breakthrough extended the range of application of liquid chromatography to synthetic polymers that used to be amenable only to thin-layer methods. The capabilities of evaporative light scattering detection in gradient elution have also been illustrated by Verhelst [15], when he reported on the analysis of organo-silicone copolymers. When silicone polymers are co-polymerised with a polyglycol, the resulting copolymer differs from the monomer by a single bond, which is often difficult to detect via spectroscopic methods such as NMR and IR, especially when high molar mass polymers are to be analysed.

2.1.2.2 Analysis of oligomers by gradient elution

Low molar mass polymers, or oligomers such as pre-polymers, and extracts of high polymers obtained during the first stages of polymerisation have also been successfully analysed by gradient elution, as reported by Van der Maeden in 1978 [16]. The problem with separation of oligomers is that successive components in an oligomeric mixture generally only differ slightly in chromatographic behaviour. Gradient elution offers a promising alternative for the analysis of such mixtures, since the activity of the stationary phase can be changed in such a subtle manner. Other chromatographic techniques such as thin layer (TLC), gas (GC) and size exclusion chromatography (SEC) used to be the most popular techniques for the analysis of oligomers, but gradient elution of oligomers offers greater selectivity and much more detailed information can be obtained. Although gradient elution is much more suitable for the analysis of oligomeric mixtures, a few complications were observed. Problems associated with the solubility of oligomeric

samples may cause a temporary disturbance of the phase system, leading to inferior separation. Another problem is the size-exclusion effect, which causes poor resolution of higher molar mass oligomers. The main cause of this problem is most probably the decreasing accessibility of higher molar mass polymers to the silica pores, leading to less retention and poorer separation.

A series of publications on gradient elution analysis of low molar mass polymers was published by Philipsen and co-workers from 1996 to 1997. Their main objective was to establish to what extent gradient elution could be used for providing information on the microstructure and composition of materials that cannot easily be obtained by other analytical methods such as SEC and NMR. They investigated the influence of several practical parameters such as: injection volume, gradient shape, temperature and sample loadability, on the separation of low molar mass polyester resins [17,18] and crystalline polyesters [19] in reversed-phase gradient elution. They proved that gradient elution is capable of providing detailed information on the molar mass and chemical composition of low molar mass polymers, and that optimum separation results can be obtained by adjusting practical parameters. Results of investigations into the gradient separation of polyesters were once again reported by Philipsen and co-workers in 1998 [20] and 1999 [21], when copolyesters were separated by gradient elution.

2.1.2.3 Normal-phase and reversed-phase gradient elution

Two modes of separation are generally recognised within gradient elution separations. The selection of normal-phase gradient separation (NP-GPEC), which uses a polar column and a less polar solvent/non-solvent combination, or reversed-phase gradient elution (RP-GPEC), where the solvent/non-solvent combination is more polar than the stationary phase, may play a significant role in the separation process. Normal-phase separation is usually employed for the separation of polymers on the basis of their polarity on a polar column, by making use of a gradient with increasing polarity, whereas reversed-phase systems use an apolar column and a gradient of decreasing polarity.

Although reversed-phase chromatography is preferred to normal-phase separation, due to poor reproducibility and unpredictable retention behaviour of the latter, normal-phase separation is still extremely useful for the separation of polymers according to the polarity of their side groups, thereby facilitating the separation of copolymers that used to be difficult to separate, or had very low resolution. Normal-phase separation was first introduced by Danieliwicz in 1981 [22]. Reversed-phase separation has become much more popular for the separation of a wide range of analytes, but normal-phase chromatography continues to be the method of choice for the separation of very hydrophilic compounds non-retained in reversed-phase, or of hydrophobic samples very strongly retained by reversed-phase separation. The advantages of normal-phase chromatography are: better stability of columns due to a lower pressure drop in non-aqueous mobile phases, greater possibilities of changing separation selectivity by varying mobile phase constituents, and better solubility of some samples in more hydrophobic solvents, which is especially important in preparative applications.

From 1993 to 1994, a series of publications by Glöckner and co-workers appeared, in which they described the use of sudden-transition gradients in both normal and reversed-phase separation [23-27]. Such gradients are ternary gradients that involve the sudden addition of a moderately polar solvent to control solvent strength and chromatographic power during a run. Sudden-transition gradients ensure proper retention of polymers and allow independent control of solubility and precipitation for the peak shape and signal drop between adjacent peaks to be optimised. Glöckner *et al.* have demonstrated the efficiency of sudden-transition gradients via the separation of styrene/methyl methacrylate copolymers according to chemical composition differences, in both normal-phase and reversed-phase systems. Here, the starting eluent, A, after injection and retention of the sample, was rapidly changed by addition of a solvent, C, of intermediate polarity. The dissolution power of the mixture was adjusted to a level where the sample was still retained, but elution could be performed if a strongly polar eluent, B, which need not be a solvent, was to be added. The elution sequence observed in the reversed-phase mode was opposite to that in the normal-phase mode, thereby complying with the polarity rules of chromatography. Sudden-transition gradients offer the

following advantages: (i) proper control of solubility and adsorption phenomena, (ii) optimization of separation with respect to selectivity and time, and (iii) the possibility of monitoring elution, without any disturbing effects, due to the application of an indispensable solvent at a constant concentration.

2.1.2.4 Separation according to chemical composition and critical conditions

The characterisation of copolymers requires the determination of chemical composition distribution in addition to molecular mass distribution. When appropriate experimental conditions are selected for gradient elution analysis of copolymers, separation will be based solely upon the chemical composition of copolymers, in a molar mass independent mode. Gradient elution therefore, allows the elimination of size exclusion effects due to interaction of molecules with the porous adsorbent and the minimisation of precipitation effects. In 1994 the separation of methyl methacrylate/methacrylic acid copolymers on a 100 Å pore silica column, with a toluene/methanol mobile phase mixture, was reported by Schunk [28]. It was found that the separation of PMMA-MAA copolymers on silica is predominantly due to adsorption interactions. Copolymers containing higher amounts of methyl methacrylate showed increased interaction with the column, causing excessive peak broadening and poorer results. Schunk did, however, establish that the addition of glacial acetic acid displaced the strongly adsorbed copolymers, thereby ensuring narrow peaks and smaller elution volumes. The normal and reversed-phase HPLC separation of styrene methacrylate copolymers by chemical composition was also reported by Sato [29], who also found that the influence of molecular weight diminished when adsorption effects are induced. The efficiency of gradient separation of copolymers was also demonstrated by Cools in 1996 [30], when the chemical composition distribution of copolymers of styrene and butadiene was determined.

Although gradient HPLC is predominantly used for the determination of chemical composition distribution, Cools and co-workers have also demonstrated how this technique can be used for the determination of the critical solvent composition (CSC) [31] and molar mass distribution (MMD) [32], respectively.

2.2 Hyphenation in liquid chromatography

2.2.1 The need for hyphenation in the characterisation of polymers

As research into polymer synthesis advanced and polymer chemists started to produce more complex polymers such as copolymers and structured multi-phase materials, it was realized that more sophisticated analytical methods were needed for the complete characterization of polymer systems. HPLC was therefore coupled to a number of selective detectors, in order to obtain structural information for the identification and/or confirmation of unknown chemical compounds. The combination of column liquid chromatography or capillary gas chromatography with a mass detector (LC-MS and GC-MS) is preferred for most trace level analyses nowadays, but additional and/or complementary information is often required. Such information can be obtained via atomic emission, Fourier transform infrared, diode-array UV-vis absorbance, fluorescence emission, or nuclear magnetic resonance spectrometry.

Most synthetic polymers are highly complex multi-component materials, characterized by a distribution in molar mass, chemical composition, functionality and molecular architecture. It is therefore often necessary to use a combination of different analytical techniques for the adequate characterization of synthetic polymers. In 1980 Hirschfeld [33] proposed the term “hyphenation” to describe the close relationship or marriage between two analytical techniques or devices. This does not necessarily imply on-line coupling, since in most cases suitable interfaces are required when combining two or more instruments.

Several approaches have been used for the analysis of multi-component mixtures. A comprehensive review article on the most important hyphenated techniques used for the characterisation of complex polymers was published by Pasch in 2000 [34]. This publication presents the basic principles of combining different analytical techniques, i.e., chromatography and spectroscopy in two-dimensional analysis schemes, as well as

hyphenation of liquid chromatography with various selective detectors. The techniques of GC-MS [35] and GC-FTIR [36,37] have been successfully used for the separation and identification of a variety of samples. Unfortunately, many compounds are thermally labile or not volatile enough for analysis by gas chromatography. Therefore, analysts have been forced to investigate the possibilities of coupling liquid chromatography with selective detectors such as MS, NMR and FTIR.

In polymer analysis, the use of a mass spectrometric detector is considered a valuable alternative to conventional detectors, since the absolute molar mass of polymer components can be obtained. As long as fragmentation does not occur, the measured molar mass of intact molecular ions can be related to the chemical composition and chain length of each component. The main limitation of LC-MS is that it cannot be used successfully for the detection of higher oligomers (molar mass above 2 000 to 3 000) since these analytes cannot be ionized without fragmentation.

NMR is one of the most powerful and versatile spectroscopic techniques, allowing the analyst to obtain structural information about almost any organic compound in solution, and to differentiate between isomers of different structures, conformations and optical orientations. NMR spectroscopy can usually supply the information necessary to unambiguously identify any unknown compound, and quantitative information can also be deduced from the number of contributing nuclei present in a certain area of the spectrum. Two major drawbacks of NMR are the poor sensitivity compared to that of mass spectrometry and the inability to sometimes identify compounds with overlapping NMR signals.

Separation of compounds prior to NMR analysis is therefore extremely useful in many cases, and the direct coupling of NMR to chromatographic separation is the method of choice in cases where overcrowded signals appear within a narrow chemical shift region of the NMR spectrum. On-line LC-NMR coupling was reported by Bayer in 1979 [38]. Sensitivity and resolution were however poor compared to other spectrometric techniques available at that time. The poor sensitivity of LC-NMR has precluded it from being used

for the trace analysis of drugs in bio-fluids, where LC-MS is considered a better alternative [39]. It has however, been used successfully for the characterization of drug impurities and the identification of drug metabolites [40,41].

2.2.2 LC-FTIR analysis

FT-IR detection became feasible in the 1970s and the combination of GC and FT-IR has long been a well-established analytical technique [42]. Compared to GC-FTIR, the development of LC-FTIR has proceeded more slowly. However, with the introduction of new interfacing techniques during the past decade, LC-FTIR has reached the stage where it is now considered a valuable analytical utility. This technique combines the merits of both liquid chromatography and infrared spectroscopy. Most organic compounds have highly specific absorption bands in the mid-IR spectral region, which provide a unique fingerprint for distinguishing an organic compound from others. It is therefore possible to unambiguously identify any compound on the basis of its IR spectrum, whenever reference spectra are available.

The first approach for coupling liquid chromatography to infrared detection involved the use of a flow-cell, through which the effluent from the LC column was passed while the IR spectra of components were recorded continuously. Although this method ensures on-line monitoring of the LC effluent, it has the disadvantage that most mobile phase solvents show strong absorption in many areas of the IR spectrum. During the 1970s mobile phase elimination LC-FTIR became possible. This is a more versatile approach and interference-free spectra of considerably smaller amounts of analytes can be obtained. The first two reports on the use of such an interface were published by Griffiths in 1977 [43] and by Kuehl and Griffiths in 1979 [44]. Although this technique has evolved since the early days, the general principle, which is to deposit the chromatographic eluent containing the sample components onto a moving substrate, still remains. The interfaces available today make use of thermospray [45], electrospray [46], particle beam [47], ultrasonic [48,49], or pneumatic nebulisers [50-52] to facilitate solvent evaporation.

In 1986 research into LC-FTIR interfaces was revolutionized by the invention of Gagel and Biemann [50]. The interface used by them was equipped with a nitrogen gas nebuliser that allowed the vaporization of solvents used in both isocratic and gradient reversed-phase HPLC. The solutes exiting a narrow-bore column were deposited onto a rotating reflective disc, allowing evaporation of the mobile phase solvent, followed by FTIR analysis in the sample compartment of the IR spectrometer. This interface offered adequate sensitivity, but some complications regarding aqueous solvent systems were experienced. In 1993 Lab Connections Inc. introduced the LC-Transform, a direct LC-FTIR solvent evaporation interface based on the invention of Gagel and Biemann. This interface can be used for the analysis of virtually any sample in any chromatographic system, even aqueous and fairly non-volatile solvents can be handled. A number of publications dealing with the application of this interface to polymer analysis have been published by Lab Connections Inc. They have illustrated how additives such as diluents in polyurethane systems, as well as UV stabilisers and antioxidants can be isolated and characterised by this interface [53], as well as its ability to be used in normal and reversed-phase systems [54]. They have also supplied information on the optimisation of chromatographic, spectroscopic and interface parameters for obtaining the best possible data from LC-FTIR analysis [55].

They have also proposed a solution to the problem of varying deposit characteristics observed for different polymers. Some polymers will form clear, transparent films upon deposition, while others may exhibit a powdery appearance. During solvent evaporation and deposition onto the IR-transparent substrate, spray droplets are transformed into discrete gel beads that do not anneal together in the deposit. These beads result in the scattering of IR energy during scanning, leading to a sloping spectral baseline. Usually, this does not affect the identification of compounds, and in most cases the software can be used to flatten the baseline. This may however, cause some complications for quantitative peak ratio analysis. Fortunately, a simple procedure, involving the annealing of a polymer deposit in solvent vapor, has been proposed to eliminate the granular nature of deposits [56].

2.2.3 Gradient elution chromatography coupled to FTIR detection

Reversed-phase gradient elution chromatography has been coupled to FTIR detection in only a few isolated cases, due to problems experienced with the evaporation of eluents with a changing water content. Possible solutions for this problem have been proposed by Gagel and Biemann [51]. They suggested that the temperature of the nebulisation gas should be increased gradually during a gradient run to facilitate evaporation of the mobile phase solvents. Vredendrecht [57], on the other hand, found that excess methanol could be added to the effluent of micro-LC columns to mask the changing water content. During this study, various polymer and oligomer mixtures were analysed by reversed-phase gradient elution chromatography coupled to FTIR spectroscopy, by means of the LC-Transform interface.

2.3 The development of scanning probe microscopy

2.3.1 From optical microscopy to scanning probe microscopy

Vast improvements in the resolution of microscopes have occurred since Hooke's discovery of the optical microscope in 1665. The main limitation of this microscope was the resolution that did not exceed the range of a few 100 nanometers even after the introduction of the confocal optical microscope. In 1933 the resolution of microscopes was extended to the nanometer range, with the discovery of the transmission electron microscope by Ruska, but it was only in 1981 that a breakthrough by Binnig and Rohrer allowed atomic resolution images for the first time [58].

The idea of a super-resolution microscope can be traced back to 1928 when the British scientist Synge introduced the concept of a scanning probe near-field optical microscope [59]. He suggested a design in which a tiny aperture at the end of a glass tip could be scanned over an illuminated sample surface in a raster pattern. The light transmitted

through sub-wavelength regions could then be used to construct an image of the sample surface. It was only in 1956 that his idea was re-investigated by O'Keefe [60]. Unfortunately he assumed that devices for scanning and positioning were not yet available, and therefore no further investigation was carried out. The first demonstration of a super-resolution near-field optical microscope was performed by Ash and Nicholls in 1972 [61] when they achieved resolution of 150 μm , by means of 3 cm wavelength microwave radiation.

In 1981 the field of microscopy was revolutionised by the introduction of the scanning tunneling microscope (STM) by Binnig and Rohrer [62]. They demonstrated the feasibility of controlled vacuum tunneling, by applying a tunneling current between a tungsten tip and a platinum surface separated by a distance of 10 \AA . The discovery of the scanning tunneling microscope has stimulated the development of a whole family of scanning probe microscopes (SPMs) that are capable of measuring chemical and physical properties on the nano-scale.

2.3.2 The atomic force microscope

2.3.2.1 The origin of atomic force microscopy

The atomic force microscope (AFM) is regarded by some as the most versatile member of this group of scanning probe microscopes. In 1986 Binnig and Quate introduced this new type of microscope capable of non-destructively measuring insulator surfaces on an atomic scale. A lateral and vertical resolution of 30 \AA and 1 \AA , respectively, was obtained by them. The system consisted of a cantilever beam to which the STM tip was mounted in order to measure the motion of the cantilever beam with an ultra-small mass.

The atomic force microscope was developed mainly for the purpose of studying non-conductive surfaces. The first system was operated in the repulsive mode, i.e., repulsive forces between a diamond stylus and the sample were measured as the stylus gently touched the surface. Initial designs used a tunneling sensor to detect this deflection, but

forces measured by such systems were limited to approximately 10^{-7} N. In more recent experiments, optical sensors have replaced the original tunneling sensor [63,64]. Wickramasinghe developed a new version of the force microscope which was capable of measuring van der Waals forces as small as 10^{-13} N and force gradients down to 10^{-6} N/m in the attractive mode [64]. This development makes it possible to measure micro-electronic systems in a non-destructive, non-contact mode. The force microscope has also been used in the attractive mode for novel measurements such as non-contact profiling of surfaces, magnetic imaging [65,66] and electrostatic imaging [67,68].

Soon after its development in 1986, the atomic force microscope, also known as the scanning force microscope (SFM), became famous for its ability to characterise polymer surfaces and thin films. Its first recognition was earned for its powerful and versatile imaging capabilities. Over the past decade, a number of improvements have occurred in the imaging possibilities of scanning force microscopes. It has become a technique of great importance, particularly because it can analyse surface structures in a physically relevant environment, and also in a completely non-destructive way. This is of particular importance for biological samples, since they can now be imaged *in-situ*, thereby retaining their native structure and activity during experiments. SFM has also been developed into a technique capable of visualising single macromolecules with sizes of about 5 nm, thereby enabling the characterisation of polymers according to their size, flexibility and conformation.

Over the past decade scanning force microscopy has been transformed from a simple imaging technique into a powerful tool for the determination of physical properties, and even the manipulation of nanoscale structures. In addition to its high resolution imaging capabilities, SFM offers a number of new contrast mechanisms for distinguishing between areas with different chemical and physical characteristics. Hereby, the microscopic capabilities of SFMs are extended far beyond morphological studies. Nowadays, mechanical properties such as visco-elasticity, friction, and adhesion, as well as long-ranged electrostatic and steric forces, can be characterised locally on the

nano-scale. This has been made possible through the ability of SPMs to measure forces as small as pico-Newtons and probe areas well below 100 nm.

One significant development in the use of AFM for the determination of physical properties such as the elastic modulus of polymers, was reported by Martin [69]. Resonant contact AFM was used to investigate the microstructure of various polymer blends. This technique is based on the measurement of the resonance frequency shift between the free resonance frequency and the resonance frequency of the cantilever in contact with the sample. This frequency shift is directly related to the material elastic properties. This technique has succeeded in eliminating most of the problems associated with other methods of obtaining the same information. Such techniques include force modulation and intermittent-contact mode analysis.

Resonant contact AFM is precise and very sensitive and it has been successfully applied for determining (i) the phase properties or/and (ii) the interface characteristics of several immiscible polymer blends. This technique has allowed the detection of a crosslinking agent within rubber particles consisting of a poly(butylene terephthalate)/epoxide blend. It also appears to be a promising tool for investigating the interfacial region of compatibilised and non-compatibilised polymer systems, since good correlation between the resonance frequency spectrum and the interfacial thickness was indeed obtained for a variety of polymer blends.

2.3.2.2 Polymer thin film characteristics

Polymer films have gained importance in a variety of technological applications, ranging from dielectric layers in electronic devices to protective coatings, adhesives and lubricants. Advances in the field of polymeric thin films have drawn increased attention to polymer surface properties. A number of polymer thin film phenomena have been investigated over the last few years, including thermal expansion, glass transitions, diffusion and wetting.

The characteristics of thin polymer films are known to differ considerably from those of the bulk polymer [70]. This can be ascribed to various factors such as confinement effects [71], chain conformation differences [72] and certain effects associated with both the air-polymer and the substrate-polymer interfaces dominating large areas of thin films [73,74]. The number of chain ends near the surface influences the free volume of the system, and may therefore also be responsible for fluctuations in polymer thin film properties [75,76].

2.3.2.3 The glass transition temperature

The glass transition temperature measured at the surface of ultrathin films, surfaces and confined geometries can differ by as much as tens of degrees from the bulk [70-72,77-80]. Such behaviour in the glass transition has been studied by a number of different techniques, including Brillouin light scattering (BLS) [70,71]; spectroscopic ellipsometry [74,81]; attenuated total reflection (ATR) [82]; X-ray diffraction [83,84]; modulated dynamic scanning calorimetry (MDSC) [85] and scanning force microscopy (SFM) [86]. Results of T_g measurements on nominally identical systems show large disagreements due to the complexity of polymer chains, since different length scales need to be considered when dynamic properties are to be interpreted. The length scales probed (i.e. end-to-end distances and persistence length) by different techniques are often difficult to quantify, making the comparison of results almost impossible.

The glass transition of polymer thin films is also strongly dependent on the thickness of the film [87] and the molar mass of the polymers under investigation [88]. In most cases, a decrease in the T_g of a film is observed for a decreasing film thickness and molar mass [70,71,89-91], although certain authors have reported no change [92,93] or even a slight increase in the T_g near the surface of the film [83]. A reduced T_g near the surface of a polymer film may play a significant role in adhesion [85], friction [94] and mechanical failure [95] of polymeric devices. It is therefore essential to have well-established analytical techniques to measure T_g s of surfaces accurately and reproducibly.

2.3.2.4 Thermal analysis by AFM

A number of SPM modes have been used to investigate the surface glass transition temperature in polymers. A significant lowering of the bulk T_g has been observed by friction force microscopy (FFM) [96]; shear modulation force microscopy (SMFM) [92]; and lateral force microscopy (LFM) [97,98]. These methods have all proved their potential as thermal analysis tools for polymer characterisation. However, the main disadvantage shared by all of the techniques mentioned above is that they are all in contact with the surface during thermal measurements. This may cause damage to surface and/or the tip, which might influence the results obtained.

A new technique for measuring thermal transitions by atomic force microscopy, was recently developed by Meincken *et al.* [99,100]. It involves the AFM being operated in the non-contact mode, in a way similar to the functioning of the dynamic mechanical analyser (DMA), but on a molecular scale. The term “nano-DMA” was therefore coined. This reliable and reproducible method measures individual glass transition temperatures (T_g) and melting points (T_m) of structured multi-phase materials and polymer blends [100,101]. Another advantage of this technique is the relatively short time necessary to perform one measurement. Depending on the temperature range over which the sample is probed, one T_g measurement may take less than one hour, opposed to approximately 20 hours for a similar measurement by Brillouin light scattering, and one to two days for a positron annihilation study of thermal properties.

In this method the AFM cantilever oscillates above the sample surface and the resonance frequency is measured as a function of temperature, as the sample is heated from a certain temperature below its T_g , to a certain temperature above its T_g . Therefore, this method is also referred to as the resonance frequency measurement (RFM) method. Polymer thermal transitions are clearly visible as a change in the characteristic resonance frequency behaviour of the cantilever. Conventional thermal analysis methods such as dynamic scanning calorimetry (DSC) and dynamic mechanical analysis (DMA) can only

provide an average value of a certain parameter measured for the bulk of the sample. This new method can, however, resolve the thermal transitions of individual polymers in blends and structured systems, without damaging the surface or the tip. This new technique may therefore become one of the most versatile techniques in the analysis and characterisation of nano-materials. The coupling of this technique with chromatography, may become extremely useful in future, since it allows the non-destructive determination of thermal properties of individual components in polymer blends, and structured multi-phase systems, directly after chromatographic separation and identification via FTIR spectroscopy.

2.4 References

- [1] A.J.P. Martin, R.L.M. Synge, *Biochem. J.* **35** (1941) 1358.
 - [2] J.F.K. Huber, *J. Chromatogr. Sci.* **7** (1969) 85.
 - [3] H. Pasch, B. Trathnigg, *HPLC of Polymers*, Springer-Verlag, Heidelberg, Berlin, 1998.
 - [4] R.S. Alm, R.J.P. Williams, A. Tiselius, *Acta Chem. Scand.* **6** (1952) 826.
 - [5] L.R. Snyder, *J. Chromatogr.* **5** (1961) 430.
 - [6] L.R. Snyder, *J. Chromatogr.* **6** (1961) 22.
 - [7] L.R. Snyder, *J. Chromatogr.* **8** (1962) 178.
 - [8] L.R. Snyder, *J. Chromatogr.* **8** (1962) 319.
 - [9] L.R. Snyder, *J. Chromatogr.* **11** (1963) 195.
 - [10] L.R. Snyder, *J. Chromatogr.* **12** (1963) 488.
 - [11] L.R. Snyder, *J. Chromatogr. A* **13** (1964) 415.
 - [12] L.R. Snyder, *Gradient Elution; High-Performance Liquid Chromatography: Advances and Perspectives*; **1** (1980) 207.
 - [13] L.R. Snyder, *Adv. Chromatogr.* **38** (1998) 115.
 - [14] T.H. Mourey, *J. Chromatogr. A* **357** (1986) 101.
 - [15] V. Verhelst, P. Vandereecken, *J. Chromatogr. A* **871** (2000) 269.
-

- [16] F.P.B. Van der Maeden, M.E.F. Boiemond, P.C.G.M. Janssen, *J. Chromatogr.* **149** (1978) 539.
- [17] H.J.A. Philipsen, B. Klumperman, A.L. German, *J. Chromatogr. A* **746** (1996) 211.
- [18] H.J.A. Philipsen, M.R. de Cooker, H.A. Claessens, B. Klumperman, A.L. German, *J. Chromatogr. A* **761** (1997) 147.
- [19] H.J.A. Philipsen, M. Oestreich, B. Klumperman, A.L. German, *J. Chromatogr. A* **775** (1997) 157.
- [20] H.J.A. Philipsen, H.A. Claessens, M. Bosman, *Chromatographia* **48** (1998) 623.
- [21] B. Klumperman, H.J.A. Philipsen, *J. Appl. Polym. Sci.* **72** (1999) 118.
- [22] M. Danielewicz, M. Kubin, *J. Appl. Polym. Sci.* **26** (1981) 951.
- [23] G. Glöckner, *Chromatographia* **37** (1993) 7.
- [24] G. Glöckner, D. Wolf, H. Engelhardt, *Chromatographia* **38** (1994) 559.
- [25] G. Glöckner, D. Wolf, H. Engelhardt, *Chromatographia* **38** (1994) 749.
- [26] G. Glöckner, D. Wolf, H. Engelhardt, *Chromatographia* **39** (1994) 170.
- [27] G. Glöckner, D. Wolf, H. Engelhardt, *Chromatographia* **39** (1994) 557.
- [28] T.C. Schunk, *J. Chromatogr. A* **661** (1994) 215.
- [29] H. Sato, K. Ogino, S. Matuo, M. Sasaki, *J. Polym. Sci., Part B: Polym. Phys.* **29** (1991) 1073.
- [30] P.J.C.H. Cools, F. Maesen, B. Klumperman, A.M. van Herk, A.L. German, *J. Chromatogr. A* **736** (1996) 125.
- [31] P.J.C.H. Cools, A.M. Van Herk, A.L. German, W.J. Staal, *J. Liq. Chromatogr.* **17** (1994) 3133.
- [32] B. Klumperman, P. Cools, H. Philipsen, W. Staal, *Macromol. Symp.* **110** (1996) 1.
- [33] T. Hirschfeld, *Anal. Chem.* **52** (1980) 279A.
- [34] H. Pasch, *Adv. Polym. Sci.* **150** (2000) 1.
- [35] J.F. Holland, C.G. Enke, J. Allison, J.T. Stults, J.D. Pinkston, B. Newcome, J.T. Watson, *Anal. Chem.* **57** (1983) 997A.
- [36] P.R. Griffiths, J.A. deHaseth, L.V. Azarraga, *Anal. Chem.* **55** (1983) 1361A.
-

- [37] G.T. Reedy, D.G. Ettinger, J.F. Schneider, S. Bourne, *Anal. Chem.* **57** (1985) 1602.
- [38] E. Bayer, K. Albert, M. Nieder, E. Grom, T. Keller, *J. Chromatogr.* **186** (1979) 497.
- [39] G.B. Wang, J.P. Santerre, R.S. Labow, *J. Chromatogr. B* **698** (1997) 69.
- [40] J.K. Roberts, R.J. Smith, *J. Chromatogr. A* **677** (1994) 385.
- [41] S.X. Peng, B. Borah, R.L.M. Dobson, Y.D. Liu, S. Pikul, *J. Pharm. Biomed. Anal.* **20** (1999) 75.
- [42] P. Jackson, G. Dent, D. Carter, D.J. Schofield, J.M. Chalmers, T. Visser, M. Vredenburg, *J. High Resolut. Chromatogr.* **16** (1993) 515.
- [43] P.R. Griffiths, *Appl. Spectrosc.* **31** (1977) 497.
- [44] D. Kuehl, P.R. Griffiths, *J. Chromatogr. Sci.* **17** (1979) 47.
- [45] J.A.J. Jansen, *Anal. Chem.* **337** (1990) 398.
- [46] M.W. Raynor, K.D. Bartle, B.W. Cook, *J. High. Resolut. Chromatogr.* **15** (1992) 361.
- [47] V.E. Turula, J.A. deHase, *Anal. Chem.* **68** (1996) 629.
- [48] A.H. Dekmezian, T. Morioka, C.E. Camp, *J. Polym. Sci., Part B: Polym. Phys.* **28** (1990) 1903.
- [49] G. Glöckner, J.H.M. van den Berg, N.L.J. Meijerink, T.G. Scholte, R. Koningsveld, *Macromolecules* **17** (1984) 962.
- [50] J.J. Gagel, K. Biemann, *Anal. Chem.* **58** (1986) 2184.
- [51] J.J. Gagel, K. Biemann, *Anal. Chem.* **59** (1987) 1266.
- [52] L.M. Wheeler, J.N. Willis, *Appl. Spectrosc.* **47** (1993) 1128.
- [53] Lab Connections, Application notes, AN-3.
- [54] Lab Connections, Application notes, AN-18.
- [55] Lab Connections, Application notes, AN-22.
- [56] A. Karami, S.T. Balke, T.C. Schunk, *J. Chromatogr. A* **911** (2001) 27.
- [57] T. Visser, M. Vredenburg, G.J. ten Hove, A.P.J.M. de Jong, G.W. Somsen, *Anal. Chim. Acta* **342** (1997) 151.
- [58] G. Binnig, H. Rohrer, C. Gerber, *Appl. Phys. Lett.* **40** (1981) 178.
- [59] E.H. Synge, *Phil. Mag.* **6** (1928) 356.
-

- [60] J.A. O'Keefe, *J. Opt. Soc. Am.* **46** (1956) 359.
- [61] E.A. Ash, G. Nicholls, *Nature* **237** (1972) 510.
- [62] G. Binnig, C.F. Quate, C. Gerber, E. Weibel, *Phys. Rev. Lett.* **49** (1982) 57 .
- [63] G. Meyer, N.M. Amer, *Appl. Phys. Lett.* **53** (1988) 1044.
- [64] A.J.P. Martin, C.C. Williams, H.K. Wickramasinghe, *J. Appl. Phys.* **61** (1987) 4723.
- [65] A.J.P. Martin, D. Rugar, H.K. Wickramasinghe, *Appl. Phys. Lett.* **52** (1988) 244.
- [66] D. Sarid, D. Iams, V. Weissenberger, *Opt. Lett.* **13** (1988) 1057.
- [67] J.E. Stern, B.D. Terris, H.J. Mamin, D. Rugar, *Appl. Phys. Lett.* **53** (1988) 2717.
- [68] J.J. Saenz, N. Garcia, P. Grutter, E. Meyer, H. Heinzelmann, R. Wiesendanger, L. Rosenthaler, H.R. Hidber, H.J. Guntherodt, *J. Appl. Phys.* **62** (1987) 4293.
- [69] P. Martin, S. Cuenot, B. Nysten, C. Bailly, R. Legras, in *Europolymer Congress*, Stockholm, Sweden, June 2003.
- [70] J. Keddie, R.A.L. Jones, R. Cory, *Europhys. Lett.* **27** (1994) 59.
- [71] J.A. Forrest, K. Dalnoki-Veress, J.R. Dutcher, *Phys. Rev. E: Stat. Phys.* **56** (1997) 5705.
- [72] T. Kajiyama, K. Tanaka, A. Takahara, *Macromolecules* **30** (1997) 280.
- [73] J.A. Forrest, K.J.A. Dalnoki-Veress, J.R. Stevens, J.R. Dutcher, *Phys. Rev. Lett.* **77** (1996) 2002.
- [74] G. DeMaggio, W. Frieze, D. Gidley, M. Zhu, H. Hristov, A. Yee, *Phys. Rev. E: Stat. Phys.* **78** (1997) 1524.
- [75] A.M. Mayes, *Macromolecules* **27** (1994) 3114 .
- [76] S. Affrossmann, M. Hartshorne, R. Jermone, R.A. Pethrick, S. Petitjean, M.R. Vilar, *Macromolecules* **26** (1993) 6251.
- [77] J.A. Forrest, K. Dalnoki-Veress, J.R. Dutcher, *Phys. Rev. E: Stat. Phys.* **58** (1998) 6109.
- [78] K. Tanaka, T. Kajiyama, A. Takahara, *Macromolecules* **33** (2000) 7588.
- [79] J.A. Forrest, J. Mattson, *Phys. Rev. E: Stat. Phys.* **61** (2000) R53.
- [80] T. Kerle, Z. Lin, H. Kim, P. Russell, *Macromolecules* **34** (2001) 3484.
- [81] Y.C. Jean, R. Zhang, H. Cao, J.P. Yuan, C.M. Huang, B. Nielsen, P. Asoka-Kumar, *Phys. Rev. B: Condens. Matter* **56** (1997) R8459.
-

-
- [82] O. Prucker, S. Christian, H. Bock, J. Ruehe, C. Frank, W. Knoll, *Macromol. Chem. Phys.* **199** (1998) 1435.
- [83] W.E. Wallace, J.H. van Zanten, W.L. Wu, *Phys. Rev. E: Stat. Phys.* **52** (1995) R3329.
- [84] J.H. van Zanten, W.E. Wallace, W. Wu, *Phys. Rev. B: Condens. Matter* **53** (1996) R2053.
- [85] X. Wang, W. Zhou, *Macromolecules* **35** (2002) 6747.
- [86] H. Fischer, *Macromolecules* **35** (2002) 3592.
- [87] D.S. Fryer, P.F. Nealey, J.J. de Pablo, *Macromolecules* **33** (2000) 6439.
- [88] D.S. Fryer, R.D. Peters, E.J. Kim, J.E. Tomaszewski, J.J. de Pablo, P.F. Nealy, C.C. White, W. Wu, *Macromolecules* **34** (2001) 5627.
- [89] S. Kawana, R.A.L. Jones, *Phys. Rev. E: Stat. Phys.* **63** (2001) 021501.
- [90] J.A. Forrest, K. Dalnoki-Veress, *Adv. Colloid Interface Sci.* **94** (2001) 167.
- [91] J. Mattsson, J.A. Forrest, L. Borjesson, *Phys. Rev. E: Stat. Phys.* **62** (2000) 5187.
- [92] S. Ge, W. Zhang, M. Rafailovich, J. Sokolov, C. Buenviaje, R. Buckmaster, R.M. Overney, *Phys. Rev. Lett.* **85** (2000) 2340.
- [93] Y. Liu, T.P. Russell, M.G. Samant, J. Stohr, H.R. Brown, A. Cossy-Favre, J. Diaz, *Macromolecules* **30** (1997) 7768.
- [94] T. Kajiyama, K. Tanaka, N. Satomi, A. Takahara, *Macromolecules* **31** (1998) 5150.
- [95] J.A. Forrest, R.A.L. Jones, *Polym. Surf. Interf. Thin Films* (2000) 251.
- [96] J.A. Hammerschmidt, W.L. Gladfelter, *Macromolecules* **32** (1999) 3360 .
- [97] K. Tanaka, A. Taura, S.R. Ge, A. Takahara, T. Kajiyama, *Macromolecules* **29** (1996) 3040.
- [98] F. Dinelli, C. Buenviaje, R.M. Overney, *J. Chem. Phys.* **113** (2000) 2043.
- [99] M. Meincken, PhD Dissertation: Stellenbosch; University of Stellenbosch, South Africa (2001).
- [100] M. Meincken, S. Graef, K. Mueller-Nedebock, R.D. Sanderson, *Appl. Phys. A* **74** (2002) 371.
- [101] M. Meincken, L.J. Balk, R.D. Sanderson, *Macromol. Mater. Eng.* **286** (2001) 412.
-

Chapter 3

Theoretical Background

3.1 Gradient polymer elution chromatography

The discussion on the theory of gradient elution high performance liquid chromatography contained within section 3.1 of this chapter, is based on work done by Snyder from 1964 to 1998 [1-3].

Based on the composition of the mobile phase, liquid chromatography can be divided into two groups of applications, i.e. isocratic and gradient elution. In most chromatographic applications the general conditions of separation are not intentionally changed between injection of the sample and completion of the elution process. In the isocratic separation regime the composition of the mobile phase as well as the elution power of the solvent remains constant during the entire separation process. Gradient elution on the other hand, is characterised by the intentional variation of the mobile phase composition, either continuously or stepwise, so as to ensure a continuous increase in the solvent strength during the chromatographic run. In this case, separation is influenced by sorption (the combination of adsorption and partition), solubility, and size exclusion. These factors, in turn, depend on the molar mass and chemical composition of the sample components.

Gradient elution was developed for the purpose of eliminating problems experienced in isocratic elution. Isocratic elution is ineffective for samples that contain many compounds of different retention values, i.e., a wide range of k' (capacity factor) values. This is known as the general elution problem, which causes early-eluting bands to have

retention times, t_R , near the column dead volume, t_0 , which causes poor resolution. Later-eluting bands may have inconveniently large t_R values, causing unnecessary long separation times, as well as band broadening. Excessive tailing, due to column overloading or solute chemi-sorption, may also cause problems in some cases.

Gradient elution offers much better resolution of early-eluting bands, while later-eluting bands have smaller t_R values, thereby eliminating excessive tailing and band broadening. Gradient elution is also preferred in cases where later-eluting components are present in a much smaller concentration than early-eluting interferences, even when isocratic separation of the group of later-eluting compounds is possible. The column can often be overloaded by a large concentration of early-eluting bands, causing later bands of interest to overlap and tail. In most cases, gradient elution may be used instead, to eliminate this problem. Another problem associated with isocratic elution is that later eluting peaks may adsorb irreversibly onto the column, thereby interfering with the analysis of successive samples. This may also cause deactivation and inefficiency of the column. To solve this problem, continuous application of a stronger solvent towards the end of separation in gradient elution will result in the strongly adsorbed components being desorbed and removed from the column prior to the next injection.

Since separation in gradient elution is facilitated by changes in the mobile phase composition, factors such as the solvent gradient or program, the nature of the solvents used, the gradient shape and steepness and a number of other variables need to be understood in order to obtain a clear understanding of gradient elution as a whole. The effect of these factors on the gradient elution process will now be discussed in detail.

3.1.1 The solvent gradient or program

The solvent gradient or program describes the manner in which the mobile phase composition is changed during the elution process and is considered the most important aspect of any gradient separation. Generally a two-solvent gradient, consisting of a weak solvent A and a strong solvent B, is employed and the composition is varied linearly from

pure A to pure B during the gradient time, t_G . The solvent gradient or program may not be the only variable affecting separation. Factors such as the nature of the solvents, the gradient shape and the steepness of the gradient, will also affect the separation process. The effect of these factors will now be discussed in more detail.

3.1.1.1 The nature of solvents A and B

The two basic requirements to which gradient elution solvents should adhere are: (i) solvent B should be a chromatographically stronger solvent than A, and (ii) they need to be miscible over the entire solvent composition range employed during the separation process.

Although binary gradients usually ensure adequate separation of most samples, ternary gradients are necessary in particular cases. The three solvents can be mixed in different ways, as long as the solvent strength of the mobile phase is increased towards the end of the elution process. After the introduction of a mixture of two weak solvents at the start of the gradient, a strong solvent might be added straight away, or a solvent of intermediate strength can first be introduced before the final, stronger solvent is added. Where a binary gradient is present, the composition of the mobile phase usually changes directly from a weak solvent to a stronger solvent. Typical solvent systems are illustrated by the following scheme:

100% (solvent A)	→	100% (solvent B)		
X% A / Y% C	→	100% (solvent C)		
X% A / Y% B	→	100% B	→	100% C
where:		A = weak solvent		
		B = intermediate solvent		
		C = strong solvent		
and:		X + Y = 100%		

Scheme 3.1: Different solvent systems in binary and ternary gradients.

The values of X and Y refer to the volume fraction of each of the solvents in the mixture, and should be selected according to the separation process in question.

3.1.1.2 Gradient steepness

The gradient steepness ϕ' , refers to the rate at which the solvent composition is changed as a function of time (in minutes) and is expressed by the following equation:

$$\phi' = (\text{change in volume fraction B}) / \text{time} \quad (3.1)$$

Where the mobile phase composition is changed from pure A to pure B, the following relationship holds, where t_G is the gradient time, i.e., time from start to end of gradient:

$$\phi' = 1 / t_G \text{ (min}^{-1}\text{)} \quad (3.2)$$

Gradient steepness can also be expressed differently in the following, more fundamental way, where t_0 is the column dead time:

$$\phi'' = (\text{change in volume fraction B}) / (t / t_0) \quad (3.3)$$

$$= \phi' t_0 = t / t_G \quad (3.4)$$

3.1.1.3 Gradient shape

A simple linear gradient (figure 3.1(a)) is often adequate for separation of most samples. Different gradient shapes should however be evaluated to ensure the most effective separation of a certain sample. The gradient may even be concave (figure 3.1(b)) or convex (figure 3.1(c)), depending on the nature of the components to be separated.

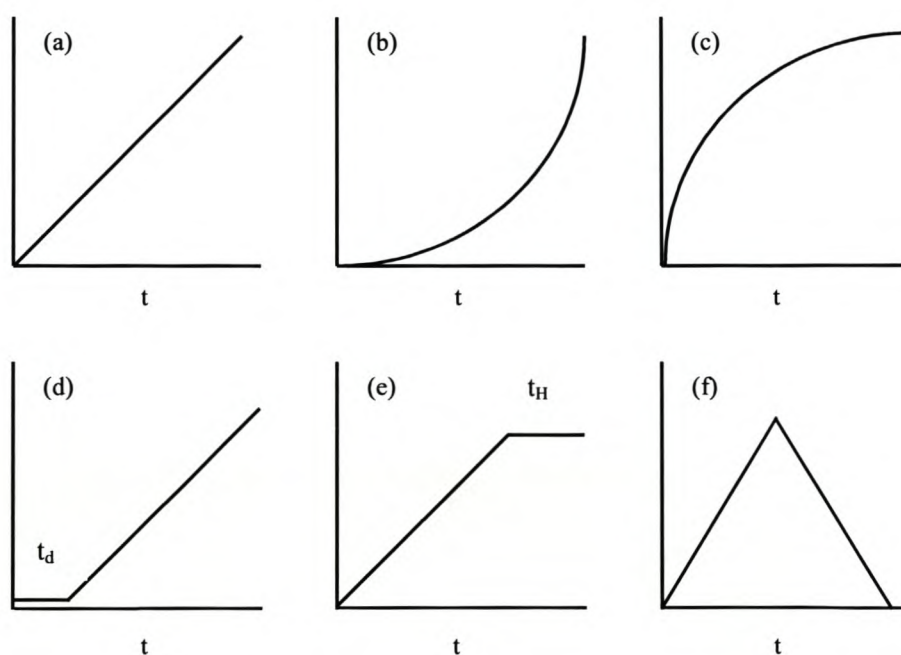


Figure 3.1: Illustration of a number of solvent gradients of various shapes [2].

As far as gradient shapes are concerned, three important terms need to be introduced, i.e., gradient delay, gradient hold and gradient reversal. Gradient delay occurs at the beginning of elution, when solvent A is applied for a certain time, t_d , before the actual gradient is started, as indicated by the initial plateau in figure 3.1(d). Gradient hold is illustrated in figure 3.1(e), where elution is continued with pure solvent B for a certain time, t_H , after completion of the gradient. Gradient reversal is a very important step in

any gradient elution process, since it restores the original column conditions before the next injection (figure 3.1(f)). This process is also referred to as column regeneration.

3.1.2 The separation process

As stated previously, one of the main disadvantages of isocratic elution is band broadening and loss of sensitivity of later eluting bands. In gradient elution this problem is usually eliminated, as explained in figure 3.2, which represents the elution of more strongly retained bands in gradient elution.

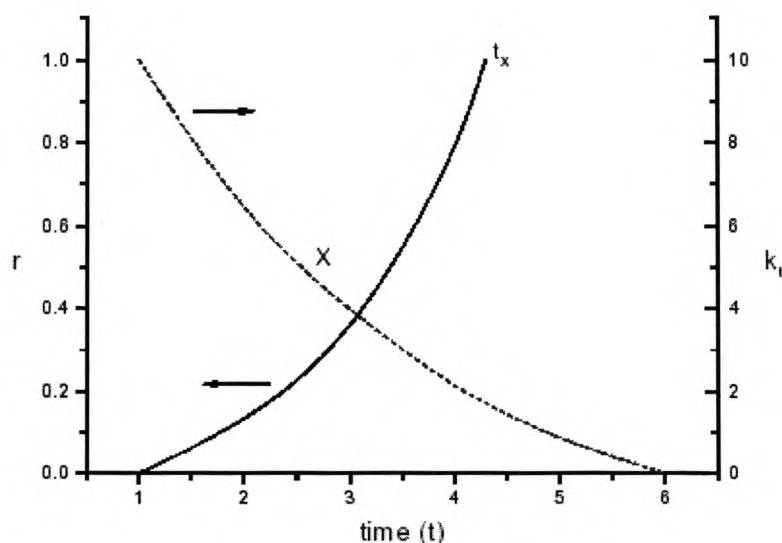


Figure 3.2: (—) The fractional migration (r) of a band of compound X along the column as a function of time; and (-----) the band k' value as a function of time (instantaneous value k_t) [2].

Consider a compound X with a large capacity factor value ($k' > 10$), which is characteristic of later eluting bands in gradient elution. The solid line in figure 3.2 represents the fractional position of a band within the column as a function of time, t , after injection. This curve therefore represents the position of a band, r , which is the fractional distance between the column inlet and outlet. The dashed curve represents the k' value (capacity factor) of a band within the column as a function of t . Since the

strength of the mobile phase is increased during gradient separation, a decrease in the k' value of this band is observed.

As far as the solid curve for the migration of the band is concerned, it is clear that at some time t_x , X will start its migration along the column. Migration of compound X indicates that the k' value of compound X has been decreased to $k' < 10$. Prior to this point, the large initial value of k_x is responsible for the retention of X near the column inlet. As the strength of the mobile phase continues to increase with time, k_x continues to decrease further, causing it to move more rapidly along the column, as illustrated by the curve of r as a function of time. At $r = 1$ the band will exit the column at its gradient retention time $t_G = t_X$.

As compound X migrates along the column, its k_x values decrease mainly in the range $1 < k_x < 10$, thereby indicating that the average k' value (k) of X during migration is adequate for good resolution from adjacent bands, as is the case in isocratic separation.

The resolution R_s , in isocratic elution is given as

$$R_s = \left(\frac{1}{4}\right)(\alpha_i - 1)N^{\frac{1}{2}}[k'/(1 + k')] \quad (3.5)$$

where α_i is the isocratic separation factor for two adjacent solute bands, which is expressed by the ratio of their retention factors, and N is the column plate number, which can be considered a constant for a given separation.

Maximum resolution is obtained when $k' \geq 2$. The baseline bandwidth, w , is given as

$$w = \left(4/N^{\frac{1}{2}}\right)t_0(1 + k') \quad (3.6)$$

From equations 3.5 and 3.6 it is evident that a small k' will ensure a narrow bandwidth. In gradient elution the capacity factor, k' , decreases as the eluent strength increases, which indicates that the widths of eluting bands will be much narrower than those in isocratic elution where k' increases towards the end of elution.

3.1.2.1 Effect of specific solvents A and B on separation

Gradient elution is characterised by the presence of a weak solvent A at the beginning of the elution process, followed by the addition of a strong solvent B towards the end of the gradient, where A is a non-solvent and B a solvent for a specific sample. To be able to understand the influence of solvents and non-solvents of different strengths on separation in gradient elution, we first need to understand what is meant by the terms strong and weak solvent, as well as strong and weak non-solvent. A strong solvent will solubilise a certain compound to a high degree, which necessitates the addition of a larger amount of non-solvent for precipitation to occur. A weak solvent will cause a lower degree of solubilisation for the compound in question, thereby making it possible to precipitate the compound through the addition of a relatively small amount of the non-solvent. A strong non-solvent by volume added, precipitates the compound to a larger degree than a weak non-solvent, with the additional result that a larger amount of solvent needs to be added for solubilisation of the compound. The choice of both the A and B solvents is a very important consideration in the design and improvement of any gradient separation, due to their significant influence on resolution and bandwidth.

If the A solvent is too strong or the B solvent too weak, separation will be of poor quality, with all elution bands appearing close to the end of the chromatogram. If the A solvent is too weak and the B solvent too strong, all of the sample bands will appear at the beginning of the chromatogram and separation time will be wasted.

If the strengths of the A and B solvents are too dissimilar, bunching of peaks in the middle of the chromatogram may occur as a result of solvent de-mixing. To obtain satisfactory results from gradient separation it is therefore extremely important to choose

the appropriate A and B solvents for each separation. Preferably, solvents A and B should both be of moderate strength for optimal separation performance.

3.1.2.2 Effect of gradient steepness on separation

The steepness of the applied gradient is defined as the rate at which the mobile phase composition changes as a function of time. If a gradient changes at 5%/min then the mobile phase composition will change from 0% to 100% B solvent in 20 minutes, ($t_G = 20$ min), which is also the approximate time required for the separation. If this gradient is slowed down to 2%/min, the gradient time will increase to 50 minutes ($t_G = 50$ min), resulting in a decrease in the gradient steepness.

A decrease in the gradient steepness may lead to the following changes: (i) band broadening and loss of sensitivity; (ii) better resolution, and (iii) longer separation times. It can be stated that a certain analogy exists between isocratic k' values and gradient steepness, as measured by the gradient time, t_G . An increase in t_G (decrease in gradient steepness) has a similar effect on separation in gradient elution as does an increase in k' values in isocratic elution. A certain intermediate gradient steepness therefore needs to be selected in order to find a compromise between sensitivity, resolution and time, which will ensure optimal results.

3.1.2.3 Effect of gradient shape on separation

A number of different gradient shapes have already been illustrated in figure 3.1. The influence of gradient shape on separation will now be discussed by using a convex (figure 3.3(a)), concave (figure 3.3(c)), and linear gradient (figure 3.3(b)). For the purpose of this illustration we shall assume that ideal separation is obtained when a linear gradient is applied, as illustrated by figure 3.3(b). If this gradient is changed to a more convex shape, it is obvious that the gradient steepness will increase at the beginning of the elution process and decrease toward the end. The effect of the increased convexity of this gradient is illustrated by figure 3.3(a), where it can be seen that the increase in

steepness at the beginning of separation causes a decrease in bandwidths and a loss of resolution for early eluting compounds. Also, the decreased steepness or flattening at the end of separation leads to an increase in bandwidth and better resolution of later eluting bands.

If however, the linear gradient is changed to a more concave shape, in which case the gradient steepness will decrease near the start and increase towards the end, the opposite effects can be observed, as illustrated by figure 3.3(c). Although linear gradients are usually adequate for separation of most samples, the application of a convex or concave gradient can be used to increase resolution or decrease bandwidth in some parts of the chromatogram.

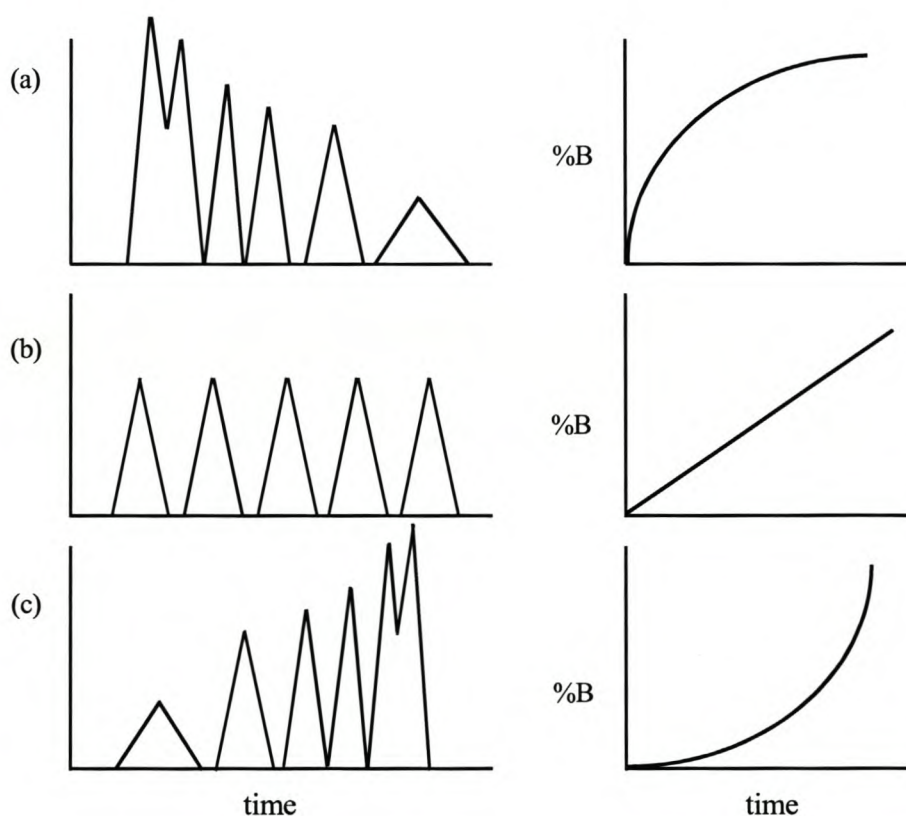


Figure 3.3: The effect of gradient shape on the peak profile appearance of the chromatogram [2]. The graphs on the left are typical peak profiles of a schematic chromatogram, while those on the right illustrate the gradient shapes responsible for each peak profile.

3.1.3 Other factors affecting separation in gradient elution

3.1.3.1 Solvent degassing

When two solvents are mixed in gradient elution, problems may arise due to dissolved gas contained in the solvents. LC solvents are usually saturated by air from the atmosphere and, because of different solubility limits, become supersaturated with respect to a specific gas when they are mixed. In high-pressure gradient systems these problems are less important. In low-pressure gradient systems, however, air bubbles can be pulled into the pump, causing interference with the accurate delivery of the pump during each pump stroke. Three approaches can be used for degassing solvents: (i) the A and B solvents may be degassed under vacuum before they are mixed within the system; (ii) on-line degassing of solvents, and (iii) helium sparging of the initial A and B solvents. Helium sparging involves the displacement of air in the initial solvents with helium, thereby saturating both solvents with helium. Since helium has a very low solubility in all solvents, spontaneous degassing of helium upon mixing of two helium-saturated solvents is not likely to occur.

3.1.3.2 Baseline stability

Baseline irregularities in gradient elution are mainly caused by the presence of impurities and dissolved oxygen in the initial solvents. The presence of dissolved oxygen is usually detected by its strong absorbance at wavelengths below 260 nm, especially near 200 nm. The interference of impurities can be eliminated by the use of HPLC-grade organic solvents and de-ionised water, whereas solvent degassing or helium sparging could eliminate baseline drift caused by dissolved oxygen.

3.1.3.3 Column regeneration

After each separation in gradient elution, the original column conditions need to be restored before the next sample is injected. This can either be done by passing a sufficient volume of solvent A through the column at the end of the first analysis, or by applying a reverse gradient from the B solvent to the A solvent and keeping the mobile phase composition as pure A for a few minutes before the next injection. A certain minimum volume, as opposed to a minimum time, of the original A solvent is required for column regeneration. The regeneration time can be decreased considerably by applying a higher mobile phase flow rate.

3.1.3.4 Sampling effects

In isocratic elution the sample is usually dissolved in the mobile phase or any weaker solvent and the injection volume should be smaller than one third of the volume of the first eluted band of interest. In gradient elution the sample should also be dissolved in the A solvent or any other weaker solvent but much larger volumes can be tolerated, especially if the bands of interest appear close to the end of separation. The sample is then concentrated at the head of the column due to it being washed onto the column by the weak A solvent.

3.1.4 Normal-phase and reversed-phase separation in gradient elution

Gradient polymer elution chromatography (GPEC) or gradient HPLC [4] separates polymers by a complex series of mechanisms. It relies on the complete retention of the sample, or at least part of it, at the initial experimental conditions, followed by its gradual elution due to the application of a solvent gradient. The separation and elution of each polymer fraction in the gradient is determined by its molar mass and chemical composition. The separation of high molar mass copolymers will be governed almost exclusively by differences in chemical composition, whereas a combination of molar mass and chemical composition effects will be responsible for separation of low molar

mass components. The choice of normal-phase GPEC, which uses a polar stationary phase and a less polar mobile phase, or reversed-phase GPEC, where an apolar stationary phase and a more polar solvent/non-solvent combination is used, plays a decisive role in the mechanism of separation [5].

3.1.4.1 The precipitation-redissolution mechanism in reversed-phase separation

In reversed-phase gradient separation, the stationary phases most often used are modified silica materials such as C18-silica materials. Generally, depending on the nature of the sample, polar solvents or non-solvents such as water or methanol are used as a mobile phase eluent at the beginning of the gradient [5]. The presence of the non-solvents at the start of the elution process causes the precipitation of the sample, or at least part of it, which leads to retention of polymer components at the head of the column (figure 3.4(a)). The solvent gradient is then started by the addition of a strong solvent in increasing amounts. Each polymer component will redissolve at a specific solvent/non-solvent composition, determined by its molar mass and chemical composition. If the mobile phase is strong enough to exclude adsorption interaction between polymers and the stationary phase, each polymer will elute in a specific solvent/non-solvent composition, corresponding to its cloud-point. The cloud-point is the solvent/non-solvent composition at which the first turbidity occurs during the titration of a polymer solution with the non-solvent [6]. The polymer component that dissolves more easily in the particular solvent mixture will elute first (sample 1 in figure 3.4(b)).

As the gradient progresses and the solvent strength continue to increase, the second polymer (sample 2) will also redissolve and elute according to its molar mass and chemical composition (figure 3.4(c)). It is therefore clear that sample 1 redissolves at a low solvent fraction and sample 2 at a high solvent fraction. As a consequence,

heterogeneous polymer samples can be separated according to differences in solubility.

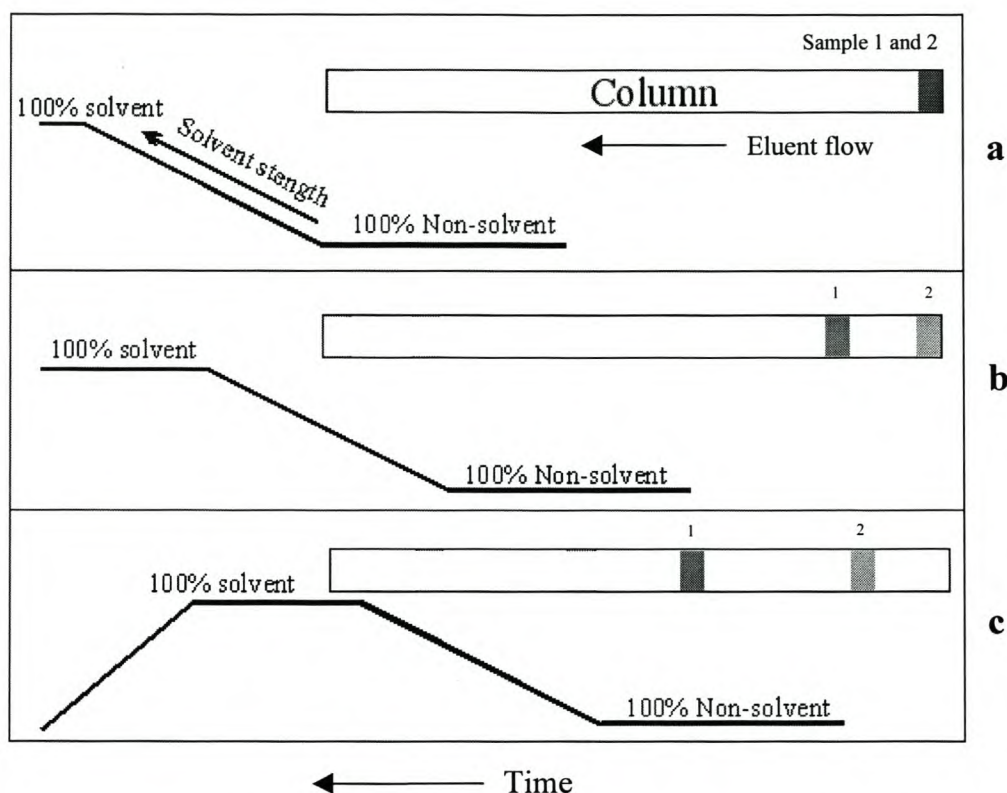


Figure 3.4: Schematic representation of three different stages a, b, and c in the precipitation-redissolution mechanism of gradient elution [7].

In reversed-phase gradient elution, weak van der Waals interactions are present between polymers and the stationary phase packing material. Since no strong adsorptive interactions are present, separation in reversed-phase mode is predominated by the precipitation-redissolution mechanism described here [5,8].

It should be mentioned that separation in such a system could also be governed by differences in molar mass. In a certain solvent/non-solvent mixture, low MM polymers will dissolve before higher MM components, and therefore elute first [9,10]. This phenomenon will now be explained in detail.

When a dissolved polymer is injected into the column it will precipitate, as it finds itself within the high % non-solvent region of figure 3.5. In this region, high molar mass

polymers will have higher retention times (RT) due to their lower solubility compared to lower molar mass molecules. As the solvent strength is increased, the polymer will enter the exclusion region, where size exclusion effects predominate. In this region high molar mass polymers will have decreased retention times since they are excluded from the pores of the stationary phase packing material. Low molar mass molecules that are able to move into the pores of the stationary phase will increase their retention time through spending time within the pores.

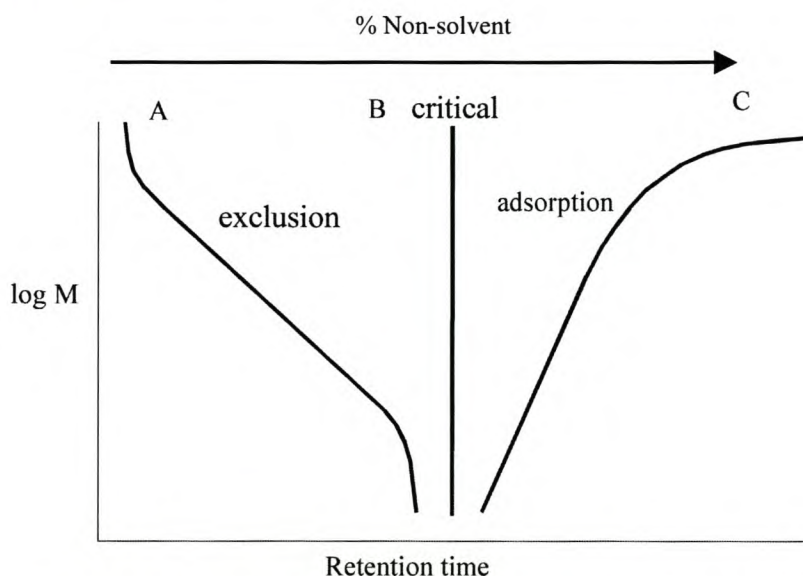


Figure 3.5: The relationship between log M and retention time (RT) for separation in gradient HPLC [11].

The following model by Glöckner [12] describes the gradient separation process when high molar mass polymers are introduced into a small pore size stationary phase such as a C₁₈ column. This model assumes that all molecules in the system are excluded completely from the pores of the packing material. Only the interstitial volume, V_I , can be accessed by any polymer molecule. The linear velocity, U_p , of a polymer in the interstitial volume is given by:

$$U_p = \frac{L}{V_I / F_{rate}} \quad (3.7)$$

where L is the length of the column and F_{rate} is the mobile phase flow rate.

The eluent, however, has access to the pore volume of the packing material, V_P , as well as the interstitial volume. The total volume accessible to the eluent is therefore given by the following:

$$V_{mob} = V_I + V_P \quad (3.8)$$

From this, the linear velocity of the eluent can be expressed as:

$$U_E = \frac{L}{V_{mob} / F_{rate}} = \frac{L}{(V_I + V_P) / F_{rate}} \quad (3.9)$$

It is therefore clear that $V_{mob} > V_I$, which implies that the velocity of the eluent is smaller than that of the polymer. The polymer bypasses the packing material and overtakes the eluent front where it reaches the mobile phase composition that favours precipitation of the polymer. The polymer is retained on the stationary phase packing material until the solvent strength is sufficient for re-dissolution. This model represents the precipitation-redissolution mechanism of gradient elution, where a molecule is precipitated in the column by passing the eluent front wherein it is dissolved and entering a poor solvent ahead of the front. In the same system, low molar mass polymers that are capable of migrating into the pores of the stationary phase will have increased retention times.

3.1.5 Normal-phase gradient elution

In normal-phase GPEC a polar stationary phase such as unmodified silica, diol-functionalised silica, or amino-modified silica is used [5]. The normal-phase regime is therefore characterised by the presence of very strong and specific interactions between polymers and the stationary phase. These hydrogen bonding and dipole-dipole interactions are much stronger and much more specific than the weak van der Waals forces present in reversed-phase gradient elution. One advantage is that weak

non-solvents can be used in normal-phase GPEC. If experimental conditions are chosen to prevent any precipitation of molecules, retention will be governed only by adsorption of solutes to the stationary phase. Molar-mass dependency of the gradient process is minimized by the reduction of precipitation effects. Hence, separation will mainly be based on chemical composition [5].

3.1.5.1 The adsorption mechanism

Adsorption in liquid chromatography is based on the retention of solute molecules by surface adsorption due to interaction with the polar groups on the surface of the stationary phase. The interaction between flexible macromolecules in solution and the column packing material depends on the magnitude of the adsorption energy. During the first step of adsorption, a part of the polymer chain binds to the active groups of the stationary phase. If the adsorption energy per unit is too low, the polymer chain will be repulsed from the surface. When the adsorption energy exceeds a certain limit, the polymer chain will be adsorbed to the surface. The adsorption of a polymer to the stationary phase is always associated with a decrease in entropy of the system, since the polymer chains need to change from their three-dimensional coil structure into a two-dimensional structure that is thermodynamically less favourable for the system. If the change in adsorption enthalpy (ΔH) is higher than the entropy losses due to conformational changes of molecules (ΔS), all repeat units of a molecule will adsorb to the stationary phase. A polymer chain is retained on the stationary phase as long as one or more of its repeat units are adsorbed. A chain can only start migrating through the column when all of its units are in the mobile phase. It can be said that separation, in this case, takes place according to an adsorption/desorption mechanism [13].

3.1.5.2 Effect of eluent strength

The strength of the mobile phase eluent plays a significant role in the retention of polymers during the adsorption process. When a weak solvent is present, the adsorbed polymer molecules can be retained indefinitely, due to the inability of the solvent to

facilitate desorption. An increase in the eluent strength may, however, prevent any retention of the polymer molecule, causing it to exit the column at the column dead volume, V_o . This behaviour is a consequence of the multiple attachment behaviour of polymers. All of the repeat units in a synthetic polymer have the chance of becoming adsorbed to the stationary phase. The magnitude of interaction with the stationary phase is considered as the sum of all the interactions of individual units, therefore, the mobility of the polymer molecule is a function of the probabilities of all repeat units and the chain length. Where weak eluents or extremely long polymer chains are present, the polymer molecule will be retained for a very long time, since at least one repeat unit will always be adsorbed to the packing material.

The solvent strength is clearly a very important consideration in the adsorption process. To ensure separation of molecules, the solvent needs to be strong enough to promote desorption of molecules from the stationary phase. The solvent strength should, on the other hand, not be too strong, otherwise an adequate adsorption-desorption equilibrium cannot be established. In order to establish appropriate solvent strengths, mixtures of different solvents are used as eluents. The strength of a solvent mixture can therefore be adjusted by changing the ratio of the components in the mixture.

3.1.5.3 Effect of solubility

Solubility usually requires a negative change in the Gibbs free energy of mixing. For low molar mass solutes this is easily obtained, due to the large entropy contribution. Here, the entropy term, $T\Delta S_m$, is so large that even positive ΔH_m values cannot prevent dissolution. The solubility of macromolecules differs from low molar mass compounds due to the following factors: (i) macromolecules have a lower order in the solid state (small entropy term), (ii) the regular arrangement of repeat units along a polymer chain remains on dissolution, and (iii) in solutions of equal weight concentrations the number of solute particles is much greater for low molar mass systems. This leads to a small ΔG_m contribution and, since the Gibbs free energy of mixing should be negative, a negative enthalpy change ($\Delta H_m < 0$) is required. As a result, the solubility parameter of

the solvent should be similar to that of the polymer. Since adsorption is an exothermic process, one expects a decrease in adsorption with an increase in temperature. For macromolecules, however, this does not apply, since at higher temperatures a thermodynamically less favourable configuration may result, which can in certain cases lead to an increase in the amount of sites capable of undergoing adsorption to the stationary phase.

3.2 Liquid chromatography-Fourier transform infrared spectroscopy

Most organic compounds have a large number of highly specific absorption bands in the mid-infrared (IR) region, which can be used to obtain detailed information on their chemical structure. The IR spectrum of any organic compound provides a unique fingerprint, which can readily be distinguished from the absorption patterns of other compounds. IR spectrometry therefore allows the identification of most compounds where reference spectra are available, making it a powerful technique for the characterisation of chromatographic peaks [14]. The need for analytical techniques that provide confirmation and/or identification of individual sample components, has led to extensive research into the coupling of liquid chromatography with infrared spectroscopy. This coupling is unfortunately not a simple task, due to the interfering absorbance of the LC mobile phase in most regions of the IR spectrum. Therefore, rather sophisticated interfaces are needed for LC-FTIR analysis.

Two approaches for the coupling of LC and FTIR are currently available. The first and simpler approach uses a flow cell through which the LC mobile phase is passed after chromatographic separation, while the IR absorbance of the eluent is recorded continuously. The second approach involves the use of an interface that eliminates the LC solvent and deposits the analytes onto a substrate suitable for IR analysis. Both these approaches have their characteristic advantages, as will be pointed out in sections 3.2.1 and 3.2.2.

3.2.1 Flow-cell LC-FTIR

The simplest way to couple LC to FTIR is to direct the column effluent through a flow cell with transparent windows, while monitoring the IR transmission of the LC eluent continuously [15-17]. Spectral information is collected and stored during the entire chromatographic run, after which IR spectra are computed and the eluent absorption subtracted. The interfering absorption of IR radiation by the LC eluent can cause a number of significant problems in the flow-cell approach. Firstly, depending on the absorption window provided by the eluent, intense absorption by the LC mobile phase may obscure analyte absorption bands and limit the spectral information that can be obtained. Secondly, the flow-cell approach cannot be used in gradient analysis, since accurate spectral subtraction is almost impossible when the eluent composition is continuously changed. Thirdly, a reduction in the signal-to-noise ratio is observed at any wavelength where appreciable solvent absorption occurs and, finally, the path length of the flow cell has to be limited to ensure that sufficient energy reaches the detector. The sensitivity and applicability of flow-cell LC-FTIR is therefore limited, but it can still be used for on-line detection of major constituents in sample mixtures. Solvent-elimination techniques are considered more versatile, and display better sensitivity when interference-free spectra from very small amounts of analytes need to be obtained. Therefore, if the objective of LC-FTIR is to identify low-level constituents of complex mixtures, semi on-line coupling using a solvent-elimination interface is generally preferred.

3.2.2 Solvent-elimination LC-FTIR

This approach involves the elimination of the mobile phase solvent prior to IR measurement. Solvent-elimination interfaces [18-21] deposit individual compounds onto an IR-compatible substrate for IR analysis after evaporation of the LC eluent. This allows interference-free FTIR spectra of deposited analytes to be recorded independent from the LC conditions. The detectability of deposited analytes can be enhanced by precise control of the interface parameters such as the rate of deposition. The deposition

step can also be repeated on the same substrate to ensure higher concentrations of low-level constituents. Chromatograms can also be stored and analysed without any time constraints. This allows for signal averaging to be performed in order to obtain better resolution of previously recorded IR spectra.

A variety of different spray-type interfaces are commercially available to suit the nature of different samples and chromatographic systems. They are classified according to the method of solvent elimination employed. The most commonly used spray-type interfaces include thermo and electrospray interfaces [22], pneumatic nebulisers [23,24], and ultrasonic nebulisers [25-27]. One example of such a commercial interface is the LC-Transform introduced by Lab Connections Inc. (Lab Connections, Inc., Marlborough, MA.) [24]. It is a direct HPLC/FTIR solvent evaporation interface based on the invention of Gagel and Biemann [18,23,28]. This was the interface used for coupling LC to FTIR during this study. It is equipped with an ultrasonic nebuliser, which transforms the LC eluent into a spray by means of a transducer that vibrates at ultrasonic frequencies. These vibrations cause the solvent to break up into small desolvating droplets that are directed onto the IR-transparent collection disc. A more detailed discussion of the design and functioning of this interface can be found in section 4.3.2 of the experimental chapter.

3.3 Scanning probe microscopy

Developments in the field of nano-technology and thin films have set new demands on chemistry and characterisation techniques. Progress in nano-technology undoubtedly depends on improvements and new developments in microscopy. Compared to other methods of characterisation used to explore the relation between macromolecular structure and macroscopic properties of polymers, microscopic techniques often supply the most direct information. Visualisation of the surface structure of polymer systems, especially heterogeneous systems, by microscopic techniques, is often more useful than indirect measurement and interpretation of scattering properties.

In earlier days scanning probe microscopy was mainly used for the topographical imaging of sample surfaces. This allowed for information such as surface roughness, particle size, form and structure to be obtained. Over the past decade, there had been a number of remarkable developments in scanning probe microscopy, which have transformed this simple, yet powerful imaging technique into a versatile tool for measuring a variety of different physical properties.

During this study the atomic force microscope was operated in the probing mode for the measurement of thermal properties of individual polymer phases in mixtures. No imaging of polymer samples was performed, therefore little attention was paid to features relevant only to the imaging mode. The following section consists of a brief introduction into the system operation of a typical scanning probe microscope, followed by a detailed discussion of the technique used to determine the thermal properties of individual components in polymer mixtures or blends.

3.3.1 System operation and signal detection

Scanning probe microscopy is the term used for all microscopes where a sharp probe (e.g. tip, optical fiber, pipette) is scanned across a sample surface in order to detect the interaction between the surface and the probe at each point on the sample. The general concept of scanning probe microscopy is illustrated by the following figure [29].

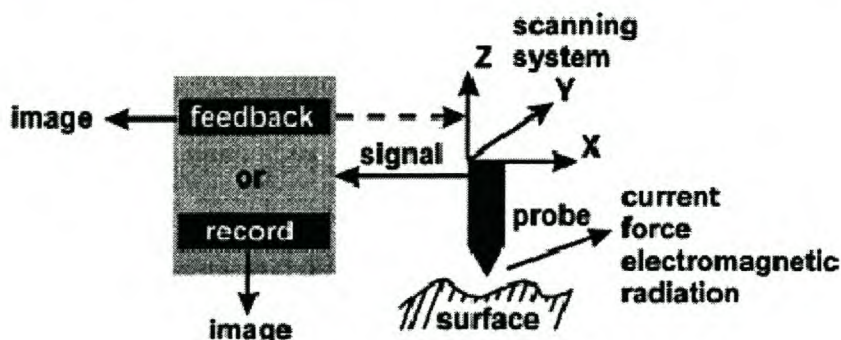


Figure 3.6: Illustration of the general design principle of all SPMs [29].

The following components can be identified as common features of all scanning probe microscopes [29]:

- A sharp probe
- Piezoelectric translator, which moves the probe relative to the sample
- Detection system for the signal sensed by the probe
- Feedback system to keep the signal constant via, height re-adjustment of the probe
- Imaging system for presenting a three-dimensional image of the scanned surface.

Two piezoelectric translators allow the probe to scan the surface in the x,y-direction, while a piezo in the z-direction controls the distance between the probe and the sample. The probe is mounted onto a metal cantilever with a low force constant. As the probe moves across the sample surface during a scan, any change in the attractive or repulsive forces between the probe and the sample will cause the cantilever to bend. A laser beam focused on the back of the cantilever is reflected by its mirror surface and directed towards a position-sensitive photo-detector with four segments. Any change in the interaction between the probe and the sample will result in a change in the cantilever curvature, causing a shift in the position of the laser beam. The difference in the light intensity of the laser beam in the four quadrants of the detector is used to calculate the force acting on the probe.

SPMs provide a number of advantages as far as the microscopic investigation of surfaces are concerned [30]. In addition to the lateral resolution obtained, SPMs are also capable of imaging the surface morphology of a vast array of different samples. Sample preparation is restricted to a minimum, which makes this technique superior to scanning electron microscopy (SEM), where rather sophisticated sample treatment procedures such as etching and metal sputtering are required. SPMs can visualize the native structure of a sample surface in a number of different environments.

Different types of scanning probe microscopes differ only in the nature of the force detected between the tip and the sample surface. Depending on the type of interaction between the probe and sample, or the signal detected, one can distinguish between scanning tunneling microscopy (STM), scanning force microscopy (SFM), scanning near-field optical microscopy (SNOM) and various other S(X)M techniques where “X” refers to the physical property measured, such as magnetic field [31], electrostatic charge [32,33] or temperature [34].

The scanning tunneling microscope (STM) [35] uses a fine tungsten tip (or other noble metal) to scan a surface at a distance of about 1 nm above the surface, while a voltage of a few millivolts is applied between the probe tip and the sample. This gives rise to a tunneling current in the order of a few nano-ampere between the tip and the sample. The small gap between the tip and the sample allows electrons to tunnel from the atom at the very end of the tip to the nearest atom on the sample surface, hereby generating a tunneling current. STM is useful for measuring the tunneling current generated over an electronic gap between a conductive sample and a conductive tip. It is however of limited use for non-conductive materials such as polymers.

3.3.2 Atomic force microscopy

The AFM is perhaps the most versatile member of the family of scanning probe microscopes. In general, the AFM allows one to detect surface morphology, nano-scale structures and molecular and atomic scale lattices. Whereas the SEM requires sample surfaces to be coated by a metal or carbon coating, the AFM requires minimal sample preparation. Such preparative methods can obscure finer features and/or damage the sample surface. The AFM can scan samples in air [36], vacuum [37], or in liquid [38], with the only requirement that the object of interest needs to be secured on a substrate for the duration of the measurement.

In atomic force microscopy, a non-conductive silicon tip is raster-scanned across a surface, detecting the repulsive contact forces and the attractive and repulsive non-contact

forces present between the tip and sample. Figure 3.7 illustrates the forces created when a sharp tip is brought into contact with a surface. In the contact area of the tip apex (ideally a single atom), repulsive forces arise due to the overlapping electronic orbitals of the atoms situated on the tip and the sample surface. These short-range interatomic repulsive forces are confined to an extremely small area and can be used to trace the surface topography at atomic resolution. However, both attractive and repulsive long-range forces, usually of the van der Waals type, also exist. Since these forces arise due to long ranged interactions between the tip and sample, they are not suited for atomic resolution imaging. Such forces are avoided during AFM imaging since they cause an increase in the total force acting on the cantilever, leading to possible deformation of the sample, especially when soft sensitive surfaces are investigated.

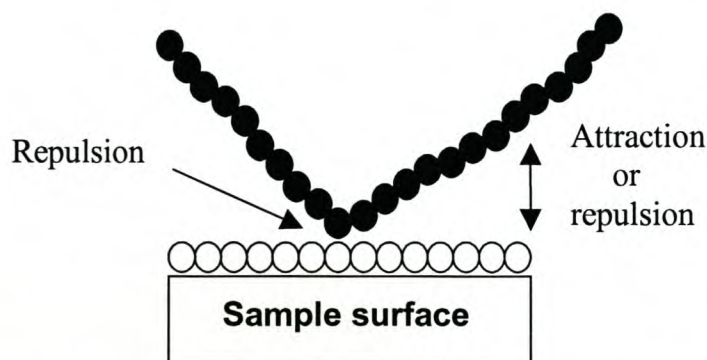


Figure 3.7: Representation of the forces present between the AFM tip and a sample surface when the tip is in close proximity of the sample. The white and black circles represent the sample and tip atoms, respectively [29].

3.3.2.1 Force-distance relationship

The following force-distance curve further illustrates the AFM's range of operation. Force-distance curves are used to illustrate the change in force between the tip and sample as a function of the distance between them.

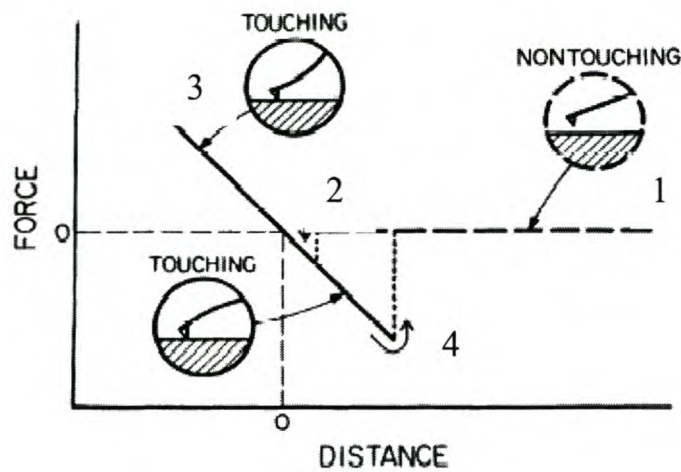


Figure 3.8: Diagram of a typical AFM force-vs-distance curve [29,39].

At very large separations, if long-range interactions are ignored, there is no interaction between the tip and sample. In this case the observed force equals zero, as illustrated by the straight line between 1 and 2 on the curve. As the tip is brought closer to the sample surface, attractive forces are being created and at a certain point the tip jumps into contact with the surface due to attractive van der Waals forces. This is called the jump-in point and indicates the transition from non-touching to touching of the sample surface. If the tip is brought even closer to the surface, the electron orbitals of the atoms on the tip and sample begin to repel each other. As this gap is decreased further, the repulsive forces begin to neutralize the attractive forces, until they become dominant. When the probe is now retracted, the force between the tip and sample is reduced along the line from point 3 to 4. Below the line indicating a force equal to zero, the net force acting on the cantilever becomes attractive due to adhesion forces holding the tip onto the surface. At position 4 on the curve, the adhesion force and the cantilever load are in equilibrium and the tip flips off the surface when it is retracted even further. During AFM measurements, forces between points 3 and 4 are aimed for, preferably closer to point 4 in order to minimize the contact force.

Depending on the distance between the tip and sample, the AFM can operate in either the contact or non-contact mode.

3.3.2.2 Contact mode AFM

When the AFM is operated in the repulsive region, it is called “contact imaging”. In this mode the cantilever is curved away from the sample due to repulsion between the atoms of the sample and tip.

3.3.2.3 Non-contact mode AFM

In contact AFM of soft materials such as polymers and bio-molecules, the tip can cause mechanical deformation of the sample surface. This can lead to an increase in the contact area, which subsequently reduces resolution. It can also lead to incorrect estimations of the height profile of the sample. One major disadvantage of such deformation is the possibility that the sample surface and/or the tip may be damaged irreversibly, especially when imaging hard samples. This problem can be overcome by operating in the non-contact mode, where the cantilever is bent towards the sample surface by attractive forces. It is, however, difficult to achieve stable imaging conditions when the probe is not in contact with the sample surface. In the non-contact mode, long-ranged interactions, such as electrostatic forces, can be easily monitored to obtain relatively stable images. The most important advantage of non-contact AFM is its ability to investigate extremely soft samples, without damaging the sample and/or the tip.

3.3.3 Micro-thermal analysis of polymers by SPM

The term ‘micro-thermal analysis’ (μ TA) [40] is used to describe all techniques where a near-field thermal probe is used to investigate the effect of thermal expansion. In modern materials technology, micro-thermal analysis plays an increasingly important role by allowing the addition of an extra dimension of, say, chemical composition information to high-resolution microscopy, or microscopic information to spectroscopy. Micro-thermal analysis is currently employed in the visualization of spatial distribution of phases,

components and contaminants in polymers, foods, biological and electronic materials as well as pharmaceuticals.

Micro-thermal analysis was launched commercially in 1998 (μ TATM Micro-Thermal Analyser (TA Instrumentations, New Castle, USA)). For the purpose of micro-thermal analysis, the SPM is provided with a thermal tip and the probe can be placed at different areas on the sample to perform localized thermal measurements. The sample is heated by heat transferred from the thermal tip to the sample. During measurements, the temperature of the tip is ramped linearly and the laser deflection of the cantilever, which results from the expansion and contraction of the sample, is recorded. Such measurements can provide information on surface expansion, film thickness, glass transition temperature, softening and melting processes, as well as changes in the hardness of the sample.

One major disadvantage of this technique is that the thermal probe is permanently in contact with the sample, which might cause detailed surface structures to be disturbed. The tip may also be contaminated, causing possible complications in heat transfer and conductivity from the tip to the sample.

3.3.3.1 Thermal analysis of polymers by AFM

Two conventional techniques used for thermal analysis of polymers are differential scanning calorimetry (DSC) [41] and dynamic mechanical analysis (DMA) [42]. The measurement of polymer thermal transitions, such as the glass transition temperature, T_g , can be carried out by these two techniques. It can however, be insufficient when trying to determine the thermal transitions of individual polymer phases of heterogeneous systems like blends and structured multiphase lattices, such as core-shell polymers. The latter are employed, for example, in the paint industry where a soft polymer shell, which will ensure a smooth film at room temperature, is combined with a hard core, necessary for sufficient stabilisation of the polymer film [43]. The T_g s of the individual phases in the core-shell system can be calculated theoretically by the Fox equation [44], but cannot be

proven experimentally by any method currently available. Conventional methods for thermal analysis, such as DSC, can only provide an average T_g for the entire sample.

A new technique for measuring T_g s and T_m s of polymers, entirely non-destructively and without any distortion of the sample surface, was recently developed by Meincken *et al.* [45]. Here the AFM is used as a “nano-DMA”, i.e., it is used in a similar manner to the DMA, but on a considerably smaller scale. This technique measures the response of surface molecules to mechanical excitation by an oscillating cantilever, making it possible to determine thermal transitions of individual polymer phases in close proximity of the tip.

During thermal analysis, the AFM is used in a stationary “probing” mode, instead of traditional raster scanning. The non-contact tip, is placed at a fairly large distance, typically about 20 μm , from the sample surface, thereby preventing distortion of the surface structure, and contamination of the tip. The cantilever oscillates above the surface, thereby exciting the underlying molecules. These molecules can respond to this excitation by absorbing energy, resulting in a change in the characteristic resonance frequency, R_f , behaviour of the cantilever. Their ability to respond to the excitation will be influenced by their degree of freedom and, therefore, their ability to move upon excitation. Unlike the μTA , a normal non-contact tip can be used instead of a thermal probe. Another difference is that, in this new AFM technique, the entire sample is heated, not just the localised area under examination, as in the case of μTA .

3.3.3.2 The interaction mode

The interaction between the polymer sample and the cantilever is influenced by two factors:

1. the distance between the sample and tip
2. viscoelastic properties of the polymer, i.e., the storage, G' , and loss modulus, G'' .

Any decrease in the distance between the tip and sample causes a decrease in the resonance frequency of the oscillating cantilever. In this technique, the resonance frequency of the cantilever is measured as a function of temperature, while the temperature is increased at a constant rate. As the temperature is increased, a material with an original length, L , and material constant, α , will expand linearly according to the relationship $L = \alpha T$. As the length of the cantilever increases, the resonance frequency, ω_r , will decrease. An increase in temperature therefore causes the resonance frequency of the oscillating cantilever, ω_r , to shift to lower values, according to the following relationship:

$$\omega_r \approx \sqrt{\frac{E}{\rho} \frac{D}{L^2}} \quad (3.10)$$

E is the elastic modulus, ρ the density, D the diameter and L the length of the cantilever as supplied by the manufacturer. The length L and diameter D increase linearly with an increase in temperature, resulting in a linear decrease of the resonance frequency.

Furthermore, as the temperature is increased, the heating stage expands and causes a decrease in the distance between the tip and sample surface, leading to a slight decrease in the resonance frequency of the cantilever. Since the distance between the tip and sample is relatively large, this effect can be neglected for polymers below their T_m .

Figure 3.9 is a plot of the resonance frequency of the cantilever as a function of temperature. The gradient of this linearly decreasing plot depends only on the material characteristics of the cantilever and the expansion coefficient of the heating stage. The characteristic form of this linear frequency plot is altered by the thermal transitions of a polymer placed between the cantilever and heating stage, characterised by kinks or plateaus at characteristic temperatures.

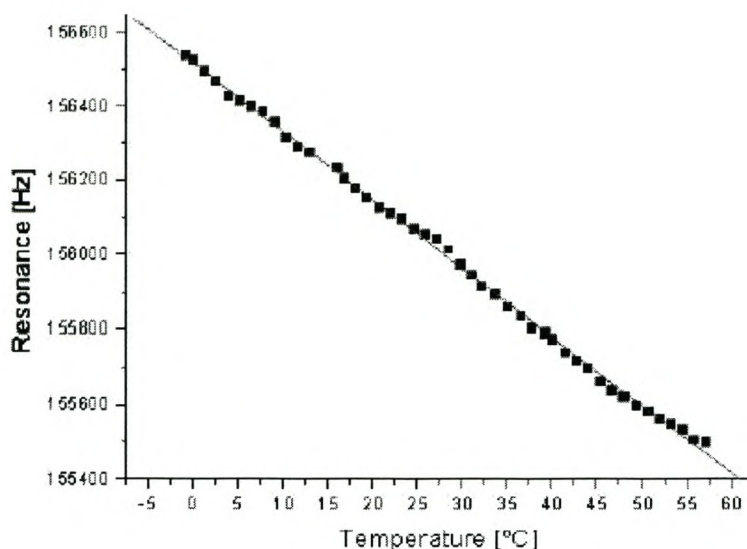


Figure 3.9: The resonance frequency of the cantilever as a function of temperature [45].

3.3.3.3 The melting point

As the polymer sample is heated, it will expand slowly, causing a decrease in the resonance frequency of the cantilever. At the melting point, the volume of the polymer increases drastically due to the ability of polymer chains to move freely at this temperature. This volume increase causes a considerable decrease in the distance between the tip and sample and, therefore, a sharp decrease in the resonance frequency. The melting point of a polymer is therefore observed as a sharp kink in the resonance frequency plot as shown by figure 3.10.

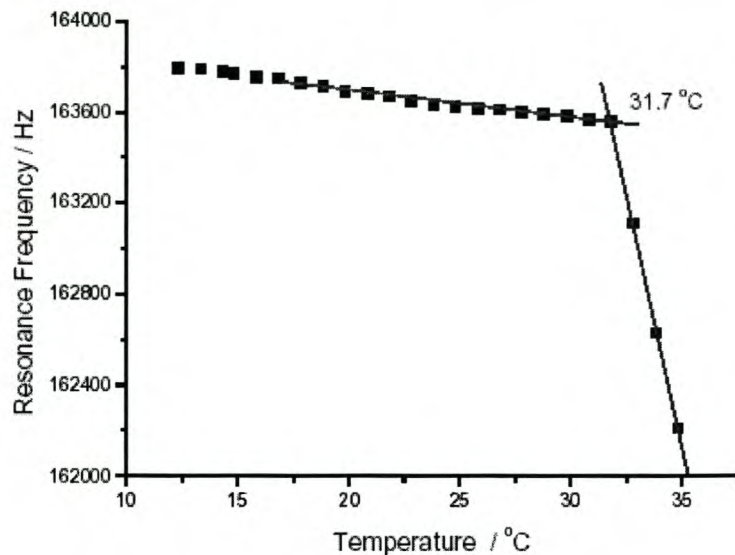


Figure 3.10: The melting point of octadecane as indicated by the kink at 31.7°C in the resonance frequency plot [45].

3.3.3.4 The glass transition

The free volume expansion in second order transitions is several orders of magnitude smaller than in first order transitions such as the melting point, and is in fact a change in the expansion coefficient of the material rather than a distinct volume expansion. The glass transition in polymers is not a true second order transition. It is characterised by a change in the elastic properties of the material rather than a change in volume. At the glass transition temperature the change in the free volume of the polymer is just enough to allow movement of individual polymer chains. This transition can therefore not be explained in terms of a free volume change inside the polymer. The glass transition is indicated by a plateau (region 2) in the frequency plot, as shown by figure 3.11. The measured frequency shift is indicated by the curve consisting of black squares, with the glass transition temperature clearly visible as a plateau region. The decreasing linear function present in regions 1 and 3 can be used as a baseline, and subtracted from the entire curve, resulting in a curve of the frequency shift represented by the hollow circles. This curve indicates that the glass transition is actually related to an increase in the resonance frequency of the cantilever.

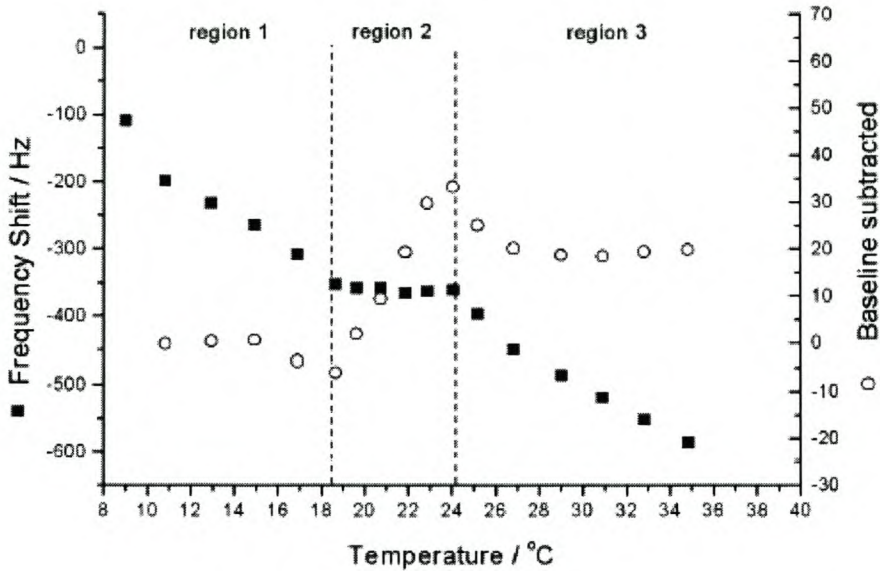


Figure 3.11: The glass transition of a random copolymer, as indicated by the plateau at about 21°C [45].

A model has been formulated by Meincken [45] to describe the behaviour of the cantilever while taking into account the elastic properties of the polymer. This model gives a possible explanation for the glass transition appearing as a plateau in the resonance frequency plot. The oscillating cantilever generates a pressure wave, transporting energy through the air molecules. The pressure wave is partly reflected at the air/polymer interface and partly absorbed by the polymer. The complex reflection coefficient, r^* , can be expressed as:

$$r^* = (Z_p^* - Z_a^*) / (Z_p^* + Z_a^*) \quad (3.11)$$

where Z_a^* and Z_p^* are the imaginary acoustic impedances of air and the polymer which depend on the shear modulus G^* of the medium and their density, ρ : $Z^{*2} = \rho^2 G^{*2}$.

The absorption coefficient a^* is given by:

$$a^* = 1 - r^* \quad (3.12)$$

At the glass transition temperature a^* and r^* change significantly, since more energy can now be absorbed by the polymer as a result of a higher degree of freedom of the molecules, as well as an increased free volume that assists the movement of polymer chains.

Therefore, at the T_g , the adsorption coefficient increases and the reflection coefficient decreases. This is also observed for the loss modulus, G'' , which is a measure of the damping abilities of the polymer, and reaches a maximum after the T_g . In the glassy state, when the polymer is harder than in the rubbery state, the pressure wave is reflected to a greater extent. At higher temperatures the cantilever's movement is less hindered, and it is able to oscillate at a value closer to its Eigenfrequency, $\omega_o \approx 190$ Hz [46]. The change in the viscoelastic properties, or rather the increased absorption coefficient, is therefore represented by a plateau in the resonance frequency plot around the T_g . The width of the plateau suggesting the T_g , is expected to be influenced by the film thickness of the sample [47], thereby implying that this method shows a certain depth sensitivity.

3.4 References

- [1] L.R. Snyder, *J. Chromatogr. A* **13** (1964) 415.
 - [2] L.R. Snyder, *Gradient Elution; High-Performance Liquid Chromatography: Advances and Perspectives*; **1** (1980) 207.
 - [3] L.R. Snyder, *Adv. Chromatogr.* **38** (1998) 115.
 - [4] R.S. Alm, R.J.P. Williams, A. Tiselius, *Acta Chem. Scand.* **6** (1952) 826.
 - [5] B. Klumperman, H.J.A. Philipsen, *LC-GC* **17** (1999) 118.
 - [6] W.J. Staal, P. Cools, A.M. van Herk, I. German, *J. Liq. Chromatogr.* **17** (1994) 3191.
-

-
- [7] W.J. Staal, PhD Dissertation: Gradient Polymer Elution Chromatography; Technische Universiteit Eindhoven; Eindhoven, Netherlands, (1997).
- [8] Glöckner G., J.H.M. van den Berg, *J.Chromatogr.* **352** (1986) 511.
- [9] P.J.C.H. Cools, A.M. Van Herk, A.L. German, W.J. Staal, *J. Liq. Chromatogr.* **17** (1994) 3133.
- [10] H.J.A. Philipsen, B. Klumperman, A.L. German, *J. Chromatogr. A* **746** (1996) 211.
- [11] H. Pasch, B. Trathnigg, *HPLC of Polymers*, Springer-Verlag, Heidelberg, Berlin, 1998.
- [12] G. Glöckner, *J. Chromatogr. A* **797** (1998) 11.
- [13] G. Glockner, *J. Appl. Polym. Sci.* **43** (1989) 39.
- [14] G.W. Somsen, C. Gooijer, U.A.T. Brinkman, *J. Chromatogr. A* **856** (1999) 213.
- [15] D.W. Vidrine, D.R. Mattson, *Appl. Spectrosc.* **32** (1978) 502.
- [16] J.W. Hellgeth, L.T. Taylor, *Anal. Chem.* **59** (1987) 295.
- [17] C.C. Johnson, J.W. Hellgeth, L.T. Taylor, *Anal. Chem.* **57** (1985) 610.
- [18] J.J. Gagel, K. Biemann, *Anal. Chem.* **59** (1987) 1266.
- [19] A. Karami, S.T. Balke, T.C. Schunk, *J. Chromatogr. A* **911** (2001) 27.
- [20] S.J. Kok, N.C. Arentsen, P.J.C.H. Cools, T. Hankemeier, P.J. Schoenmakers, *J. Chromatogr. A* **948** (2002) 257.
- [21] S.L. Jordan, L.T. Taylor, B. McPherson, H.T. Rasmussen, *J. Chromatogr. A* **755** (1996) 211.
- [22] M.W. Raynor, K.D. Bartle, B.W. Cook, *J. High. Resolut. Chromatogr.* **15** (1992) 361.
- [23] J.J. Gagel, K. Biemann, *Anal. Chem.* **58** (1986) 2184.
- [24] L.M. Wheeler, J.N. Willis, *Appl. Spectrosc.* **47** (1993) 1128.
- [25] G. Glöckner, J.H.M. van den Berg, N.L.J. Meijerink, T.G. Scholte, R. Koningsveld, *Macromolecules* **17** (1984) 962.
- [26] A.H. Dekmezian, T. Morioka, C.E. Camp, *J. Polym. Sci., Part B: Polym. Phys.* **28** (1990) 1903.
- [27] J.L. Dwyer, A.E. Chapman, X.J. Liu, *LC-GC* **8** (1995) 704.
- [28] J.J. Gagel, K. Biemann, *Mikrochim. Acta* **11** (1988) 185.
-

-
- [29] H. Friedbacher, G.Fuchs, *Pure Appl. Chem.* **71** (1999) 1337.
- [30] S.S. Sheiko, *Adv. Polym. Sci.* **151** (2000) 61.
- [31] A.J.P. Martin, C.C. Williams, H.K. Wickramasinghe, *J. Appl. Phys.* **61** (1987) 4723.
- [32] B.D. Terris, J.E. Stern, D. Rugar, H.J. Mamin, *Phys. Rev. Lett.* **63** (1989).
- [33] F. Saurenbach, B.D. Terris, *Appl. Phys. Lett.* **56** (1990) 1704.
- [34] M. Stopka, L. Hadjiiski, E. Oesterschulze, R. Kassing, *J. Vac. Sci. Technol. B* **13** (1995).
- [35] G. Binnig, C.F. Quate, C. Gerber, E. Weibel, *Phys. Rev. Lett.* **49** (1982) 57.
- [36] T.R. Albrecht, C.F. Quate, *J. Appl. Phys.* **62** (1987) 2599.
- [37] G. Meyer, N.M. Amer, *Appl. Phys. Lett.* **53** (1988) 1044.
- [38] S. Manne, H.J. Butt, S.A.C. Gould, P.K. Hansma, *Appl. Phys. Lett.* **56** (1990) 1758.
- [39] A.L. Weisenhorn, P. Maivald, H.-J. Butt, P.K. Hansma, *Phys. Rev. B: Condens. Matter* **45** (1992) 11 226.
- [40] H.M. Pollock, A. Hammiche, *J. Phys. D: Appl. Phys.* **34** (2000) R23.
- [41] E. Dargent, C. Cabot, J. Saiter, J. Bayard, J. Grenet, *J Therm. Anal.* **47** (1996) 887.
- [42] B. Twombly, *Instrum. Sci. Technol.* **22** (1994) 259.
- [43] M. Meincken, PhD Dissertation: University of Stellenbosch; Stellenbosch, South Africa (2001).
- [44] T. Fox, *Bull. Am. Phys. Soc.* **1** (1956) 123.
- [45] M. Meincken, S. Graef, K. Mueller-Nedebock, R.D. Sanderson, *Appl. Phys. A* **74** (2002) 371.
- [46] Nanosensors: Nanosensors, product specification, 2000.
- [47] V.N. Bliznyuk, H.E. Assender, G.A.D. Briggs, *Macromolecules* **35** (2002) 6613.
-

Chapter 4

Experimental

4.1. Materials

4.1.1 Choice of materials

The polymers and oligomers used for HPLC analysis were as follows:

- Narrow molar mass oligoethylene standards, (M_w 282 and 394 g.mol⁻¹), from Polymer Standards Service. Molar mass values were supplied by the manufacturer, and the polydispersity, D ($D = M_w/M_n$) of both standards was 1.0.
 - Narrow molar mass polystyrene (PS) standards, (M_w 4 000; 30 740; 400 000; 942 000 g.mol⁻¹), supplied by Pressure Chemical. Polydispersities of all standards were below 1.06.
 - Poly(ethyl methacrylate) (PEMA), (M_w 850 000 g.mol⁻¹), from Aldrich Chemical Company Inc.
 - EasiCal PS-2 polystyrene calibration standards, containing five standards of the following molar masses: 377 000; 96 000; 20 650; 5 460; and 1 300 g.mol⁻¹, supplied by Polymer Laboratories.
 - Sample of an unknown paper coating emulsion system supplied by Swale chemicals (Pty) Ltd.
-

4.1.2 Sample preparation

Samples were prepared by weighing out 20 mg of each compound and dissolving it in 2 ml THF to obtain solutions with a concentration of 10 mg/ml. High molar mass samples that are usually more difficult to dissolve were stirred overnight to ensure complete dissolution.

The EasiCal PS standards were prepared according to the instructions supplied on the sample cards accompanying the two unlabeled plastic strips or spatulas containing five standards each. One sample contained PS standards with molar masses ranging from 580 to 210 500 $\text{g}\cdot\text{mol}^{-1}$, while the polystyrenes of the other sample had molar masses from 1 300 to 377 400 $\text{g}\cdot\text{mol}^{-1}$. Only the solution containing the standards of higher molar mass (1 300 to 377 400 $\text{g}\cdot\text{mol}^{-1}$) was used for analyses.

The following mixtures were also prepared for analysis by gradient elution chromatography:

- C20 oligoethylene (M_w 282 $\text{g}\cdot\text{mol}^{-1}$) and C28 oligoethylene (M_w 394 $\text{g}\cdot\text{mol}^{-1}$)
- C20 oligoethylene (M_w 282 $\text{g}\cdot\text{mol}^{-1}$) and polystyrene (M_w 400 000 $\text{g}\cdot\text{mol}^{-1}$)
- Polystyrene (M_w 942 000 $\text{g}\cdot\text{mol}^{-1}$) and poly(ethyl methacrylate) (M_w 850 000 $\text{g}\cdot\text{mol}^{-1}$)

For the preparation of all mixtures, equal amounts of both components were weighed out (20 mg of each) and dissolved in 2 ml THF, to ensure a final concentration of 10 mg/ml.

The unknown commercial polymer coating was supplied as an emulsion system. The commercial product was precipitated by dripping the emulsion into methanol, after which the sample was centrifuged and the methanol layer decanted. The sample was again washed with methanol to ensure the removal of all unwanted impurities. The washed sample was then dried overnight in a vacuum oven at room temperature. After drying,

20 mg of the sample was dissolved in 2 ml THF, and stirred for a period of 24 hours.

Prior to injection into the HPLC system, all dissolved samples were filtered through 25 mm Nylon syringe filters with a pore size of 0.45 μm , supplied by Anatech Instruments (Pty) Ltd.

4.2 HPLC analysis

4.2.1 HPLC equipment and experimental conditions

All HPLC experiments were performed on a Waters Alliance system, consisting of the following components:

- Waters 2690 Separations module (Alliance)
- Waters 717_{plus} Autosampler
- Waters 600E System controller
- Waters 610 Fluid unit
- Polymer Laboratories PL-ELS 1000, Evaporative light scattering detector (ELSD)
- Waters Millennium³² V3.05 Software

The columns used during this study are listed in table 4.1, together with their characteristic particle sizes and dimensions.

Table 4.1: Specifications of the columns used for HPLC analysis

Column	Supplier	Particle size (μm)	Dimensions (mm)
Nucleosil C18	Macherey-Nagel	5	125 × 4
Nucleosil ODS	SGE Analytical products	5	250 × 4.6
PLgel Mixed-D	Polymer Laboratories	5	300 × 7.5

PS EasiCal standards were separated by means of the PLgel mixed-D column, whereas all other samples were separated by either of the two Nucleosil columns. A constant column temperature of 30°C was maintained through the use of an oven.

The evaporator and nebuliser temperature of the ELSD detector was fixed at 80°C and 40°C, respectively. The feed of the chromatographic effluent to the ELSD detector was carried out under the continuous flow of N₂ carrier gas, at a rate of 1.0 SLM. The mobile phase flow rate was 1.0 ml/min in all cases, except for the analysis of the EasiCal PS standards, where a flow rate of 0.5 ml/min was employed. A sample volume of 25 µl was injected for all HPLC analyses.

4.2.2 Solvents

The solvents used for HPLC analysis were tetrahydrofuran (THF) and acetonitrile (ACN), both HPLC grade, supplied by Riedel-de Haën. During all experiments, solvents were sparged with helium at a flow rate of 10 ml/min. All solvent mixtures were prepared through volumetric mixing by the HPLC pump, and no premixes were used. Methanol (MeOH), supplied by BDH solvents, was used for the precipitation of the unknown emulsion system.

4.2.3 Experimental setup for gradient analysis

The experimental setup for gradient HPLC analysis used during this study is illustrated in figure 4.1, which shows the most important components of a general gradient HPLC system. The gradient pump, autosampler, valve switch, controller as well as the UV and ELSD detectors are all connected to a computer.

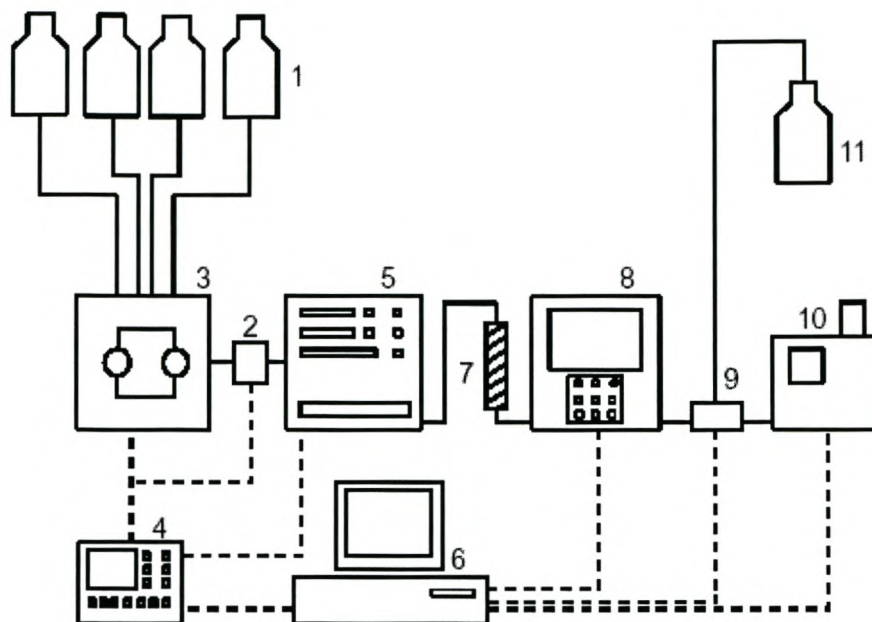


Figure 4.1: Schematic representation of the gradient HPLC experimental setup used [1].

The setup consists of the following components:

- (1) Solvent reservoirs
- (2) Mixing chamber
- (3) Gradient pump
- (4) Controller
- (5) Autosampler/Injector
- (6) Computer
- (7) Column situated inside column oven
- (8) UV detector
- (9) Switch valve
- (10) ELSD
- (11) Solvent waste bottle

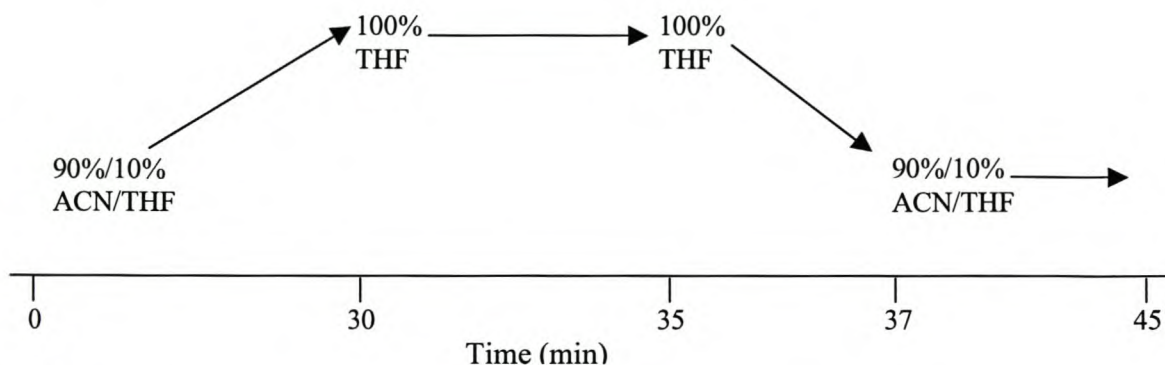
Experimental parameters such as the flow rate, injection volume, and gradient profile can either be set by the controller, which forms part of the separations unit, or the computer software, since the gradient pump, auto-sampler, valve switch, controller, and detectors

are all connected to the computer. During experiments, the solvents are continuously sparged with helium to eliminate any interferences due to air present in the reservoirs. Furthermore, degassers are installed inside the separations module, for degassing of solvents during analyses.

A typical chromatographic run commences when the sample is extracted from the sample vial situated inside the auto-sampler, and injected into the system. The solvents are pumped by the gradient pump towards the mixing chamber where solvents are mixed in the right proportions, as stipulated by the gradient program, at the starting conditions of the run. After injection, the mixed mobile phase flows through the column and carries separated sample components towards the detectors. If UV detection is desired, the column effluent enters this detector first. A switch valve can either direct the solvent stream towards the ELSD or the waste bottle as it exits the UV detector, depending on the necessity of light scattering detection of the sample involved. Continuous data collection is done automatically by the Millennium³² software, which displays results as chromatograms suitable for data analysis and interpretation purposes.

4.2.4 The solvent gradient

The following gradient profile was used for all gradient analyses:



Scheme 4.1: Representation of the gradient used during gradient analysis.

This schematic representation indicates how the mobile phase composition changes with time during a chromatographic run.

At the start of the solvent gradient or program, the mobile phase mixture contains 90% ACN and 10% THF. Within the first 30 minutes of the gradient, the solvent composition is changed to 100% THF. The gradient steepness, which is defined as the rate of change of the solvent composition as a function of time, can be calculated by the following equation [2]:

$$\phi' = (\text{change in volume fraction B})/\text{time} \quad (4.1)$$

The steepness of the gradient during this first part is therefore 3%/min. During the next 5 minutes the gradient remains unchanged, which results in a gradient steepness of 0%/min. Thereafter, the original conditions are restored within 2 minutes, and these conditions prevail for the next 8 minutes until the end of the run. This brings the total run time to 45 minutes. During this step, the gradient steepness is increased drastically to 45%/min. This last stage of the gradient, where the original solvent composition is restored, is known as the column regeneration step. This step is extremely important, since it ensures that all traces of a current sample are removed prior to injection of a new sample.

4.3. LC-FTIR analysis

4.3.1 Sample preparation

All samples were prepared in the same way as in the case of the standard HPLC analyses (section 4.1.2), except that higher concentrations were used. Samples were prepared to a concentration of 20 mg/ml in THF and 50 to 80 μ l of each sample was injected.

4.3.2 The LC-FTIR interface

The LC-FTIR interface used during this study was a Lab Connections LC-Transform. This interface is a direct HPLC/FTIR solvent evaporation interface based on the invention of Gagel and Biemann [3-5]. The main system is composed of two independent modules: the sample collection module (A) and the optics module (B), illustrated in figure 4.2.

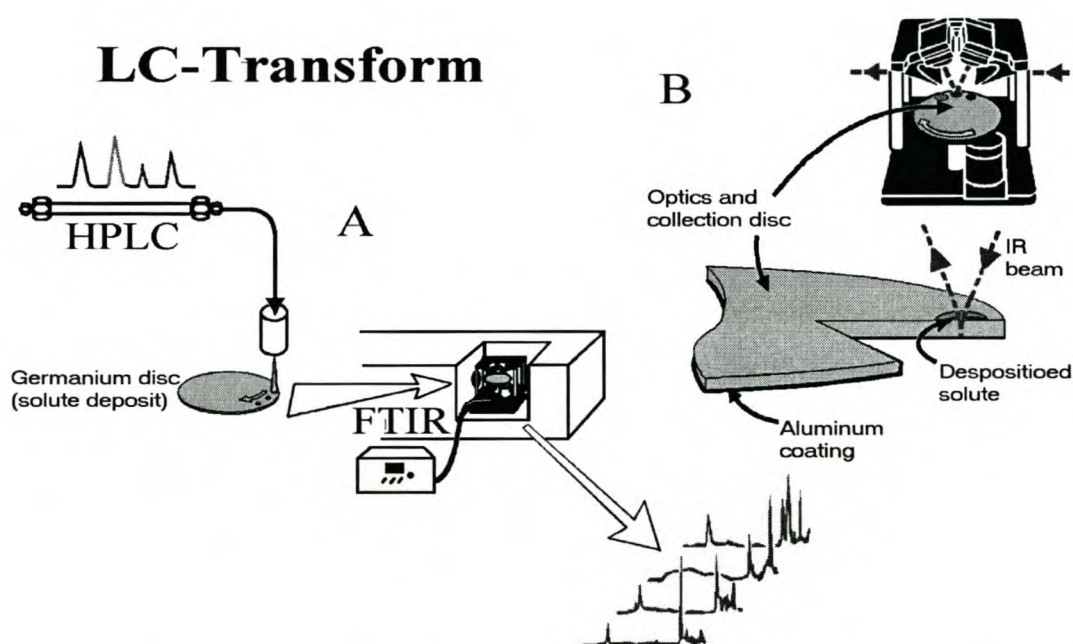


Figure 4.2: The LC-Transform design concept, illustrating the two independent modules: (A) the sample collection module, and (B) the optics module [6].

Upon exiting the liquid chromatographic system, the LC effluent is passed through a flow splitter that splits the effluent stream in a 90/10 ratio, with 90% entering the detector and 10% being directed towards the interface.

The fraction of the eluent that enters the interface is passed through a nebuliser nozzle which is located above a rotating sample collection disc. The disc surface is coated by a germanium composite, which is transparent to IR energy in the region from

450 to 6 000 cm^{-1} . The nebuliser nozzle rapidly evaporated the mobile phase solvents while depositing a tightly focused solute track onto the IR-transparent substrate. This deposition process is indicated by figure 4.3.

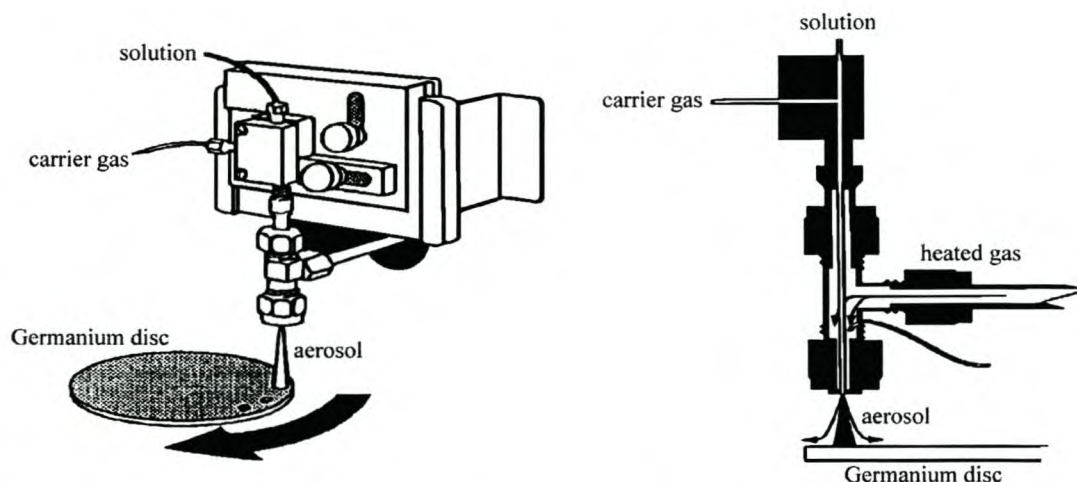


Figure 4.3: Schematic diagram of the nozzle depositing a solute track onto the germanium substrate [6].

The collection module is responsible for controlling parameters such as the gas flow and temperature to ensure sufficient evaporation for IR analysis. The position and rotation rate of the collection disc is also controlled by this module, for compatibility with the run time and peak resolution of the chromatographic separation.

After deposition of sample solutes on the collection disc, the disc is transferred to the optics module of the interface, situated inside the IR sample compartment. This module consists of a beam condenser and reflective optical bench with a motor drive onto which the collection disc is placed. During IR analysis, the incident IR beam passes through an aperture, then through optics that focus the beam onto the deposited track. The deposited solute film absorbs IR energy as the beam passes through it, after which the beam is reflected from the aluminised back surface of the collection disc, and once again passed through the film before reaching the IR detector. The IR beam therefore penetrates the sample twice, allowing optimum absorption of IR energy. This double absorption mechanism is illustrated by the part labeled B in figure 4.2.

The speed at which the disc is rotated within the optics module is tuned to the rate at which deposition was done, to ensure a compatible run time with the chromatographic run. The variable speed motor drive allows scanning of the entire track on the collection disc. Greater spectral resolution can be achieved by slowing the disc down, or stopping it at certain intervals, to obtain multiple co-added scans. Data collection is accomplished through software packages available from FTIR vendors.

Data obtained by LC-FTIR analysis is presented as a so-called Gram-Schmidt chromatogram. The shape of this representation closely resembles that of the GPEC chromatogram, and the same degree of resolution is maintained [6]. The Gram-Schmidt is a graphical representation of how the IR response changes over the duration of the experiment. In other words, the Gram-Schmidt representation illustrates the total IR absorbance as a function of time, where the time axis can be correlated with the retention time in the GPEC chromatogram. The IR spectra of components separated by chromatography can be obtained at certain positions along the perimeter of the collection disc. These IR spectra can be used to identify unknown components in polymer samples when reference spectra are available for comparison.

4.3.3 Experimental conditions

All LC-FTIR analyses were done by means of the Lab Connections series 300 LC-Transform system (model 303). The temperature of the stage onto which the disc is placed during deposition was set at 70°C for the ACN/THF mixture used during gradient analysis. The nebuliser nozzle temperature was set at 21°C to ensure sufficient nebulisation of the given solvent mixture. The nozzle was fixed at a distance of 8 mm above the collection disc surface. The germanium collection disc was rotated at a speed of 10°/min in all cases. The pressure inside the vacuum chamber was maintained at 13 Torr, using a dry ice trapped vacuum pump to remove solvent vapours. LC-FTIR data was collected and processed by means of the Timebase software V6.0 supplied by Perkin Elmer. The FTIR spectrometer that formed part of the LC-FTIR setup was a

Perkin Elmer Paragon 1000 with an internal LiTaO₃ detector. IR absorption was scanned from 4 000 to 500 cm⁻¹ at a resolution of 2.00 cm⁻¹, and only one accumulation was performed at each point along the perimeter of the germanium disc. The run time for accumulation of IR data was in each case determined by the time at which the last chromatographic peak eluted in the LC system. The disc was rotated at 10°/min inside the optics module, which agrees with the speed at which deposition was performed.

4.4. AFM analysis

4.4.1 AFM instrumentation

The atomic force microscope used for all thermal measurements was a Topometrix Explorer. The AFM was operated in the low-frequency non-contact mode, with a driving amplitude of the oscillating cantilever between 0.2 and 0.5 V. Silicon cantilevers with a nominal resonance frequency of approximately 170 kHz, and a force constant of about 50 N/m, were supplied by Nanosensors (GmbH, Germany). The dimensions of these cantilevers are more or less 225 μm × 28 μm × 7 μm, and the tip has a pyramidal shape with a height of 10 to 15 μm and a tip radius smaller than 10 nm.

The specifications of the silicon discs onto which the sample components were deposited for AFM analysis after separation by gradient analysis are presented in table 4.2.

Table 4.2: Specifications of the silicon discs used for sample collection

Diameter (mm)	50.8 ± 0.3
Thickness (μm)	280 ± 25
Orientation	<100>
Resistivity (Ωcm)	4.0 – 7.0

4.4.2 System operation for resonance frequency measurements

Contact between the tip and polymer surface was avoided at all times by keeping a fairly large distance between the tip and the sample. Although the exact distance between the sample surface and the tip could not be measured with current technology, it could be estimated by making use of the Topometrix video monitor which has a 1 000 times magnification, that the distance between the sample and tip was about 20 μm . The automatic tip approach was performed before each measurement. This procedure causes the approaching tip to stop immediately when the sample surface is reached. The tip is then retracted from the sample surface with a motor in the z direction, which allows the movement of the cantilever to be independent of the software, but still ensures a fixed distance of approximately 20 μm between the tip and surface.

The prepared sample is mounted on a stage consisting of two Peltier elements, capable of either heating or cooling the sample. The AFM is placed on top of the sample and Peltier elements, as illustrated by figure 4.4. The temperature range of these elements is between -20°C and 120°C . The temperature of the sample is measured by a PT 100 resistive temperature sensor, attached to a copper block, which ensures good conduction of heat to the sample. The sensor is situated directly below the sample, hence the temperature measured may differ from the actual temperature at the surface of the polymer sample. This difference in temperature is however not much, since very thin films are usually examined. As a result of this, the acquired temperature values are not absolute, but the relative temperature change during a thermal measurement is correct.

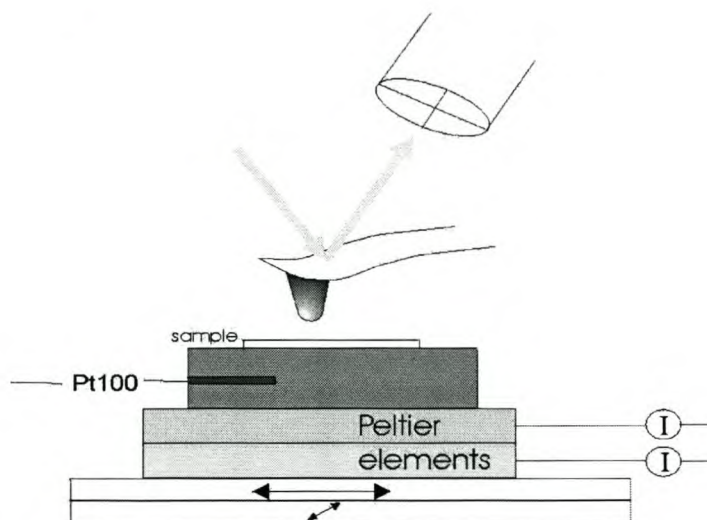


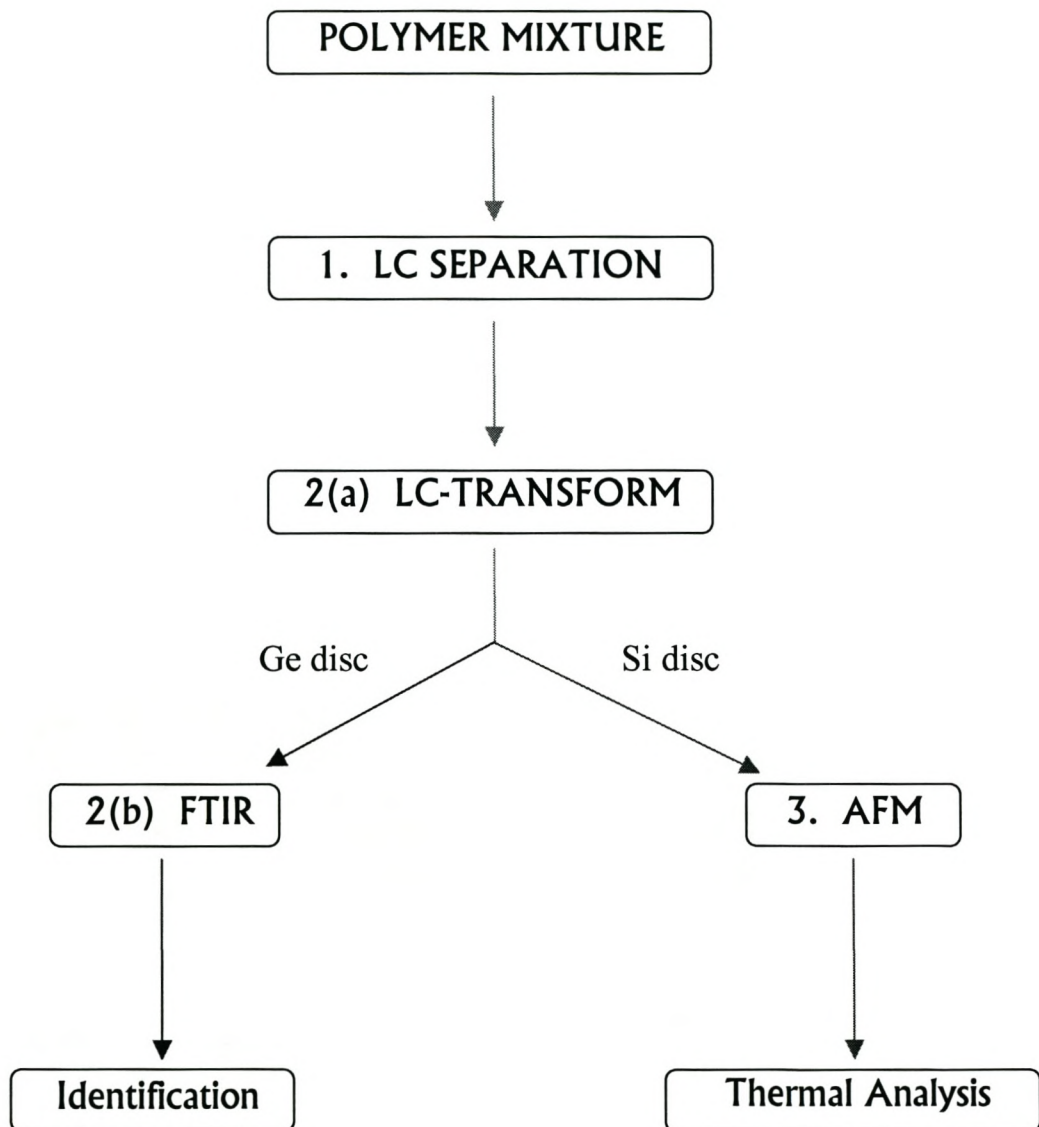
Figure 4.4: The position of the sample during AFM measurements [7].

During a thermal measurement, the temperature of the system is increased at a constant rate of approximately $2^{\circ}\text{C}/\text{min}$. For each polymer sample, a certain starting temperature below the transition point of the polymer is chosen, and the temperature is increased at this fixed rate until a maximum temperature somewhere above the transition point is reached. A polymer with a known thermal transition at 25°C will therefore be heated from, say, 10°C to 40°C .

The resonance frequency of the cantilever is determined by the internal oscilloscope in the Topometrix software, which displays the magnitude of the oscillation as a function of the frequency. The resonance frequency of the cantilever is recorded at intervals of one or two degrees, by determining its value at the maximum amplitude of the oscillation curve obtained at each point during heating. The rate at which the sample is heated is adjusted manually by increasing the current through the Peltier elements. The temperature of the sample is displayed on a computer monitor, coupled to the K20 control unit, which is in turn, connected to the PT 100 temperature sensor. The accuracy of the PT 100 temperature sensor is in the order of 1°C . During all measurements, the AFM is placed on an air table to eliminate interferences caused by vibrations.

4.5. Proposed strategy for the development of the LC-FTIR-AFM technique

4.5.1. Route diagram of the work proposed



Scheme 4.2: Route diagram of the path followed during the development of the new LC-FTIR-AFM technique.

4.5.2. Strategy followed during LC-FTIR analysis

The diagram above illustrates the different analytical routes followed during the analysis of each sample. The first step involves the separation of a polymer mixture or blend by means of HPLC. All samples, except the EasiCal PSs, were separated by gradient elution during this step. The EasiCal PS standards were separated via isocratic elution, where the column used was a PLgel mixed-D, and 100% THF was used as the mobile phase eluent. All conditions for separation were identical to those used in gradient analysis, except for the mobile phase flow rate that was 0.5 ml/min instead of 1.0 ml used in all other experiments.

During this step, the main purpose was to obtain separation of components in each mixture or blend. An evaporative light scattering detection (ELSD) was used to monitor the HPLC separation process.

The second step of the analysis scheme involves the use of the LC-Transform interface for the identification of components after separation by HPLC, via IR spectroscopy. The strategy followed during this step corresponds to the general functioning of the LC-FTIR interface, described in section 4.3.2 above. The HPLC separation of the mixed polymer sample is repeated, but the individual solutes are deposited onto the rotating germanium disc inside the sample collection module of the interface, as they leave the HPLC separations module. After deposition, the disc is transferred to the optics module of the interface situated inside the sample compartment of the IR spectrometer, and the IR absorption of the entire track is recorded. The IR spectra of individual components can be obtained from the Gram-Schmidt chromatogram to facilitate their identification through comparison with spectra in the library of IR spectra contained within the IR software.

4.5.3. Development of the LC-FTIR-AFM technique

The third step involves the coupling of HPLC with AFM in a novel way to create a new hyphenated technique, LC-FTIR-AFM. During this step, the separation step is once again performed, and the column effluent directed towards the LC-FTIR solvent evaporation interface but in this case, deposition does not take place onto a germanium disc. A silicon disc is placed onto the heating stage of the sample collection module, and the separate solutes are subsequently deposited onto the silicon disc in the same manner as was explained for LC-FTIR analysis. Silicon is used as a substrate, since it is inexpensive and easy to cut into pieces for the isolation of individual solute spots. After deposition, a glass knife is used to cut the silicon disc into pieces at all places along the perimeter of the disc where solute spots are seen. Each silicon piece onto which a sample solute has been deposited is then transferred manually to the AFM for thermal analysis by means of the technique developed by Meincken [8], as described in section 3.3.1.1.

Thermal analysis data is presented as the shift in the resonance frequency of the cantilever as a function of temperature, as the temperature is increased at a constant rate of just below 2°C/min. Thermal transitions in polymers are visible as changes in the characteristic linearly decreasing resonance frequency curve of the cantilever. Glass transitions in amorphous sections of a polymer sample will appear as a plateau, ranging over a few degrees, whereas melting points for crystalline sections of the sample will give rise to a sharp kink in the characteristic resonance frequency function.

4.6. References

- [1] A.J.P. van Zyl, MSc Thesis: University of Stellenbosch; Stellenbosch, South Africa (1999).
- [2] L.R. Snyder, Gradient Elution; High-Performance Liquid Chromatography: Advances and Perspectives; **1** (1980) 207.

- [3] J.J. Gagel, K. Biemann, *Anal. Chem.* **58** (1986) 2184.
 - [4] J.J. Gagel, K. Biemann, *Anal. Chem.* **59** (1987) 1266.
 - [5] J.J. Gagel, K. Biemann, *Mikrochim. Acta* **11** (1988) 185.
 - [6] T. Provder, M. Whited, D. Huddleston, C. Kuo, *Prog. Org. Coat.* **32** (1997) 155.
 - [7] M. Meincken, *Surf. Interface Anal.* *Accepted* (2003).
 - [8] M. Meincken, S. Graef, K. Mueller-Nedebock, R.D. Sanderson, *Appl. Phys. A* **74** (2002) 371.
-

Chapter 5

Results and Discussion

5.1 Analysis of oligoethylenes

The ability of the LC-FTIR-AFM technique to separate, identify and measure the melting points of individual mixture components, was demonstrated through the analysis of a mixture containing two oligoethylenes with molar masses of 282 and 394 g.mol⁻¹, respectively. The mixture was prepared and analysed according to the procedures described in sections 4.1.2, 4.5.2 and 4.5.3 of the experimental chapter.

5.1.1 HPLC separation of an oligoethylene mixture

The gradient separation of the oligoethylene mixture is shown in figure 5.1. At the start of the gradient, where a 90/10 (v/v) mixture of ACN and THF constitutes the mobile phase, both oligoethylenes will be precipitated and retained at the head of the column. The two components of the mixture will adsorb to the stationary phase and remain retained until the solvent strength is increased sufficiently for redissolution to occur. Throughout the gradient process, the solvent strength is continuously being enhanced through the addition of increasing amounts of the stronger solvent, THF. At a certain mobile phase composition the oligomers are re-dissolved in the solvent, and find themselves in the adsorption region (figure 3.5, section 3.1.4.1). Here, the highest molar mass oligomer (C28) will have the highest retention time (RT) due to the fact that it is slightly less soluble than the lower molar mass (C20) component [1,2] and a higher percentage solvent is required to facilitate the redissolution of the C28 oligomer. The

peak at 3.73 minutes therefore corresponds to the retention time of the C20 oligomer, while the peak at 5.88 minutes is that of the C28 oligoethylene.

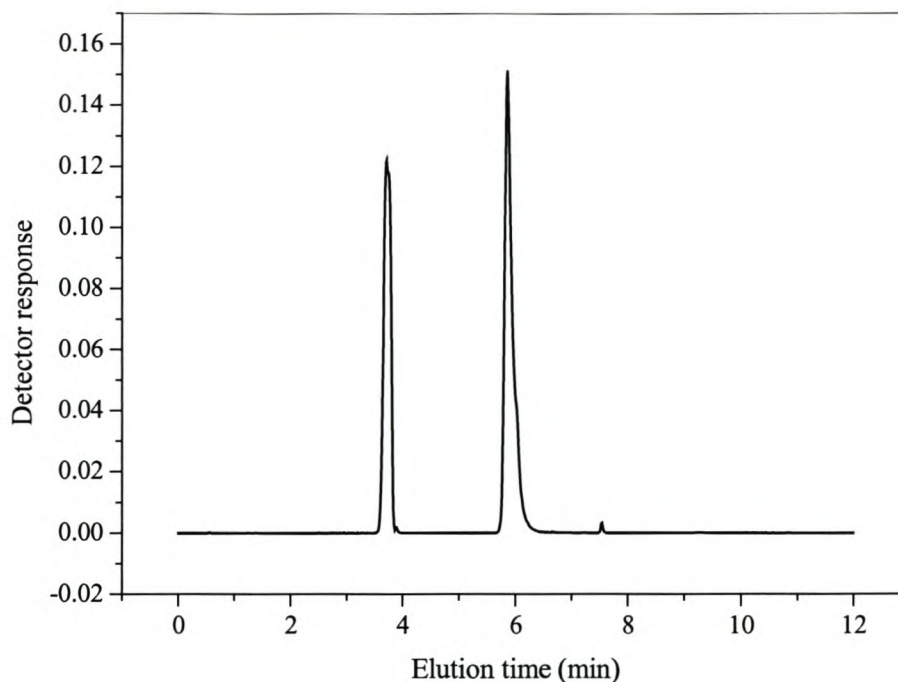


Figure 5.1: GPEC chromatogram of a mixture of two oligoethylene standards.

5.1.2 LC-FTIR analysis of an oligoethylene mixture

Figure 5.2 is the Gram-Schmidt representation obtained from the LC-FTIR analysis of a mixture of two oligoethylene standards of different molar masses. The x-axis displays the time (in minutes) that corresponds to the retention time in the GPEC separation, while the intensity of IR absorbance is given by the y-axis. The C20 oligoethylene appears at 6.15 minutes and the C28 oligoethylene at 11.13 minutes in the Gram-Schmidt representation. The nebuliser does cause peak broadening, which can be easily established from the Gram-Schmidt representation after special normalisation.

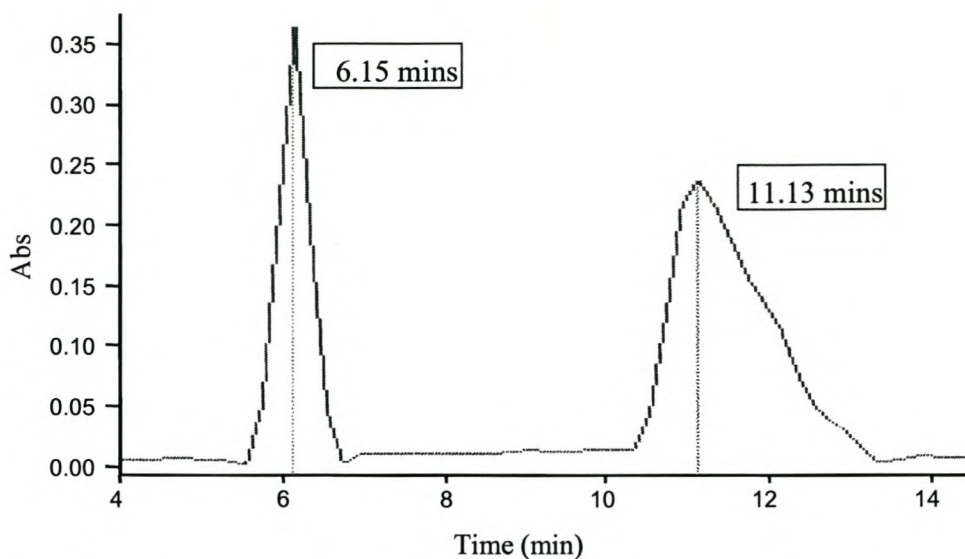


Figure 5.2: Gram-Schmidt chromatogram of a mixture of two oligoethylenes.

Figure 5.3 is the IR spectrum of the C₂₀ oligoethylene, while figure 5.4 is that of the C₂₈ component of the mixture. These spectra were recorded at the maxima of each of the two peaks in the Gram-Schmidt representation.

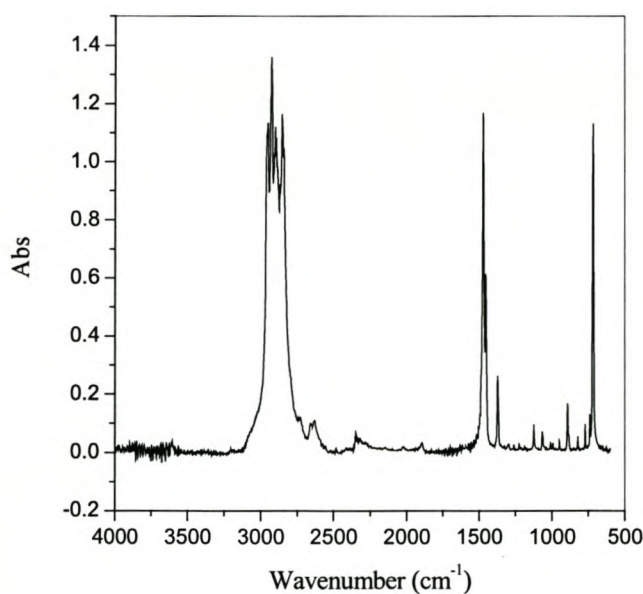


Figure 5.3: IR spectrum of the C₂₀ oligoethylene.

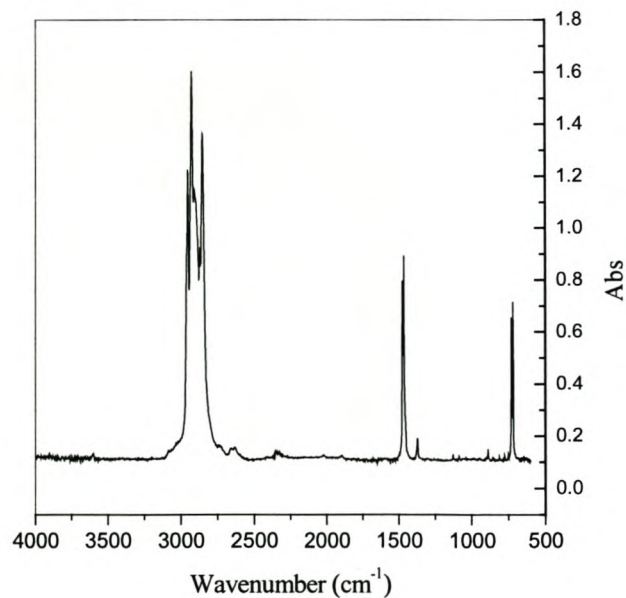


Figure 5.4: IR spectrum of the C₂₈ oligoethylene.

Oligoethylene is characterized by the presence of IR absorption bands in three regions of the IR spectrum. The position of these three major absorption bands, as well as the functional groups responsible for them, are presented in table 5.1.

Table 5.1: IR absorption data for oligoethylene

Wavenumber (cm ⁻¹)	Functional group	Spectral range (cm ⁻¹)	Bond mode	Peak intensity
722.2	CC	750 - 720	Skeletal vibration	Medium
1 470.7	CH	1 485 - 1 445	Deformation	Strong
2 854.8	CH	2 863 - 2 843	Symmetrical stretching	Strong
2 922.5	CH	2 936 - 2 916	Asymmetrical stretching	Strong

5.1.3 LC-AFM analysis of an oligoethylene mixture

After the LC-FTIR deposition step was repeated and the sample deposited onto a silicon disc, the two individual components were cut from the disc and transferred to the AFM for thermal analysis via the resonance frequency method (RFM), described in section 3.3.3.1. The melting temperature of the C20 oligoethylene appears as a kink at 32.2°C in the resonance frequency plot, as illustrated by figure 5.5.

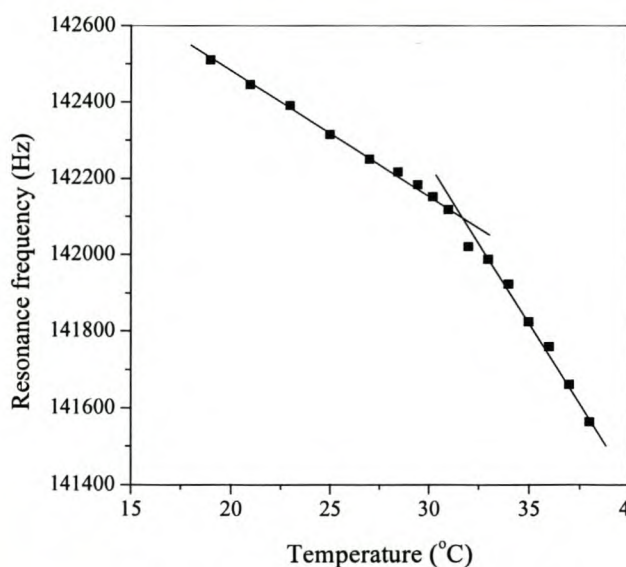


Figure 5.5: R_f spectrum of the C20 oligoethylene.

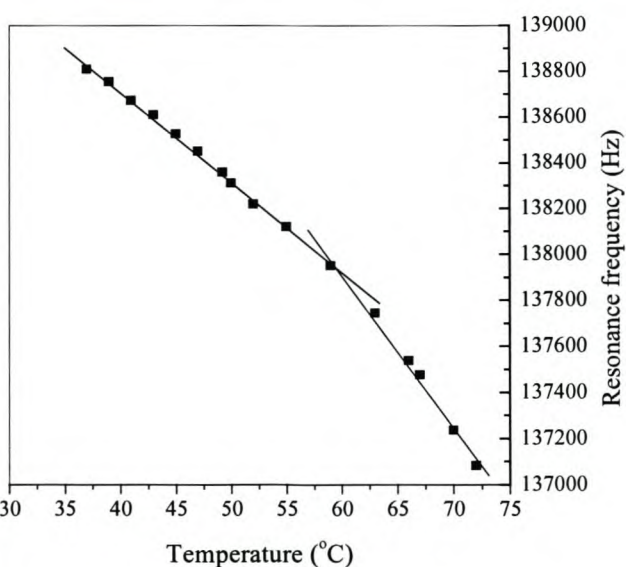


Figure 5.6: R_f spectrum of the C28 oligoethylene.

The theoretical melting point for the C20 oligoethylene with a molar mass of $282 \text{ g}\cdot\text{mol}^{-1}$ is 36.6°C [3]. The slight deviation from this value, as measured by RFM ($T_m = 32.2^\circ\text{C}$), may be ascribed to impurities in the sample, as indicated by the large number of low intensity peaks present in the IR spectrum of this component (figure 5.3). By means of similar resonance frequency measurements, the T_m of the C28 oligoethylene with a molar mass of $394 \text{ g}\cdot\text{mol}^{-1}$, (which has a theoretical $T_m = 61.4^\circ\text{C}$) [3], was measured as 62.0°C , as indicated by the kink in the resonance frequency plot, figure 5.6. The better match in this case is however, expected, since a much cleaner IR spectrum was obtained for this component (figure 5.4).

5.2 Analysis of polystyrenes

The ability of the LC-FTIR-AFM technique to separate, identify and measure the glass transition temperature of individual polymers in a mixture was demonstrated by the analysis of a mixture of five polystyrene standards of the following molar masses: 1 300, 5 460, 20 650, 96 000 and 377 400 $\text{g}\cdot\text{mol}^{-1}$. This mixture was prepared according to the procedure described in section 4.1.2, and subjected to the analysis procedure described in sections 4.5.2. and 4.5.3.

5.2.1 HPLC separation of a polystyrene mixture

Polymer samples that are homogeneous with respect to chemical composition exhibit the same elution behaviour and can therefore be separated by means of isocratic elution. In this elution regime, the composition of the mobile phase eluent remains constant throughout the chromatographic run. The mixture containing five PS standard samples can therefore be separated into single components on a C18 column, using 100% THF as the mobile phase eluent. Since a thermodynamically good solvent is used, adsorption effects are limited, and on porous packing materials the size exclusion mode will be operational.

Size exclusion chromatography is characterised by the separation of polymers according to their hydrodynamic volume, and not their molar mass [4]. For homopolymers, the hydrodynamic volume is directly related to the molar mass, and a calibration for the specific polymer under investigation can be used to obtain molar mass and polydispersity information.

Figure 3.5 (section 3.1.4.1) shows the relationship between molar mass and retention volume for the elution of polymers in the size exclusion mode. Very large polymer molecules are incapable of accessing the pore volume and are therefore excluded from the entire pore volume. Smaller, lower molar mass molecules are able to access the pore volume to a certain degree, depending on their size. They can therefore move in and out of pores, and are retained longer within the stationary phase.

The smaller a molecule, the higher the portion of the pore volume that can be penetrated, and the longer its retention time will be. The result of the isocratic separation of the five PS standards is shown in figure 5.7.

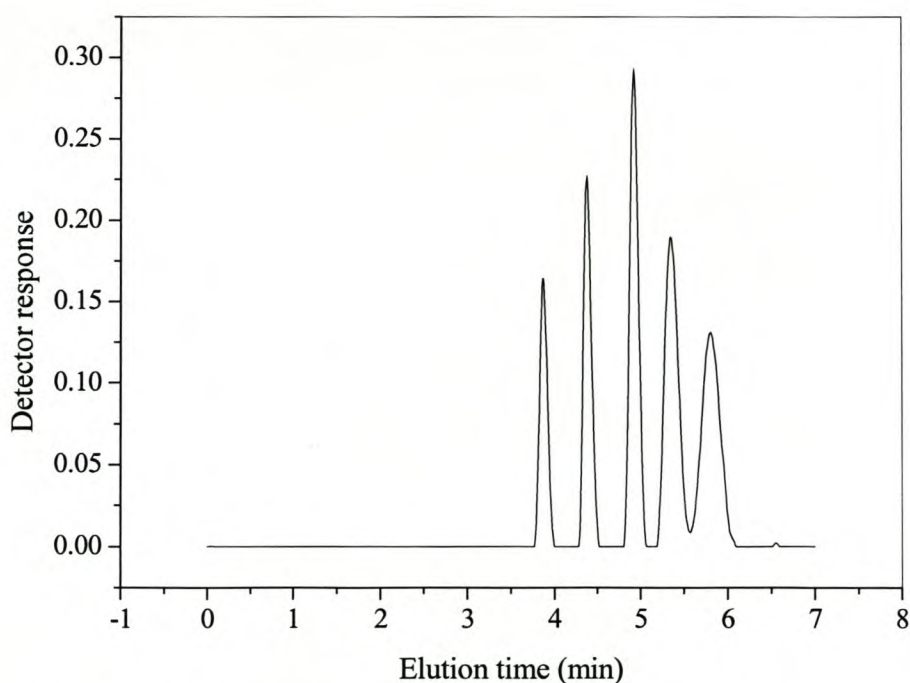


Figure 5.7: GPEC chromatogram of a mixture of five PS standards.

It can therefore be concluded that the highest molar mass standard with a molar mass of $377\,400\text{ g}\cdot\text{mol}^{-1}$ elutes first at 3.95 minutes, followed by the remaining PS standards in order of decreasing molar mass, until the lowest molar mass sample ($1\,300\text{ g}\cdot\text{mol}^{-1}$) elutes at 5.83 minutes.

5.2.2 LC-FTIR analysis of a polystyrene mixture

During the sample deposition step, the five polystyrene components were not deposited as individual spots, but rather as one continuous deposit from about 14.60 to 19.25 minutes in the Gram-Schmidt representation (figure 5.8). From the GPEC chromatogram it can be seen that the five PS components eluted relatively close to one another. The small difference in their retention times, causes the poor resolution observed in this experiment.

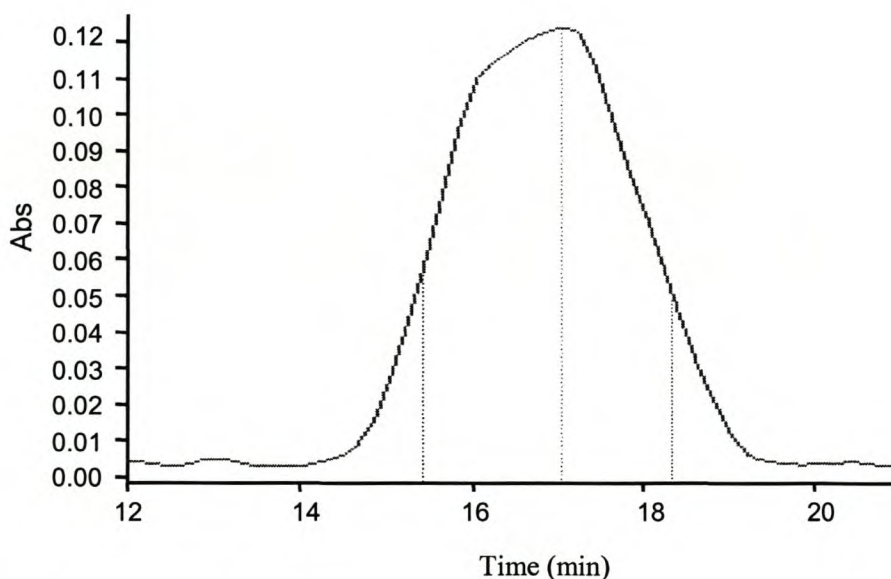


Figure 5.8: Gram-Schmidt representation of the mixture of five PS standards.

The resolution obtained during deposition of solutes by the nebuliser is determined by the rotation speed of the sample collection disc. A higher disc rotation rate will generally ensure better resolution of closely eluting peaks. The disc rotation rate of

10°/min used during the analysis of the PS mixture was therefore not high enough. A higher rotation speed might possibly have ensured complete resolution of the five individual components. An increase in the disc rotation rate does however have some disadvantages associated with it, such as a considerable decrease in the total elution time that can be accommodated. A higher rotation speed will also spread eluting peaks over a longer path, thereby decreasing the film thickness of the deposit, which usually leads to a decrease in the sensitivity of the IR measurement.

Since the five PS standards all have the same chemical composition, the IR spectrum at each point along the GS representation will be identical to the spectrum obtained at about 17.18 minutes, shown in figure 5.9.

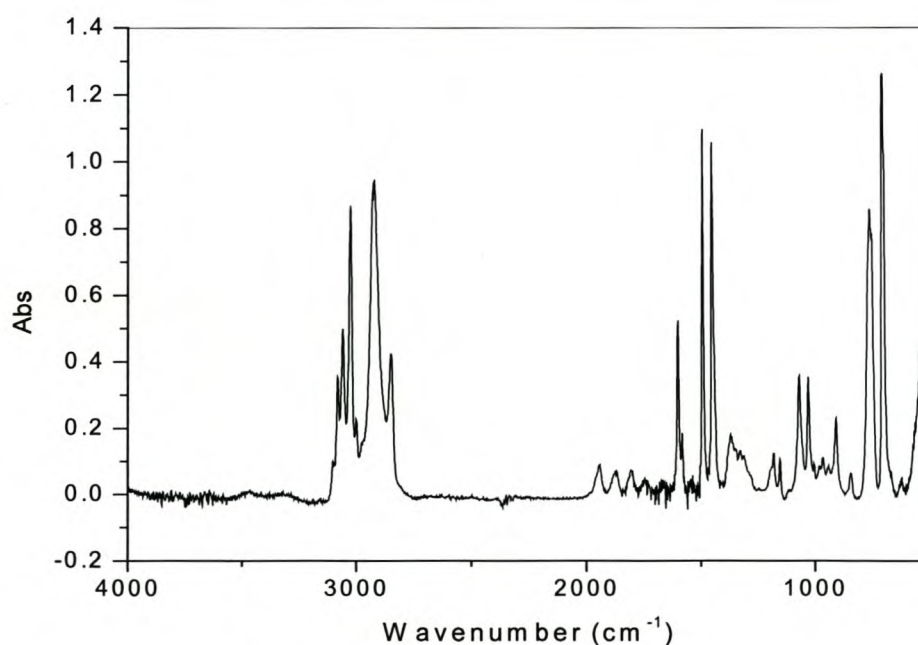


Figure 5.9: IR spectrum of PS taken at 17.18 minutes.

The characteristic IR absorbance frequencies are given in table 5.2, together with the functional groups responsible for IR absorption at each point.

Table 5.2: IR absorption data for PS

Wavenumber (cm^{-1})	Functional group	Spectral range (cm^{-1})	Bond mode	Peak intensity
700.7	Ring	710 - 690	Bend	Strong
760.2	CH (5 adjacent)	770 - 730	Deformation	Strong
902.8	CH (5 adjacent)	900 - 800	Deformation (out-of-plane)	Medium
1 026.2	CH	1 030 - 1 024	Bend (in-plane H bend)	Weak
1 072.4	CH	1 085 - 1 069	Bend (in-plane H bend)	Weak
1 180.5	CH	1 185 - 1 165	Bend (in-plane H bend)	Weak
1 239.4	CH	1 250 - 1 230	Bend	Weak
1 492.6	Ring	1 525 - 1 470	Stretching	Variable
1 600.5	Ring	1 625 - 1 590	Stretching	Variable
3 023.1, 3 057.3, 3 076.8	CH	3 079 - 3 010	Stretching	Weak

5.2.3 LC-AFM analysis of a polystyrene mixture

Since the five PSs were deposited as one continuous track along the perimeter of the collection disc, the thermal transitions of each individual component could not be determined. Instead, only three measurements were made, one at the high molar mass end of the deposit, one at the low molar mass end, and another one approximately in the center of these two regions, where the mid-molar mass components were supposed to have eluted. Three sections were cut from the disc at these points along the deposit. The three samples were transferred to the AFM for thermal analysis via the resonance frequency method (RFM) [5].

The highest molar mass sample was analysed first, and the result is given as the resonance frequency plot in figure 5.10.

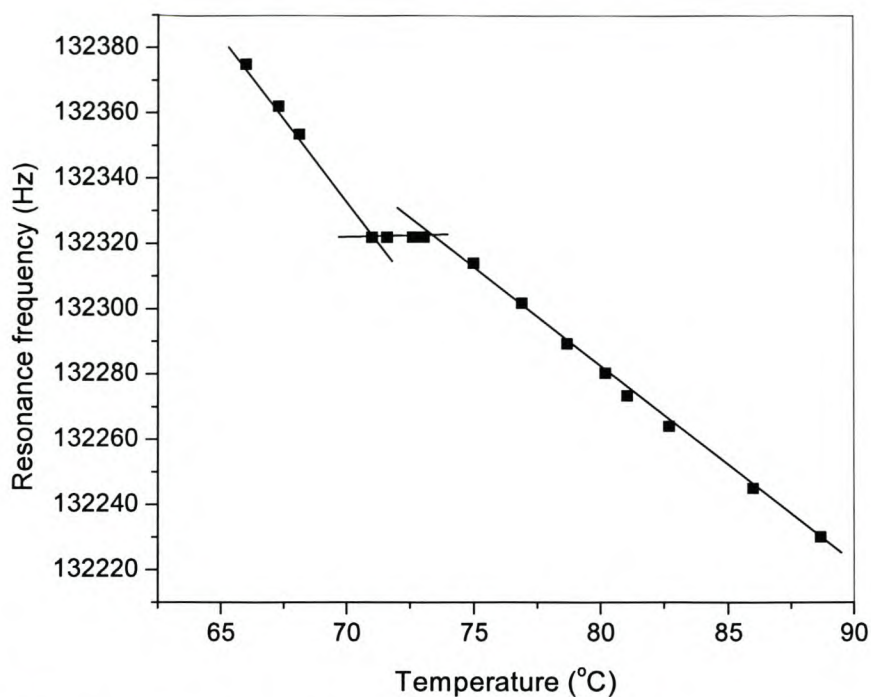


Figure 5.10: R_f plot of the highest molar mass region of the mixture of the five PS standards.

A glass transition is observed as a plateau from 71.0 to 73.1 °C in the resonance frequency plot. The AFM resonance frequency method presents the T_g of a polymer over a temperature range of a few degrees. The lowest temperature might correspond to the T_g of the surface, followed by a slightly higher T_g for the bulk sample. The width of the T_g plateau seems to depend on the thickness of the film, thereby implying that this method shows a certain depth sensitivity [6]. A thicker film, consisting of more layers of molecules, can absorb more energy to be converted into kinetic energy for chain movement at temperatures above the T_g .

Thermal analysis of the two remaining samples was also done via the resonance frequency method. The T_g of the low molar mass sample was measured at 43.8 to 46.0 °C, as indicated by the plateau in figure 5.11. Thermal analysis of the mid-molar mass sample yielded two plateaus in the resonance frequency plot (figure 5.12), one at 42.85 to 45.4 °C, and another at 55.85 to 59.0 °C. The plateau at 43.8 to 46.0 °C appears over exactly the same temperature range as that of the lower molar mass sample, thereby

indicating an overlap between the two samples taken at the low molar mass and mid-molar mass regions. The T_g of the mid-molar mass sample therefore appears at 56.1 to 59.0 °C.

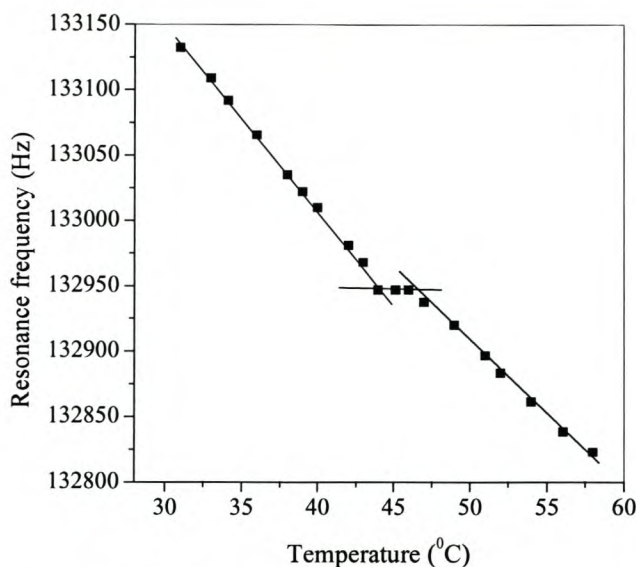


Figure 5.11: T_g of the lowest MM region of the PS deposit.

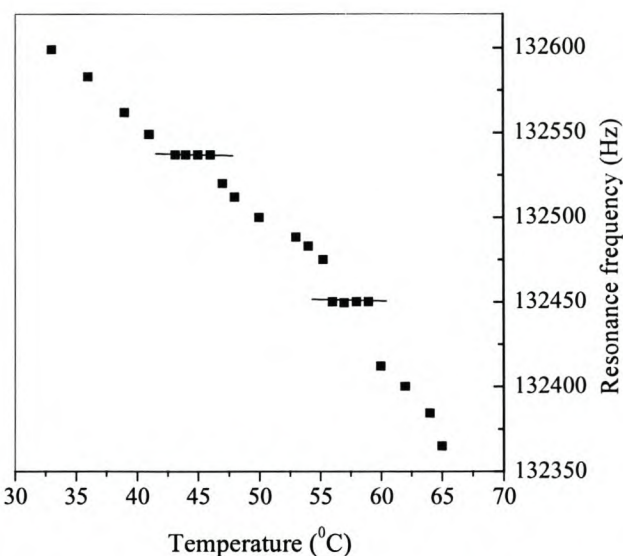


Figure 5.12: T_g of the mid-MM region of the PS deposit.

The theoretical T_g for PS is 100°C. The reason for the difference between the bulk T_g value and the values measured by the resonance frequency method, is twofold. The T_g of a polymer film is influenced by (i) the film thickness and (ii) the molar mass of the polymer under investigation. The influence of these two factors on the T_g of a polymer will now be discussed.

5.2.3.1 Molar mass dependence of the T_g

The relationship between the bulk T_g of a polymer and its molar mass (M_n) is generally given by the Fox-Flory relation [7]:

$$T_g = T_g^\infty - \frac{K}{M_n} \quad (5.6)$$

For polystyrene, the T_g at an infinitely large molar mass, T_g^∞ , is 100°C, while the empirical constant K , is taken as 1.2×10^5 [8]. Although good correlation between the bulk T_g and that of the surface is observed at higher molar mass values, a number of publications have reported a decrease in the T_g with decreasing molar mass [8-13]. The resonance frequency method confirmed the dependence of the T_g on molar mass, although the depression of the T_g is much larger than theoretically calculated with equation 5.6. This suggests that, in addition to the molar mass influence, surface effects contribute to a further decrease in the T_g of polymer films. Segregation of polymer chain ends near the surface is considered to be responsible for this phenomenon. These chain ends increase the free volume near the surface, thereby enhancing chain mobility, which subsequently leads to a lowering of the T_g of the surface layers. If the influence of chain ends is also taken into account, then the T_g of the surface, T_{g0} , can be expressed by the following equation [8]:

$$T_{g0} = T_g^\infty - CN^{-0.5} \frac{a}{D} \quad (5.7)$$

where a is the chain segment length, N is the average length of the polymer chains in units of segments, D is the depth of the surface layer and C is an empirical parameter.

Alternatively, the additional depression of the surface T_g can also be ascribed to chain entanglement effects. Bliznyuk [8] predicted the empirical constant, K , to be approximately 3.5 times larger near the surface of a polymer sample. This is due to a smaller thermal expansion as well as a reduction in the number of chain ends near the surface. Chain end effects may therefore account for the additional lowering of the T_g measured by surface sensitive methods such as the AFM thermal analysis method used in this study.

5.2.3.2 Film thickness dependence of the T_g

The dependence of the T_g of a film on its thickness, h , can be expressed as follows [8]:

$$T_g = T_g^\infty \left[1 - \left(\frac{d}{h} \right)^\delta \right] \quad (5.8)$$

where the parameters δ and d represent the strength of film-surface interaction and the depth of the correlated near-interface polymer layer, respectively.

The depth sensitivity of the AFM thermal analysis technique is evidenced by the change in the T_g plateau width and position. Figure 5.13 shows the T_g s of a range of PS films (142 500 g.mol⁻¹ molar mass) with different film thicknesses, ranging from 13 nm to about 136 nm. Clearer and wider plateaus are observed for thicker films, and the onset of the plateau shifts to higher temperature values.

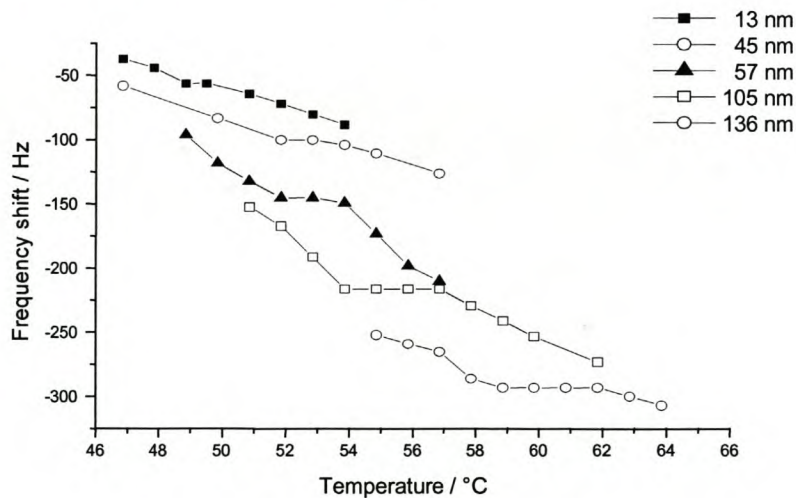


Figure 5.13: The change in the T_g plateau width and onset as a function of film thickness for PS with a molar mass of 142 500 g.mol⁻¹ [6].

The relationship between the film thickness and the width of the plateau is illustrated in figure 5.14. Here it is seen that a certain value is reached after which the plateau width does not increase for increasingly thicker films. This saturation shows that the depth

sensitivity of the RFM is limited to a certain value. For the PSs investigated here, this was found to be between 0.5 and 1 μm .

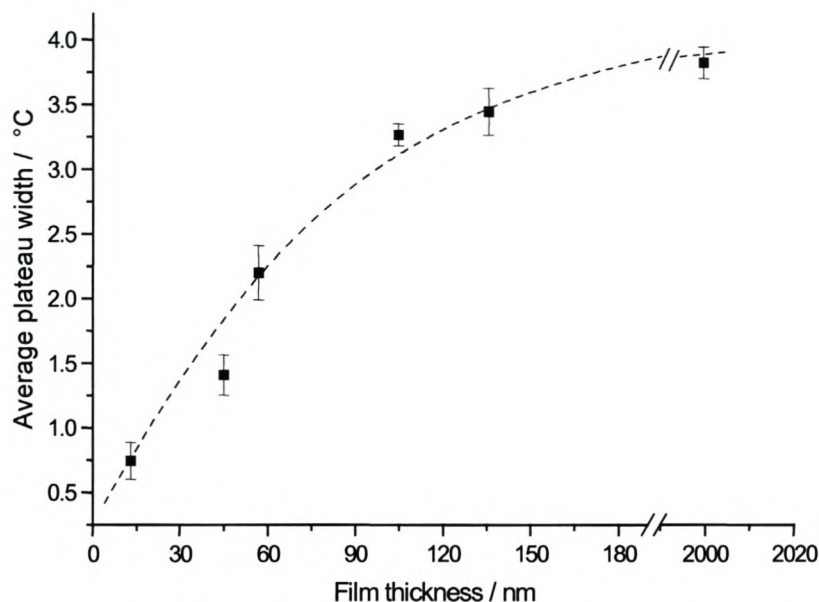


Figure 5.14: Average T_g plateau width as a function of film thickness for PS with a molar mass of $142\,500\text{ g}\cdot\text{mol}^{-1}$ [6].

In figure 5.15 the onset temperature of the T_g plateau is plotted against film thickness. Unfortunately, the curve relies on extrapolation, as many film thicknesses were not available, but it can be deduced that the onset temperature shifts to increasingly higher values as the film thickness is increased. A saturation value is expected to be reached at thicknesses higher than those measured in this experiment.

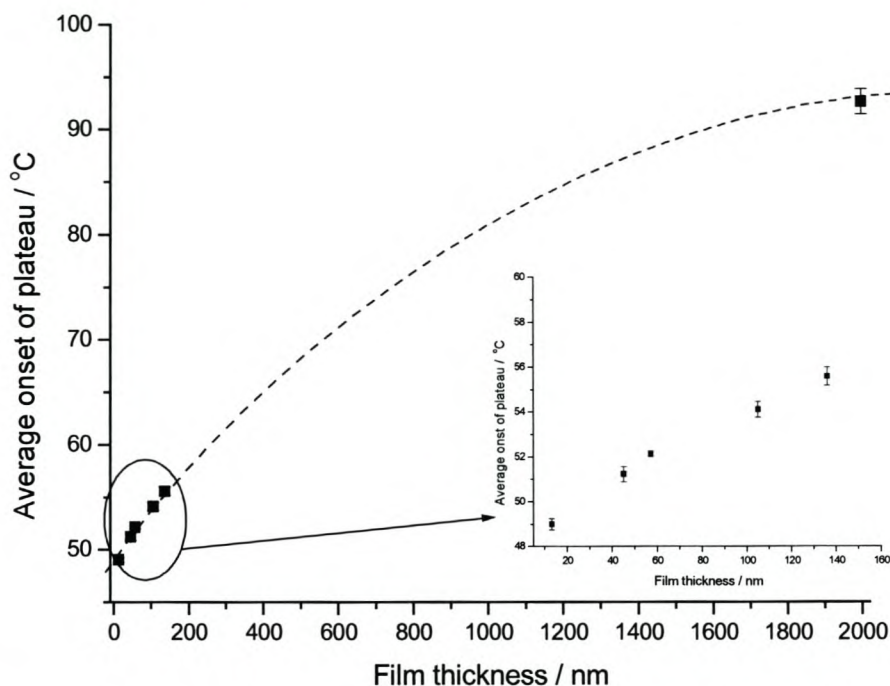


Figure 5.15: The onset of the T_g plateau as a function of film thickness [6].

These changes in the plateau width and onset temperature may be ascribed to surface effects. A lower T_g is measured for the surface compared to that of the bulk, which is 100°C for PS. During a thermal measurement the T_g of the surface is therefore measured first (onset of the plateau), followed by that of the underlying layers, resulting in a broad plateau. A decrease in the T_g with decreasing film thickness has also been observed with other techniques such as Brillouin light scattering [14], ellipsometry [15] and positron annihilation [16].

5.3 Analysis of a mixture of oligoethylene and polystyrene

The mixture of oligoethylene (282 g.mol⁻¹ molar mass) and PS (400 000 g.mol⁻¹ molar mass) was prepared according to the procedure in section 4.1.2, after which it was analysed as described in sections 4.5.2. and 4.5.3.

5.3.1 HPLC separation of a mixture of oligoethylene and polystyrene

Oligoethylene is capable of interacting more strongly with the non-polar stationary phase than PS is. Therefore, higher amounts of the less polar eluent, THF, ought to be necessary to desorb oligoethylene molecules from the stationary phase in order for elution to take place. One therefore expects the PS to elute first in this system, but the opposite is observed in figure 5.16. The oligoethylene elutes first at 7.53 minutes, while the PS is retained to 15.37 minutes. The cause of this elution pattern can be assigned to the very low molar mass of the oligoethylene molecules. They are evidently far more soluble than the higher molar mass PS molecules, and therefore elute long before them.

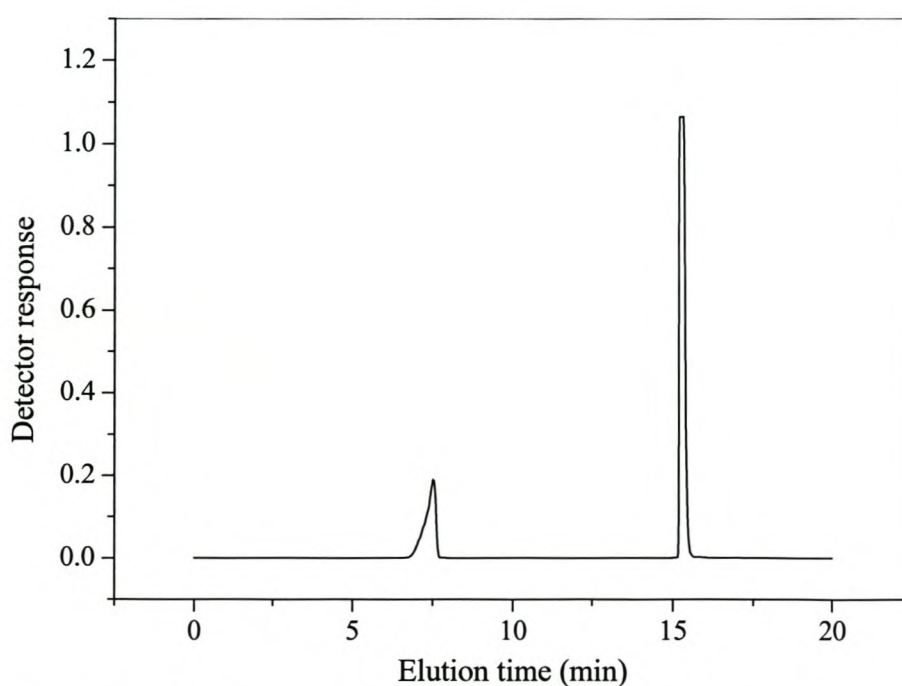


Figure 5.16: GPEC chromatogram of a mixture of oligoethylene and PS.

5.3.2 LC-FTIR analysis of a mixture of oligoethylene and polystyrene

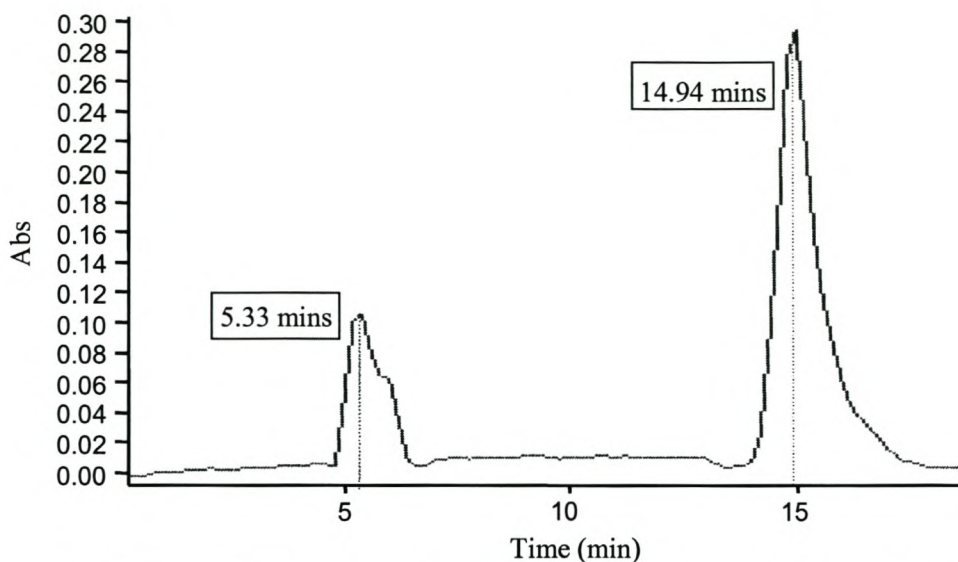


Figure 5.17: Gram-Schmidt representation of the mixture of oligoethylene and PS.

The Gram-Schmidt representation in figure 5.17 once again resembles that of the GPEC chromatogram, with two peaks present at 5.33 minutes and 14.94 minutes respectively. From the IR spectra obtained at the maxima of the two peaks in the GS representation, the identity of the two components in the mixture could be confirmed. The IR spectrum at 5.33 minutes (figure 5.18) is identical to that of the oligoethylenes in figures 5.3 and 5.4, section 5.1.2.

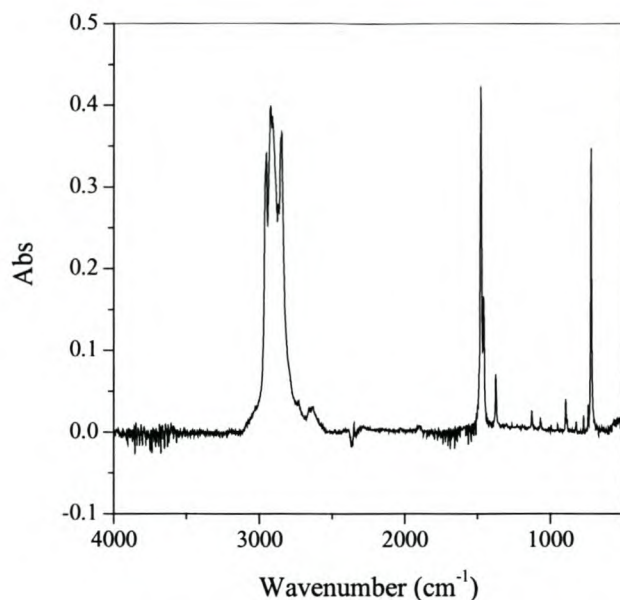


Figure 5.18: IR spectrum of the oligoethylene component of the mixture.

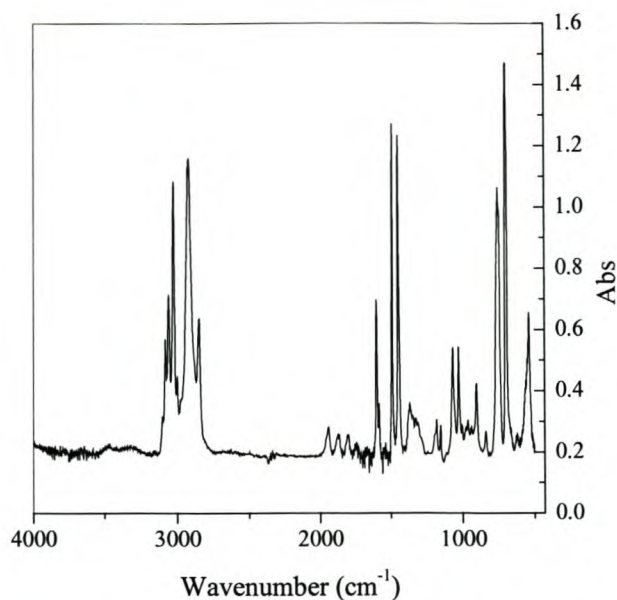


Figure 5.19: IR spectrum of the PS component of the mixture.

The IR absorption spectrum of the component eluting at 14.94 minutes (figure 5.19) is similar to those recorded for each of the PSs in section 5.2.2. LC-FTIR analysis therefore confirmed the identities of the two components that were separated by chromatography as well as their elution order. A summary of the absorption bands of the oligoethylene and PS are tabulated in tables 5.1 and 5.2 respectively.

5.3.3 LC-AFM analysis of a mixture of oligoethylene and polystyrene

After LC-FTIR analysis and the deposition of the individual components onto the silicon disc, thermal analysis of each component was done via the resonance frequency method. The oligoethylene component at 5.33 minutes in the GS representation was analysed first. Figure 5.20 shows the results of the thermal measurement. The T_m of the oligoethylene is illustrated by the kink at 33.5°C in the resonance frequency plot. This value agrees well with the T_m measured for the same oligoethylene, in figure 5.5, when it was part of a mixture containing two oligoethylenes (32.2°C). The slight difference between the two

T_m values measured for the same oligoethylene sample may be ascribed to a difference in the thickness.

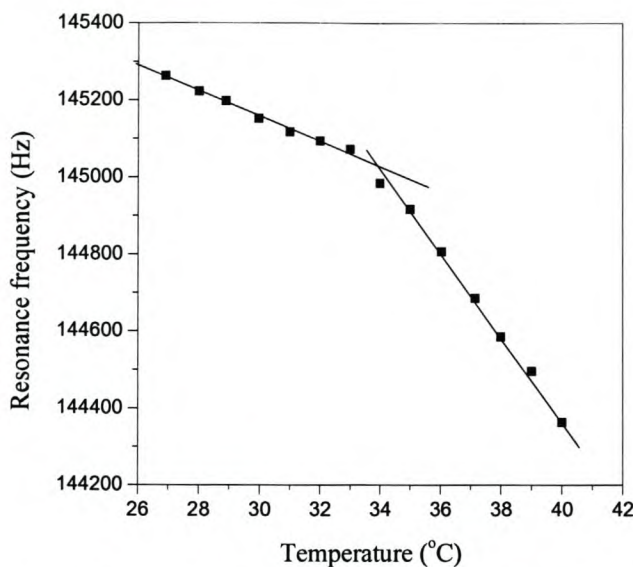


Figure 5.20: R_f plot of the oligoethylene component of the mixture.

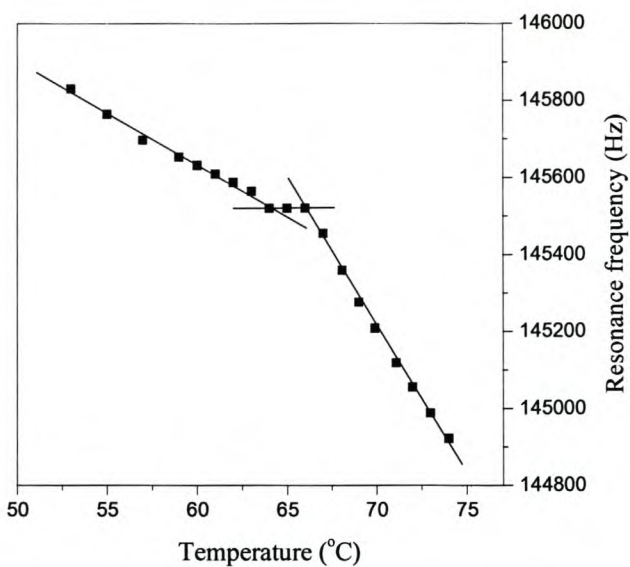


Figure 5.21: R_f plot of the PS component of the mixture.

The glass transition of the PS at 14.94 minutes in the Gram-Schmidt, appears as a plateau from 63.9 to 65.9°C in figure 5.21. The relatively narrow plateau (a broadness of 2°C) indicates a very thin film of PS. According to figure 5.14, this plateau width corresponds to a film thickness of approximately 53 nm. Figure 5.15 indicates a T_g onset of about 52°C for PS with a molar mass of 142 000 g.mol⁻¹. A T_g value of 63.9 to 65.9°C for a 400 000 g.mol⁻¹ PS is therefore considered reasonable. More calibration curves for a larger variety of molar masses are however required to establish the accuracy of this technique.

5.4 Analysis of a mixture of poly(ethyl methacrylate) and polystyrene

A mixture of poly(ethyl methacrylate) (PEMA) and polystyrene (PS) with molar masses of 850 000 and 942 000 g.mol⁻¹ respectively, was prepared (section 4.1.2) and analysed according to the procedure stipulated in sections 4.5.2. and 4.5.3.

5.4.1 HPLC separation of a mixture of PEMA and PS

PEMA is more polar than PS and will therefore be more soluble in the starting eluent composition, where a higher amount of the more polar solvent ACN, is present. Furthermore, there will be very little adsorptive interaction between the non-polar stationary phase and the more polar PEMA molecules. PS is therefore retained longer, and elutes at 15.74 minutes in this chromatographic system. PEMA elutes first, as represented by the peak at 8.26 minutes in figure 5.22.

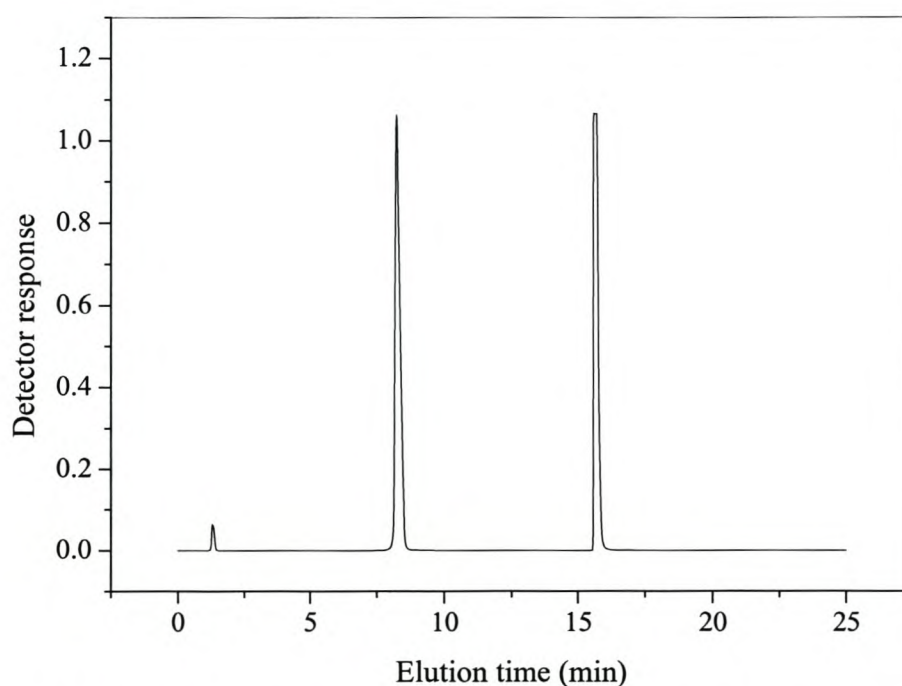


Figure 5.22: GPEC chromatogram of a mixture containing PEMA and PS.

The extremely small peak visible at 1.31 minutes is caused by column breakthrough, which results from column overloading. In such a case, when the sample volume injected is too high, the entire sample could not be adsorbed onto the column, leading to a small amount passing through the column without it being retained.

5.4.2 LC-FTIR analysis of the mixture of PEMA and PS

LC-FTIR analysis of the mixture containing PS and PEMA yielded the Gram-Schmidt as shown in figure 5.23. The shape resembles that of the GPEC chromatogram, with two peaks found at 7.71 and 15.24 minutes, respectively.

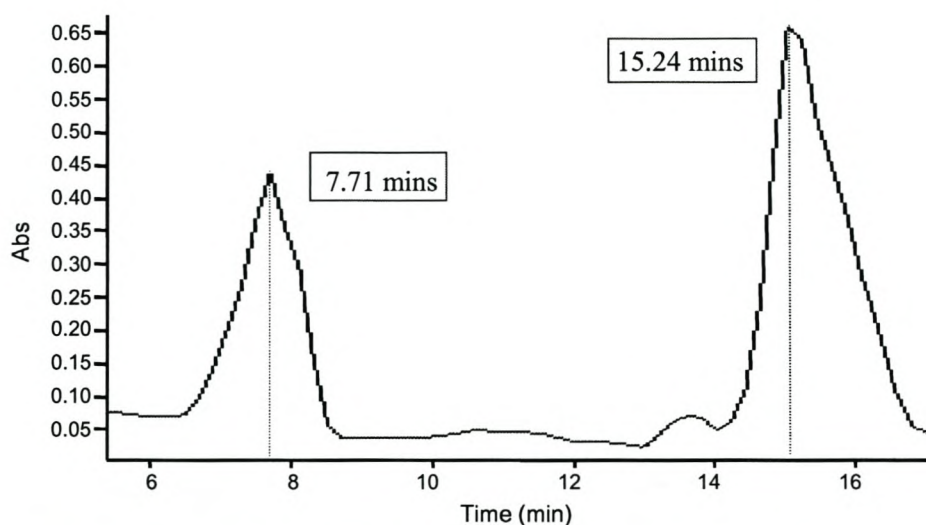


Figure 5.23: Gram-Schmidt representation of a mixture of PEMA and PS.

The IR spectrum recorded at 7.71 minutes is given in figure 5.24, where the characteristic IR absorbancies of PEMA are clearly visible. The IR spectrum of the PS component at 15.24 minutes in the GS (figure 5.25) is identical to that of the PSs in figure 5.9.

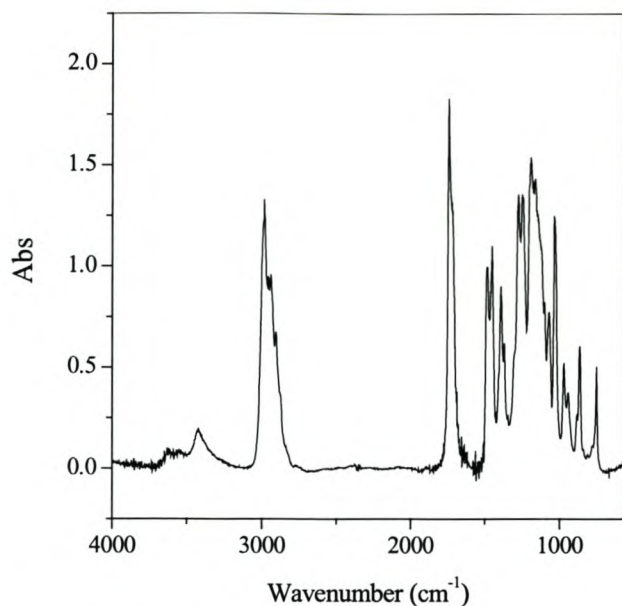


Figure 5.24: IR spectrum of PEMA at 7.71 minutes.

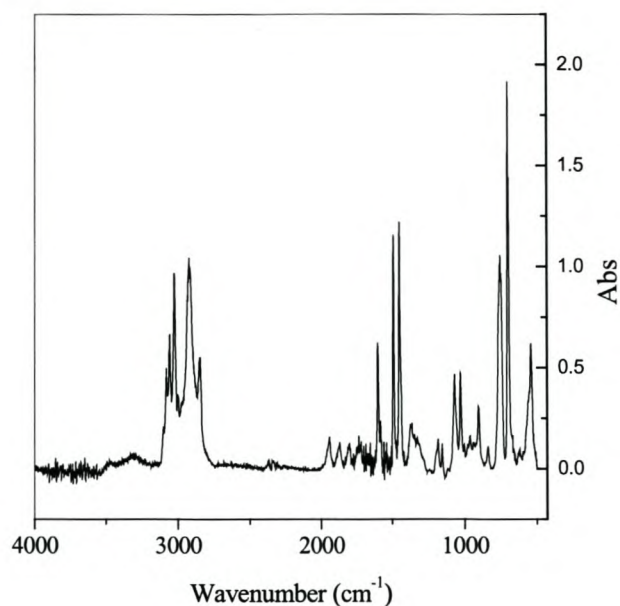


Figure 5.25: IR spectrum of PS at 15.24 minutes.

The position of the absorption bands of the characteristic groups for PEMA are given in table 5.3, together with the groups responsible for each band.

Table 5.3: IR data of the functional groups of PEMA

Wavenumber (cm ⁻¹)	Functional group	Spectral range (cm ⁻¹)	Bond mode	Peak intensity
1 160.2	C=O	1 210 - 1 160	Stretching	Strong
1 730.5	C-O	1 750 - 1 735	Stretching	Strong

5.4.3 LC-AFM analysis of a mixture of PEMA and PS

Analysis of the PEMA component by the RFM provided the resonance frequency plot shown in figure 5.26. The plateau at 57.8 to 59.9°C is representative of the T_g of a thin film of PEMA. The PS component has a T_g of 78.0 to 81.1°C, as indicated by the plateau in figure 5.27.

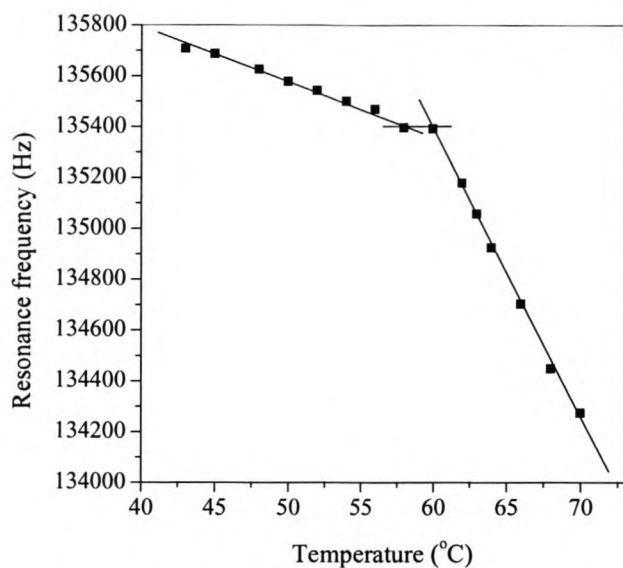


Figure 5.26: The R_f plot of the PEMA in the mixture.

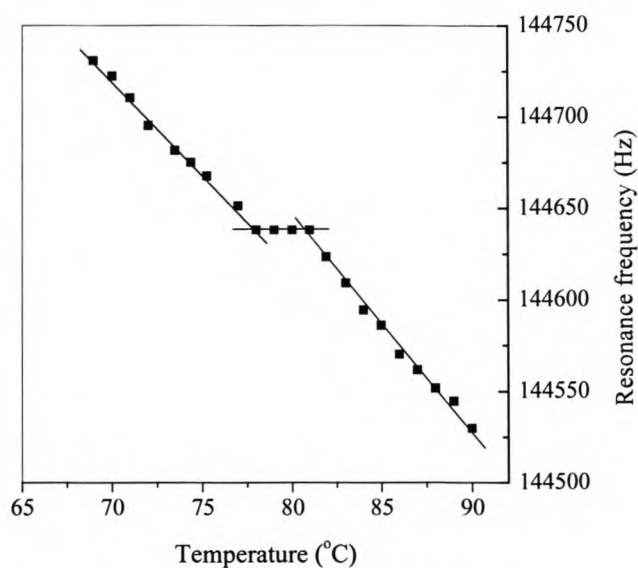


Figure 5.27: The R_f plot of the PS in the mixture.

According to figure 5.14, the thickness of the PS film in figure 5.27, which has a plateau width of 3.1°C, is approximately 105 nm. The T_g of this film (78.0 to 81.1°C) is therefore expected to be higher than the value measured for the much thinner PS film in figure 5.21, which has a T_g of 63.9 to 65.9°C.

5.5 Analysis of an unknown emulsion

The emulsion of unknown composition was prepared according to the procedure stipulated in section 4.1.2, after which it was analysed by the procedure discussed in sections 4.5.2. and 4.5.3.

5.5.1 HPLC analysis of an unknown emulsion

A sample of a commercial paper coating emulsion system was analysed by gradient elution in order to separate the individual components, and identify them via LC-FTIR. Furthermore, thermal analysis of the individual components was done via the AFM

resonance frequency method. Figure 5.28 is the GPEC chromatogram of the dissolved paper coating sample.

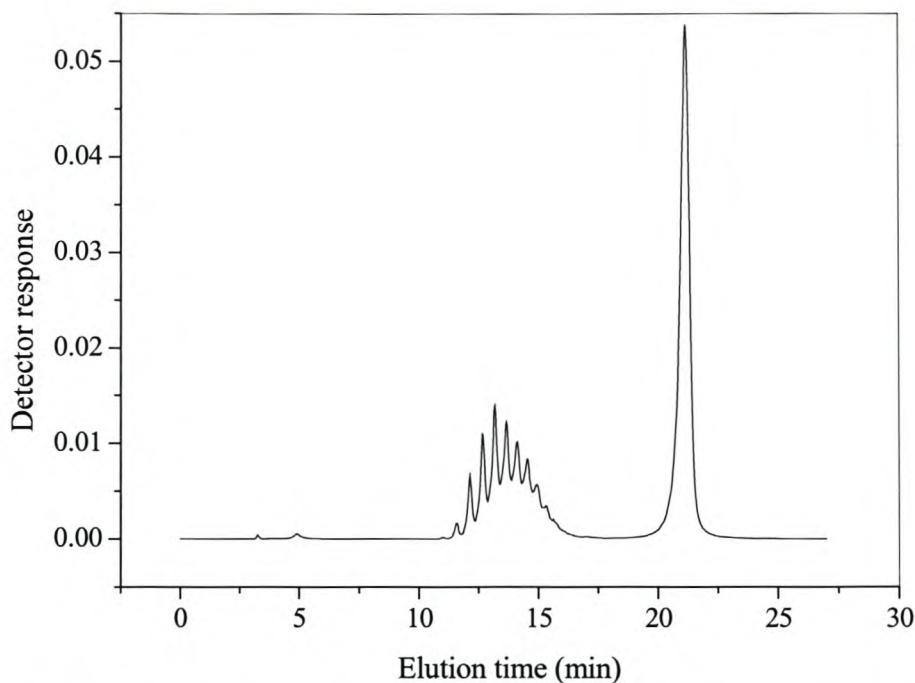


Figure 5.28: GPEC chromatogram of a commercial paper coating emulsion system.

From the GPEC chromatogram it can be seen that the sample consists of two major components. One sharp, well-defined peak appears at 21.17 minutes, while a complex series of smaller peaks is observed from 11.59 to 15.32 minutes. The pattern observed here usually indicates that oligomers are present within a sample. Depending on the complexity of the sample and the molar mass range, such a series can be separated into individual oligomers, especially when the sample is chemically homogeneous. In figure 5.28 we do not observe complete separation of individual oligomer components due to the experimental conditions used. The quality of the separation is influenced by the surface activity of the stationary phase and the composition of the mobile phase. Different stationary phases and eluents should be tried until complete separation of individual components are obtained.

If the series in figure 5.28 were to be resolved completely, each peak would have been separated by one monomer addition in the degree of polymerisation. The series is separated in the order of increasing degree of polymerisation. However, in the present case, separation is directed by hydrophobic interactions. Long chain oligomers (high degree of polymerisation) are more hydrophobic than the lower oligomers, and will therefore elute after the oligomers with a lower degree of polymerisation. If completely separated single oligomers are obtained, the degree of polymerisation and the molar mass of each oligomer can be obtained by analytical techniques such as matrix-assisted laser desorption/ionization mass spectrometry (MALDI-MS). After separation of the two main components of the sample by gradient elution, LC-FTIR analysis was performed in order to determine the identity of both components.

5.5.2 LC-FTIR analysis of an unknown emulsion

The shape of the Gram-Schmidt representation, figure 5.29, is similar to the GPEC chromatogram, with one relatively sharp peak at 20.74 minutes and a broad peak of lower intensity at 14.12 minutes, that corresponds to the series of oligomers.

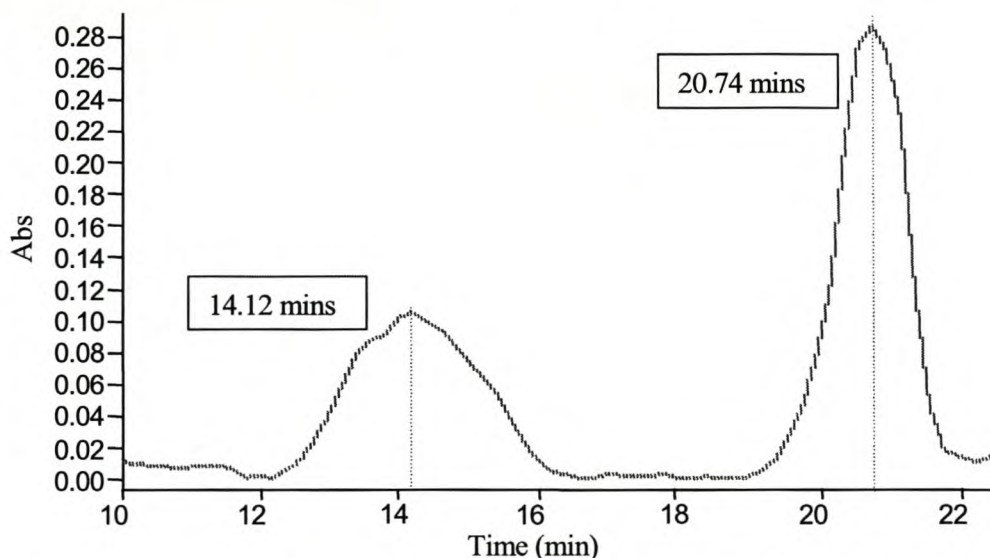


Figure 5.29: Gram-Schmidt representation of the commercial paper coating emulsion.

The IR chromatogram of the series of oligomers was recorded at 14.15 minutes, and the result is shown in figure 5.30. Three IR bands appear at 729.13 to 718.96 cm^{-1} , 1 462.2 to 1 472 cm^{-1} and 2 849.4 to 2 957.3 cm^{-1} . This absorption pattern is identical to the spectra obtained for the oligoethylenes analysed in section 5.1.2 of this chapter. It was therefore concluded that one of the components of the paper coating system is oligoethylene wax.

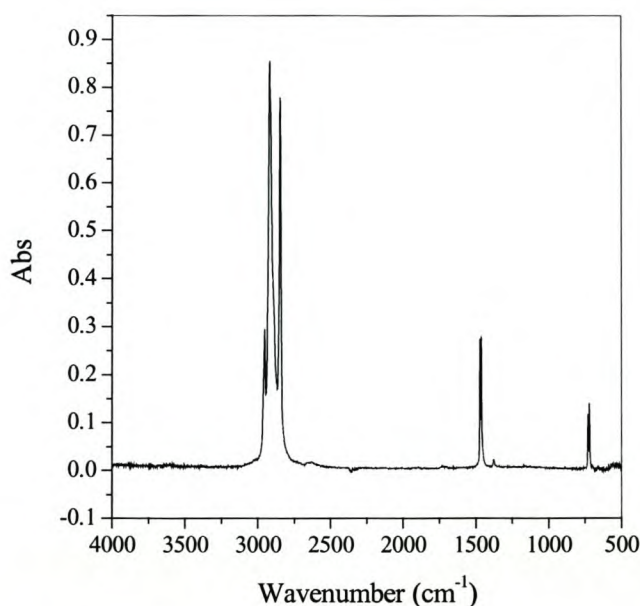


Figure 5.30: IR spectrum of the component at 14.12 minutes.

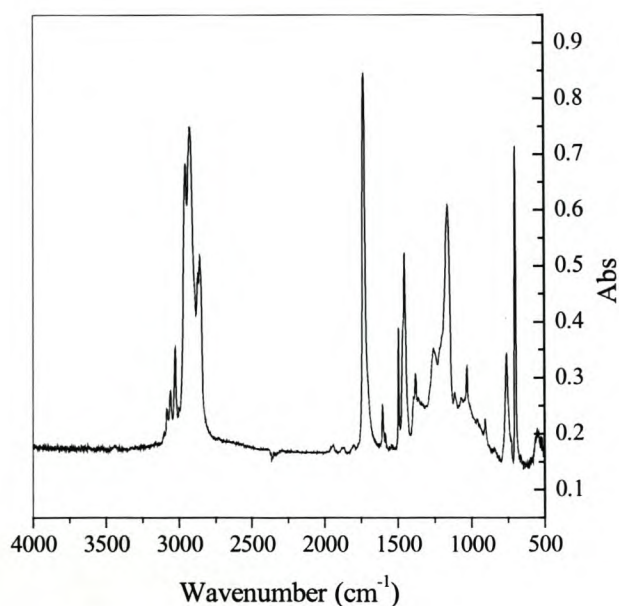


Figure 5.31: IR spectrum of the component at 20.74 minutes.

The IR spectrum of the second component is shown in figure 5.31. This spectrum was compared to reference spectra, supplied as part of our IR software package, and the result of the closest match (96.4% similar) is shown in figure 5.32. From this reference spectrum it was concluded that the major component of the paper coating emulsion is a styrene-acrylate copolymer.

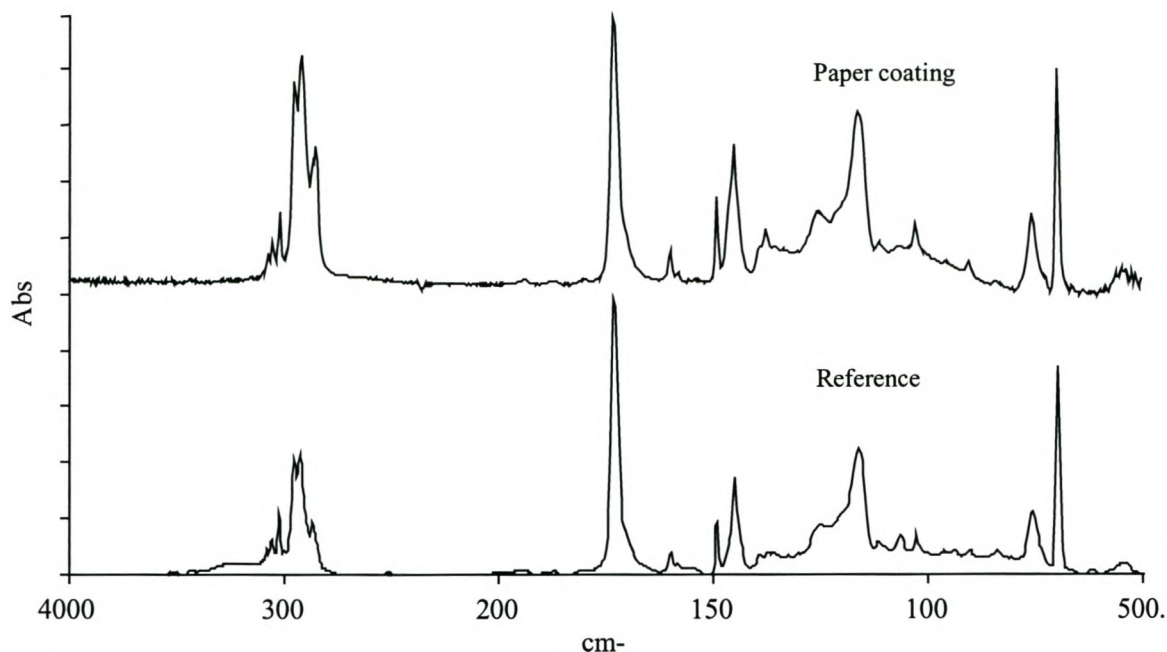


Figure 5.32: Comparison of the unknown second component of the paper coating emulsion with a reference spectrum in the IR library (closest match).

Figure 5.33 is a three-dimensional representation of the LC-FTIR data obtained for the paper coating emulsion system. This representation is called a stack plot, or “waterfall” presentation [17]. It can provide valuable information on the chemical composition of each chromatographic fraction obtained by LC-FTIR analysis and can easily be interpreted. This also provides an attractive way to represent chromatographic data.

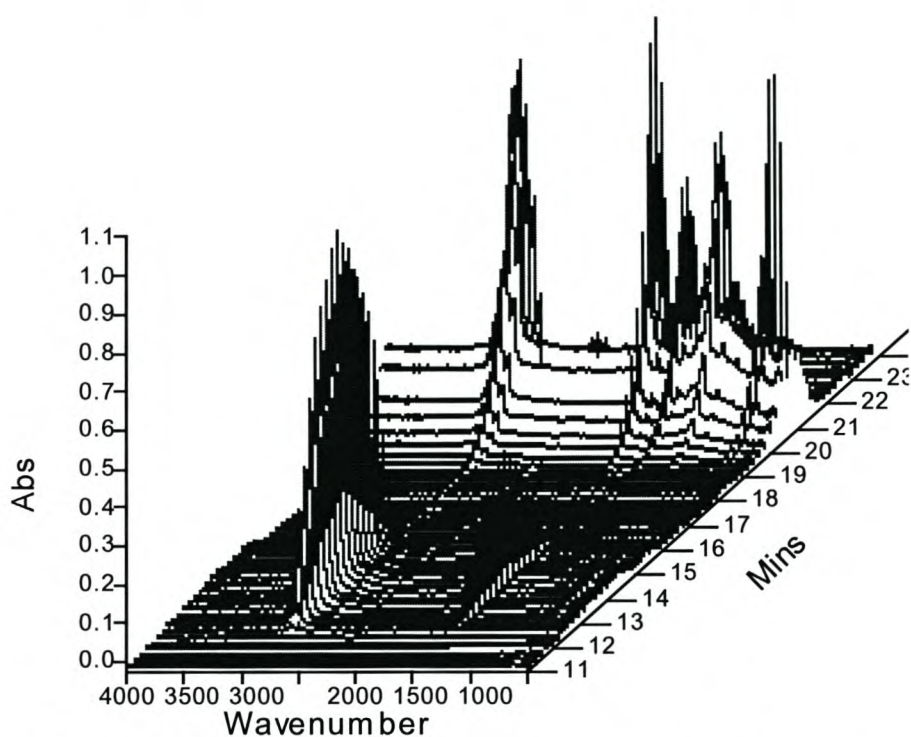


Figure 5.33: Stack plot of the two major components in the paper coating emulsion system.

The deposition step was repeated on a silicon substrate using the LC-FTIR equipment, after which each component was cut from the disc and transferred to the AFM for thermal analysis.

5.5.3 LC-AFM analysis of an unknown emulsion

The result of the AFM thermal analysis of the oligoethylene component is presented in figure 5.34. A melting point is observed at 79.5°C, as indicated by the kink in the resonance frequency plot. This is much higher than the melting points of the two oligoethylenes analysed in section 5.1.3. According to Brandrup and Immergut [3] this T_m value corresponds to an oligoethylene with a molar mass of about 535 g.mol⁻¹ (79.2°C).

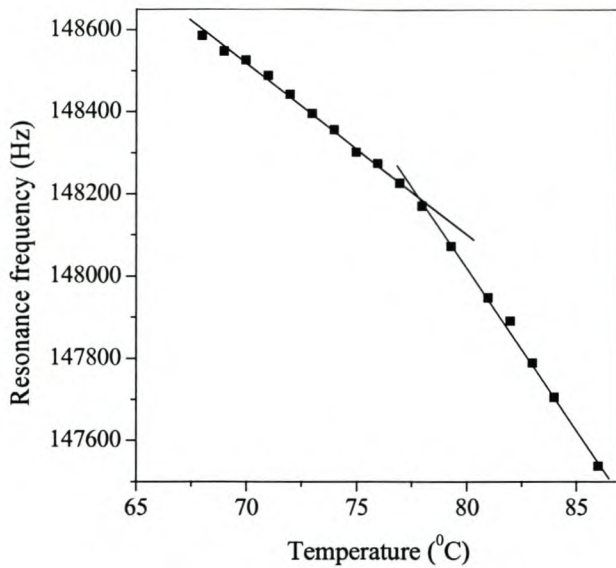


Figure 5.34: R_f plot of the oligoethylene component of the unknown sample.

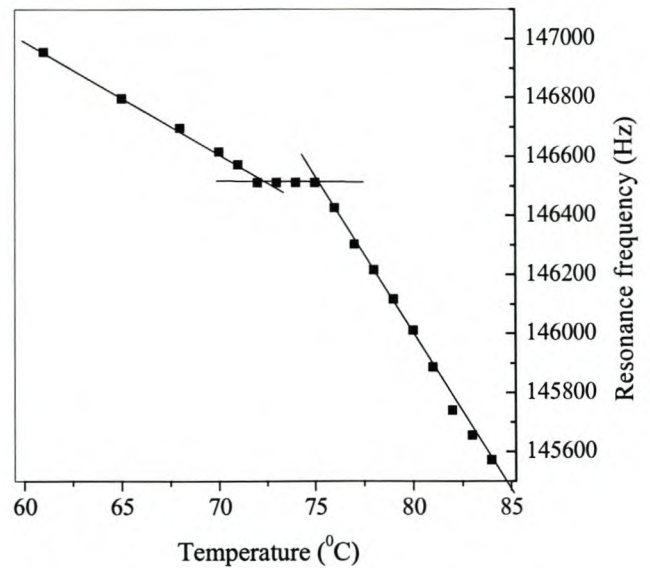


Figure 5.35: R_f plot of the copolymer component of the unknown sample.

Figure 5.35 is the result of thermal analysis of the copolymer fraction of the sample. The T_g of this component is indicated by the plateau from 71.8 to 75.1°C, and is indicative of the T_g of a thin film of the styrene-acrylate copolymer with a high styrene content and molar mass.

From the AFM thermal measurement and the IR spectrum of the unknown component, it is difficult to determine which acrylic ester is incorporated in the styrene-acrylate copolymer. If, however, the film thickness, h , is known, the parameters δ and d can be estimated and equation 5.8 can be used to determine the T_g of the copolymer film. It is also known that the T_g of a copolymer consisting of two polymers can be expressed as follows [18]:

$$\frac{1}{T_g} = \frac{W_{PS}}{T_{gPS}} + \frac{W_{Acrylic}}{T_{gAcrylic}} \quad (5.9)$$

where T_g is the T_g of the copolymer, W is the weight fraction of each of the two monomers and T_{gPS} and $T_{gAcrylic}$ is the bulk T_g for polystyrene and the acrylic ester,

respectively. Since the T_g of the copolymer is known (through calculation by means of equation 5.9) as well as the bulk T_g of PS [3], only the weight fractions of the two polymers have to be determined in order to obtain the T_g of the acrylic ester polymer. NMR spectroscopy may be used to obtain the weight fraction information through comparison of the signal intensities of the two polymer components in the NMR spectrum.

A much easier way to establish the identity of the unknown acrylic ester, would be to couple LC-FTIR to NMR spectroscopy, using a nano-probe method, since such a small quantity of the unknown sample is available after LC-FTIR analysis. The sample can be recovered from the sample collection disc through careful solvent application by means of a syringe needle [19]. A small droplet from a 1 μ l syringe should be applied to a single solute peak, withdrawing the solvent to recover the solubilised deposit, as illustrated in figure 5.36.

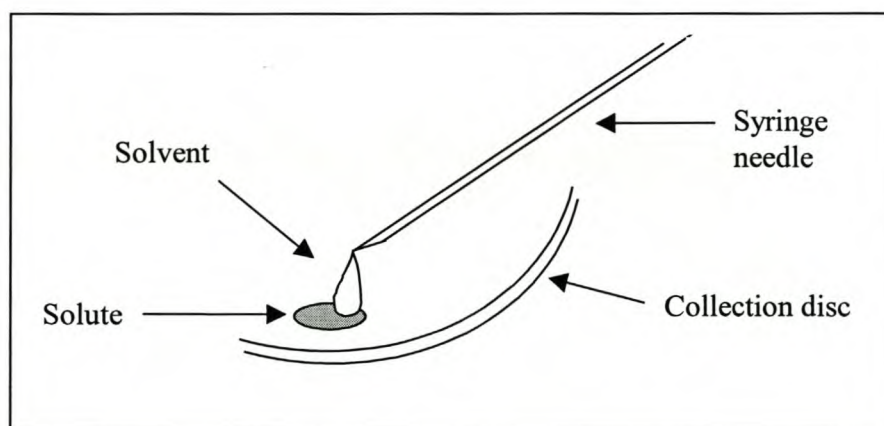


Figure 5.36: Illustration of the technique used to recover deposits from the LC-FTIR collection disc [19].

Another advantage of the LC-FTIR solvent elimination technique is therefore the ability to archive a chromatographic collection disc for subsequent solute recovery when further analyses are necessary for identification of unknown sample components. The success of storage of the sample collection disc, however, depends on the volatility of the deposits.

For samples with a tendency to sublime, storage in a freezer will greatly extend the life of the sample.

5.6 References

- [1] P.J.C.H. Cools, A.M. Van Herk, A.L. German, W.J. Staal, *J. Liq. Chromatogr.* **17** (1994) 3133.
 - [2] H.J.A. Philipsen, B. Klumperman, A.L. German, *J. Chromatogr. A* **746** (1996) 211.
 - [3] J. Brandrup, E.H. Immergut, *Polymer Handbook*, Wiley Interscience, New York, 1975.
 - [4] H. Pasch, B. Trathnigg, *HPLC of Polymers*, Springer-Verlag, Heidelberg, Berlin, 1998.
 - [5] M. Meincken, PhD Dissertation: University of Stellenbosch; Stellenbosch, South Africa (2001).
 - [6] M. Meincken, *Surf. Interface Anal.* *Accepted* (2003).
 - [7] T. Fox, P. Flory, *J. Polym. Sci.* **14** (1954) 315.
 - [8] V.N. Bliznyuk, H.E. Assender, G.A.D. Briggs, *Macromolecules* **35** (2002) 6613.
 - [9] K. Tanaka, A. Taura, S.R. Ge, A. Takahara, T. Kajiyama, *Macromolecules* **29** (1996) 3040.
 - [10] F. Dinelli, C. Buenviaje, R.M. Overney, *J. Chem. Phys.* **113** (2000) 2043.
 - [11] J.A. Hammerschmidt, W.L. Gladfelter, *Macromolecules* **32** (1999) 3360.
 - [12] S. Ge, W. Zhang, M. Rafailovich, J. Sokolov, C. Buenviaje, R. Buckmaster, R.M. Overney, *Phys. Rev. Lett.* **85** (2000) 2340.
 - [13] F. Oulevey, H. Burnham, G. Gremaud, A. Kulik, H. Pollock, A. Hammische, M. Reading, M. Song, D. Hourston, *Polymer* **41** (2000) 3087.
 - [14] J.A. Forrest, K. Dalnoki-Veress, J.R. Dutcher, *Phys. Rev. E: Stat. Phys.* **56** (1997) 5705.
 - [15] J. Mattsson, J.A. Forrest, L. Borjesson, *Phys. Rev. E: Stat. Phys.* **62** (2000) 5187.
-

-
- [16] Y.C. Jean, H. Cao, G. Dai, T. Suzuki, T. Ohdaira, Y. Kobayashi, K. Hirata, *Appl. Surf. Sci.* **116** (1997) 251.
 - [17] H. Pasch, *Adv. Polym. Sci.* **150** (2000) 1.
 - [18] R.E. Kirk, D.F. Othmer, *Encyclopedia of Chemical Engineering*, Wiley Interscience, New York, 2001.
 - [19] Lab Connections, *Instruction Manual, LC-Transform Series 300*.
-

Chapter 6

Summary and Conclusions

6.1 Summary

The main objective of this study was to develop a new analytical technique for the simultaneous separation, identification and determination of thermal properties of individual components in polymer mixtures or blends. This novel technique involved the combination of three well-established analytical methods often used for the characterisation of macromolecules, namely HPLC, LC-FTIR and AFM.

During the first stage of this technique all samples were successfully separated by means of various modes in HPLC, of which reversed-phase gradient elution was used predominantly. The second stage involved the identification of the components of each mixture according to their IR spectra via LC-FTIR analysis. For the purpose of coupling HPLC to FTIR spectroscopy, a solvent evaporation interface was used to obtain interference-free IR spectra for conclusive identification of sample components. In the case of an unknown sample, the IR spectrum of the species in question was compared to reference spectra for positive identification. During the final stage of this novel technique, thermal analysis of individual sample components was performed and information such as melting points and glass transition temperatures could be obtained. Thermal analysis was performed by means of a recently developed AFM technique, the resonance frequency measurement (RFM) method, which relates changes in the characteristic resonance behaviour of the cantilever to thermal transitions within a polymer.

6.2 Conclusions

From this study, the following conclusions have been reached:

1. The LC-FTIR interface can be successfully coupled to HPLC, more specifically gradient analysis, for the determination of the chemical composition of polymer mixtures.
 2. Unknown sample components can easily be identified through comparison of their IR spectra with those of reference materials.
 3. LC-FTIR data can be obtained within a short period of time. By contrast, weeks of effort may be required to obtain the same array of data from conventional means of preparative chromatography followed by IR analysis.
 4. LC-FTIR provides a very attractive way to present data through the use of contour plots that are easy to interpret.
 5. The AFM was successfully coupled to HPLC through the use of the LC-FTIR interface, which allowed the deposition of individual sample components onto a substrate suitable for AFM analysis.
 6. The thermal transitions of both crystalline and amorphous polymers could be measured within a localized region on the sample surface by means of the recently developed AFM resonance frequency method (RFM).
 7. The RFM allows an entirely non-destructive measurement of the thermal properties of polymers, without any contamination of the AFM tip.
-

8. Thermal analysis via the RFM ensures comparably short measurement times. Depending on the temperature range, one thermal measurement may take about one hour, as opposed to about twenty hours for similar analysis via Brillouin light scattering and up to two days for a positron annihilation depth probing measurement.

9. Since all organic substances have their own unique IR fingerprint, IR spectroscopy (or LC-FTIR) can usually supply sufficient information to unambiguously identify unknown sample components. If, however, uncertainty concerning the identity of an unknown sample still exists after LC-FTIR analysis, NMR spectroscopy may be used additionally to confirm the identity of such a sample. In this case, the analyte in question can be recovered from the deposition disc and its structure resolved via a NMR nano-probe method.

The coupling of HPLC with FTIR spectroscopy and AFM is undoubtedly of great value to the analyst interested in fast, effortless analysis of polymer mixtures or blends. Since three well established analytical techniques were combined to create this novel hyphenated technique, one can be sure of reliable, reproducible results. Other possible applications of this technique still need to be explored, and optimisation of the current experimental conditions should most certainly ensure superior results in future.
